RESEARCH ARTICLE SUMMARY

COGNITIVE MAPS

Hippocampal coding of identity, sex, hierarchy, and affiliation in a social group of wild fruit bats

Saikat Ray, Itay Yona, Nadav Elami, Shaked Palgi, Kenneth W. Latimer, Bente Jacobsen, Menno P. Witter, Liora Las*, Nachum Ulanovsky*

INTRODUCTION: Social animals live in groups and interact volitionally in complex ways. To perform real-life social behaviors, the brain needs to code other individuals' identities, represent various types of social interactions, and encode key social factors such as the sex, dominance hierarchy, and social affiliation of multiple other individuals. However, our understanding of how the brain deals with such diverse requirements stems from constrained laboratory experiments in which an animal typically exhibits one specific behavior with one other animal in one particular task. This leaves the fundamental question unexplored: How does the brain actually represent the real world with its complex, multianimal settings?

RATIONALE: To understand natural social coding in the mammalian brain, we studied Egyptian fruit bats (*Rousettus aegyptiacus*), which are highly social mammals, and focused on the hippocampus, a brain area that in previous studies has been shown to be important for memories of social identities, episodic events, and spatial locations. We hypothesized that in natural scenarios, when all of these disparate aspects occur simultaneously, hippocampal neurons would bind together all of these different types of information. To create a naturalistic environment, we established a laboratory-based "cave," housing mixed-sex groups of five to 10 wild-caught bats. The bats lived together continuously (24/7) for several months, engaging in natural social behaviors without any imposed tasks. During this time, we conducted wireless neural recordings from the dorsal hippocampus area CA1 of both male and female bats and tracked their positions, head directions, and social interactions with each other.

RESULTS: The freely behaving bats formed a stable social network and displayed three key behaviors: (i) flying between two nets located at opposite corners of the setup, (ii) engaging in social interactions, and (iii) being active on the net and observing each other. We found that hippocampal "place cells," neurons known to represent the animal's own position, were modulated during flight by the social context, i.e., whether the bat was flying to meet another bat or to be alone. These cells also encoded the identities of other bats. This identity coding was invariant to the bat's flight direction. We also found that many hippocampal cells encoded social-interaction events, with different neurons typically encoding distinct types of social interactions such as affiliative grooming or aggressive boxing. During active observation on the nets, we used methods from machine learning and game theory to reveal that neurons encoded the bat's own position and head direction, together with the positions, directions, and identities of multiple other individuals. Identity-coding neurons encoded the same specific bat across different locations and different behavioral states, both in-flight and on the net, providing another example of social invariance. The strength of identity coding was modulated by the sex, dominance hierarchy, and social affiliation of the other bats.

CONCLUSION: Our use of a naturalistic social colony allowed us to discover that the classical hippocampal cognitive map of space also integrates rich social information, forming a sociospatial cognitive map. We found neurons that encoded social interaction events, identities and sex of other individuals, dominance hierarchy, and social affiliation, along with the position and direction of both self and others. These findings combine the historically disparate views on hippocampal function, which suggested that the hippocampus is important for encoding memory, social identity, or spatial maps. Here, we have shown that all of these factors are represented together in the same neural network. ■

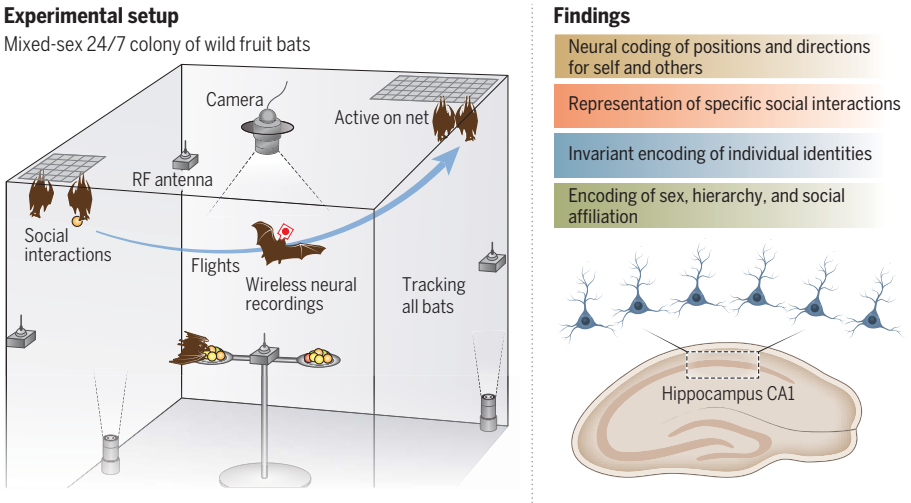

Hippocampal place cells also encode social information, forming a sociospatial cognitive map. In a naturalistic mixed-sex colony of freely behaving wild Egyptian fruit bats, hippocampal CA1 neurons encoded social interactions with other bats and represented the identity, sex, dominance hierarchy, and social affiliation of other individuals. [Map illustrations: Juliana Brykova/Shutterstock]

The list of author affiliations is available in the full article online.
*Corresponding author. Email: nachum.ulanovsky@weizmann.ac.il (N.U.); liora.las@weizmann.ac.il (L.L.)
Cite this article as S. Ray *et al.*, *Science* **387**, eadk9385 (2025). DOI: 10.1126/science.adk9385

READ THE FULL ARTICLE AT
https://doi.org/10.1126/science.adk9385

RESEARCH ARTICLE

COGNITIVE MAPS

Hippocampal coding of identity, sex, hierarchy, and affiliation in a social group of wild fruit bats

Saikat Ray[1], Itay Yona[1], Nadav Elami[1], Shaked Palgi[1], Kenneth W. Latimer[2], Bente Jacobsen[1,3], Menno P. Witter[3], Liora Las[1]*, Nachum Ulanovsky[1]*

Social animals live in groups and interact volitionally in complex ways. However, little is known about neural responses under such natural conditions. Here, we investigated hippocampal CA1 neurons in a mixed-sex group of five to 10 freely behaving wild Egyptian fruit bats that lived continuously in a laboratory-based cave and formed a stable social network. In-flight, most hippocampal place cells were socially modulated and represented the identity and sex of conspecifics. Upon social interactions, neurons represented specific interaction types. During active observation, neurons encoded the bat's own position and head direction, together with the position, direction, and identity of multiple conspecifics. Identity-coding neurons encoded the same bat across contexts. The strength of identity coding was modulated by sex, hierarchy, and social affiliation. Thus, hippocampal neurons form a multidimensional sociospatial representation of the natural world.

From a hive of bees (*1*) to a troop of baboons (*2*) or a society of humans, social groups are ubiquitous in nature, and social interactions in a group are crucial for survival (*3*). However, neurophysiological investigations of social interactions are typically conducted in pairs of animals (*4*–*10*), not in a group. Furthermore, social group behavior in the natural world is complex. For example, one may choose to mate with one individual, fight with another, and play with a third, a widespread scenario in real life that is not captured by typical laboratory experiments in social neuroscience. Such real-life situations require the representation of individuals' identities and of features pertinent to it, such as the sex, social hierarchy, and social affiliation of multiple other individuals, and representing the social interactions themselves. To date, no studies have examined together the representation of identity, sex, hierarchy, social affiliation, and social interactions in the same neuronal population. Further, there have been no studies that performed neural recordings in a mixed-sex group or in a group of wild social animals—in any species and in any brain area. Here, we aimed to close these three major gaps to elucidate how the brain represents social information in rich multianimal settings like those that would be encountered in the natural world. We focused on the hippocampus, which was shown in recent years to be important for social memory (*4*, *11*–*13*). In particular, we studied its output structure, CA1, an area containing neurons that represent the animal's own position (*14*–*16*) as well as neurons representing other animals' positions in a pairwise social setting (*5*, *6*). We investigated highly social wild mammals, Egyptian fruit bats (*Rousettus aegyptiacus*) (*17*–*20*), and allowed them to socialize freely to understand how hippocampal neurons represent identity, sex, hierarchy, social affiliation, and social interactions in natural social groups.

[1]Department of Brain Sciences, Weizmann Institute of Science, Rehovot, Israel. [2]Department of Neurobiology, University of Chicago, Chicago, IL, USA. [3]Faculty of Medicine and Health Science, Kavli Institute for Systems Neuroscience, NTNU Norwegian University for Science and Technology, Trondheim, Norway.
*Corresponding author. Email: nachum.ulanovsky@weizmann.ac.il (N.U.); liora.las@weizmann.ac.il (L.L.)

Continously monitoring a mixed-sex social group of wild bats

We established a laboratory-based cave for housing mixed-sex colonies of five to 10 wild-caught Egyptian fruit bats (Fig. 1A; $n = 5$ groups for the $n = 5$ recorded bats, with approximately equal proportions of males and females in each group). The composition of the group was stable over long periods of time (weeks to months) and was changed only when we replaced the recorded bats. Egyptian fruit bats are a long-lived, highly social species with complex social structures (*17*–*20*). The bats in our experiment were familiar with one another and lived in this setup continuously (24/7) for several months. They were free to fly and interact with each other and could choose between two nets to roost on (Fig. 1A; room dimensions: 2.7 × 2.3 × 2.6 m; large net, 40 × 80 cm; small net, 40 × 40 cm). We tracked the locations and identities of all the bats continuously during the recording session. During the flights, we tracked them in three dimensions (3D) using a radiofrequency-based system with a set of unique tags that the bats carried (10-cm precision) (*21*). We also placed barcodes on all of the bats (fig. S1) (*22*) and used a set of video cameras to track their identities, positions, and head directions at high resolution (millimeter-level precision) while they were on the nets. We also used video recordings to document in detail the bats' social interactions (movie 1). We performed wireless electrophysiological recordings from one or two bats for up to 3 hours per experimental day for a total of 99 recording days. These recording sessions commenced shortly after the beginning of the day's dark phase (Fig. 1B), when the bats are most active (*17*, *18*). No humans were present inside the room during the recordings.

A key aspect of natural social groups is stability in their social structure (*23*, *24*). Our bat colony exhibited a stable social network over weeks, with stable social-affiliation preferences (Fig. 1, C and D) (*21*). Another integral aspect of stable social groups is the stability of their social hierarchy (*25*, *26*). Indeed, our bat colony displayed a stable social hierarchy over many months (Fig. 1E and fig. S2). The social hierarchy was also transitive and linear (transitivity: 84%, $n = 113/134$ triads; linearity: $h = 0.80$, $P < 10^{-6}$; h ranges from 0 to 1, with 1 indicating perfect linear hierarchy and 0 indicating perfect equality) (*21*). Together, these features indicate that we successfully created a highly social, naturalistic, multianimal society and that bats could recognize each other—i.e., they formed internal representations of the identities of individual conspecifics within the group, which allowed them to maintain social preferences.

Social behavior in the natural world is unconstrained, so we did not constrain the behavior of our colony of bats to any particular task. Rather, the bats volitionally chose which behaviors to perform and when, where, and with which other bats. We focused our analysis on the three most prominent behavioral states that the bats exhibited: (i) flying between the two nets, (ii) engaging in social interactions on the nets, and (iii) being active on the nets and observing other bats (Fig. 1, F and G). The bats' activity on the nets in state iii was evident by their substantial head rotations and very low rate of sharp-wave ripples during that period (fig. S3). These three behavioral states occurred in an interleaved manner, with the bats spending the largest fraction of time on the large net and being active on it while intermittently engaging in social interactions and flights (Fig. 1G). While bats engaged in these three behaviors, we recorded 489 well-isolated neurons from the dorsal CA1 region of the hippocampus from five adult bats (three males and two females) (Fig. 1H). Of the 489 neurons, 444 cells met the inclusion criteria of having sufficient behavioral data and enough spikes to be valid for analysis in at least one of the three behaviors (see table S1 for the numbers of cells that were valid for analyzing each of the three types of behaviors) (*21*).

Hippocampal neurons exhibit social modulation and identity coding in flight

We first investigated how hippocampal cells respond in the flight state. The bats flew mostly

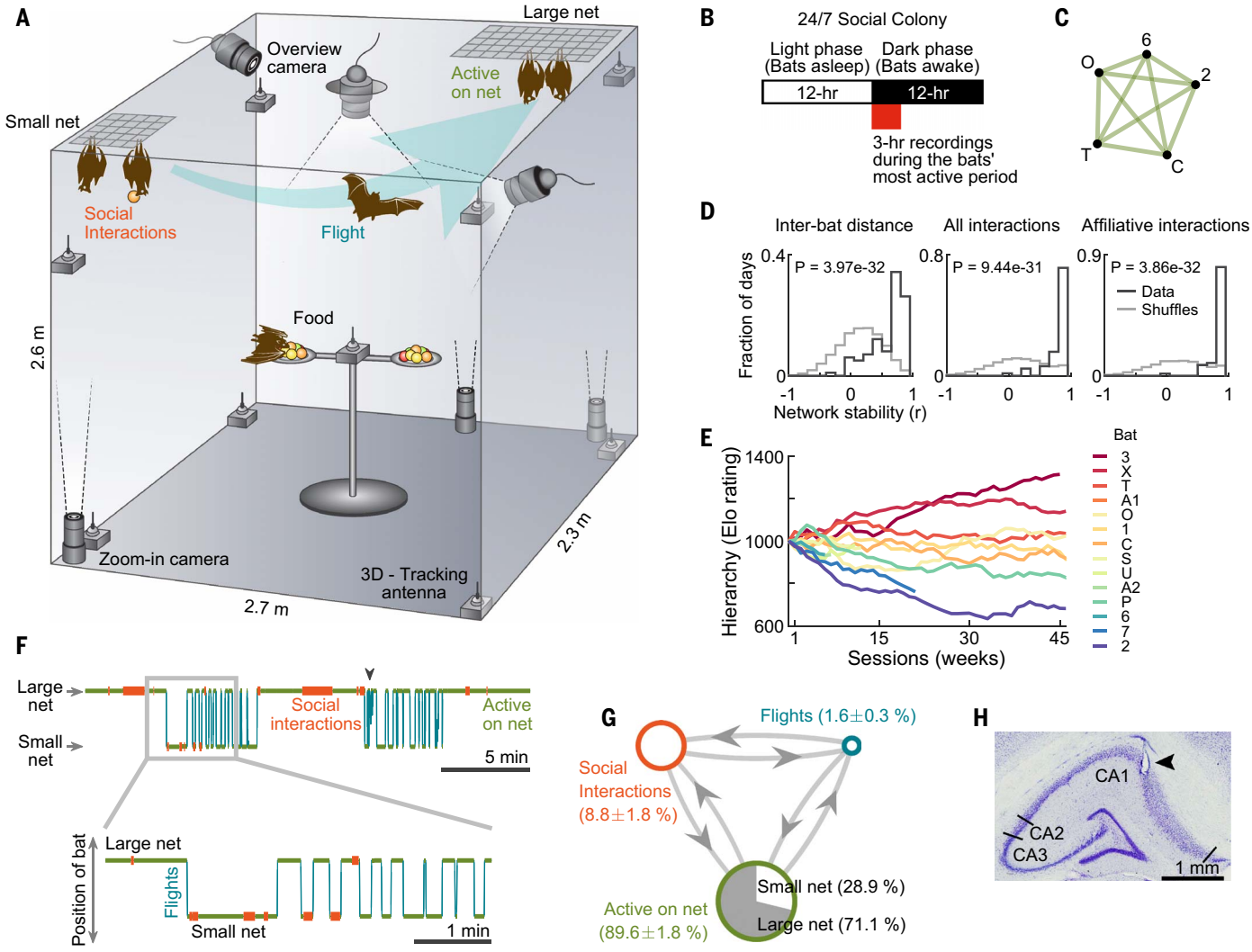

Fig. 1. Setup and behavior: A stable social network in a colony of freely behaving bats. (**A**) Five to 10 male and female bats lived continuously in a room (2.7 × 2.3 × 2.6 m) simulating a bat cave. Their social interactions and activity on two nets were observed using video cameras, and their flights were tracked by a radiofrequency-based 3D tracking system. (**B**) Schematic illustration of the daily timeline in the colony. (**C**) The average social network for all days in which this group of five bats were together. The network was constructed based on the physical distances between all pairs of bats, which is a proxy for social affiliation (n = 47 days; the colony's social composition was the same throughout these 47 days) (*21*). Nodes of the graph correspond to individual bats (bats C and T are males; bats O, 6, and 2 are females; bat 6 is the recorded bat), and distances between nodes are proportional to the median distances between the bats. (**D**) Distributions of social network stability quantified by correlation (Pearson's r) between the vector of graph centralities for each recording day and the vector of median graph centralities of that social network across all days [n = 99 days in total; n = 5 different networks (groups) for the five recorded bats] (*21*). Network stability was computed based on distances between all pairs of bats (left), rate of all social interactions (middle), or rate of affiliative social interactions with the recorded bat (right). Black line is the data; gray line is the shuffled network (*21*). Shown are P values for Wilcoxon rank-sum test between distributions of data versus shuffles; note the high network stability for the data compared with shuffles. (**E**) Dominance hierarchy (Elo rating) of individual bats over time (weeks). Each curve corresponds to an individual bat (n = 14 bats that participated in our five groups; bats 3, O, 1, 6, 7, and 2 are females, and bats X, T, A1, C, S, U, A2, and P are males). The hierarchy was determined in a separate setup using a pairwise hierarchy test (fig. S2A) (*21*). Hierarchy testing for some bats started later than others; the Elo ratings were determined in the original timing of the hierarchy tests, and then the curves for individual bats were shifted to their first session for display purposes. (**F**) Example ethogram of a recorded bat (top, 25 min from a typical session of 2 to 3 hours; bottom inset, zoom-in on 5 min). Shown are three interleaved behavioral states during the session: flights (blue), social interactions of the recorded bat with other bats (red), and activity on the two nets (green). Black arrowhead at top indicates an instance of irregular flights. (**G**) Summary of time spent by all the recorded bats in the three behavioral states and transitions between the states. Blue indicates time spent flying; red, engaging in social interactions; and green, being active on the nets. The bats spent most of their time being active on the large net, intermittently engaging in social interactions and flying. (**H**) Coronal section through dorsal hippocampus of one recorded bat; arrowhead, electrolytic lesion in CA1 at the end of a tetrode track.

in direct flights between the two nets, and we only used these direct flights for analysis. We analyzed the two flight directions separately, as is commonly done in studies of hippocampal place cells (*27*, *28*). We found that 61% of the cells were significant place cells in-flight (n = 149/243 cells × directions; significance was assessed by comparing them with spike shuffles; 243 cells × directions contained enough behavioral data and enough spikes to analyze place tuning in-flight) (*21*). This fraction of 61% place cells is consistent with previous reports on

bats flying in directed trajectories in a medium-sized room (*6*, *28*). We then investigated whether place tuning during flight depends on social context. For example, do neurons represent locations similarly when a bat flies to "meet" another bat and when it flies to be alone? We were able to investigate this question because of the natural asymmetry in the social preference of the two nets, with bats being only intermittently present on the small net (Fig. 1, F and G). We found that hippocampal cells were highly affected by social context (Fig. 2, A to D). Firing rate (FR) maps were strongly modulated in-flight between the condition when the bat was landing alone on the net or when it was landing while other bats were present on the net [Fig. 2, A and B, "landing," compare social maps (right) with alone maps (left)]. In addition to prospective social modulation, which depended on where the bat was going (landing), we also found retrospective social modulation, which depended on where it came from, i.e., whether the bat took off from a net when it was alone or if the net had other bats on it (Fig. 2, C and D, "takeoff"). The firing rate of socially modulated cells could be up-modulated or down-modulated in the social condition compared with the alone condition (Fig. 2, A to D), with simultaneously recorded cells showing heterogeneous responses (e.g., Fig. 2B, cells 70 and 71).

We defined significant socially modulated cells based on a bootstrap shuffle analysis in which individual flights were randomly redistributed between the social and alone conditions. A cell was considered significant if the root-mean-square difference (RMSD) in the 2D firing-rate maps between the social and alone conditions was greater than or equal to the 95th percentile of the shuffles (Bonferroni corrected for the two tests for landing and takeoff) (*21*). A majority of hippocampal cells (67%) were significantly socially modulated in-flight in at least one flight direction (Fig. 2E, "all cells," left bar; 67 of the 100 cells that were valid for analysis, i.e., with sufficient behavioral data in both social and alone conditions; see fig. S4D for counterexamples of cells that did not show social modulation) (*21*). We found similar proportions of cells that were socially modulated by bat presence or absence at the landing net (55 of 67) and at the takeoff net (49 of 67); 37 cells were modulated by both the landing net and the takeoff net.

To control for effects of spatial coverage and flight kinematics, we took several steps. (i) Comparisons between maps were only made on the overlapping regions of the maps (fig. S4, A to C). (ii) The landing and takeoff locations and 3D flight trajectories between the social and alone conditions were highly overlapping (fig. S5, A and B). (iii) Social coding was similar for the subset of social flights with the most similar trajectories or the most different trajectories to the alone flights (fig. S6C). (iv) Social modulation of neurons was not correlated with trajectory variability (fig. S6, E and F) (*21*), thus ruling out the possibility that the neural-activity differences between social and alone flights might arise from differing trajectories (*29*). (v) Flight velocity, acceleration, and flight curvature (straightness index) were very similar between the social and alone conditions (fig. S5, C and D), indicating that kinematic differences could not underlie the neural-activity differences between social and alone flights. (vi) Finally, we also controlled for the different number of flights in the social and alone conditions by matching the numbers of flights, and did not find substantial changes in the fraction of social-coding cells (fig. S6B).

Significant socially modulated place fields were found throughout the flight trajectory (Fig. 2F; n = 82 cells × directions). There was a slight overrepresentation of social modulation near the landing and takeoff locations (Fig. 2G), which was similar to the general distribution of place fields, as well as to the distribution on nonsocially modulated place fields (fig. S5, E and F; Kolmogorov-Smirnov tests comparing Fig. 2G with fig. S5E, P = 0.79 and P = 0.64 for the two directions; comparing Fig. 2G with fig. S5F: P = 0.54 and P = 0.59).

The socially modulated neurons showed a large effect size: The mean social modulation depth was twofold compared with nonsocial cells (Fig. 2H, compare the black and gray lines; Wilcoxon rank-sum test: $P = 2.94 \times 10^{-26}$; see also fig. S7A) (*21*), and the mean ratio of peak firing rates between the social and alone maps was 2.4-fold (Fig. 2I, mean of the black line). The social modulation was best explained by "rate remapping" of cells, which is a change in peak firing rate, rather than by "global remapping," which is a complete change in the map pattern (fig. S7B, note the high Pearson correlations between the two maps). The rate remapping was particularly prominent for cells showing large social modulation (fig. S7C, red histogram).

We observed a distinct behavior in which a bat would land on top of another bat instead of near it (Fig. 2J, right). This was likely an affiliative-landing behavior because it was typically followed by affiliative interactions such as allogrooming rather than by aggressive interactions. We then investigated whether neurons were modulated by this affiliative-landing behavior. Although this event was too rare on most days to allow systematic analysis, there were a small number of days when it occurred often enough to analyze (*21*). On these days, we found cells that were significantly modulated in-flight by the affiliative-landing behavior. The representative cell shown in Fig. 2J almost did not respond when the bat landed alone, responded moderately but significantly higher when it landed near other bats [nearby versus alone: effect size (social modulation depth) = 3.9, $P < 0.001$], and responded strongly when the bat landed on top of other bats (on top versus alone: effect size = 8.6, $P < 0.001$; on top versus near: effect size = 5.4, $P < 0.001$). Overall, of nine cells that had enough data for analysis and no velocity differences between the three conditions, we found four cells that were significantly modulated by affiliative landing. This further indicates a social modulation of place tuning in-flight.

Does the social modulation of cells depend on the identity of the conspecific involved (Fig. 3A)? To answer this, we analyzed a subset of the socially modulated cells that had enough data to compare social modulation for at least two other bats (Fig. 3, B to D; n = 84 cells). Many of these cells were identity coding and exhibited a significant difference between the social and alone conditions only for a particular conspecific bat, but not for others (Fig. 3B: examples; n = 34/84 cells) (*21*). The percentage of identity-coding cells was higher among the neurons that were nonplace cells (53%) compared with place cells (37%) (Fig. 3D). We also found a smaller subset of cells that were identity generalizing and exhibited a significant difference in firing when a bat was present or absent regardless of the bat's identity (Fig. 3C: examples; n = 15/84 cells). More than twice as many cells were significantly identity coding in-flight than identity generalizing (Fig. 3D, all cells: 40.5% identity-coding cells, 34/84; 17.9% identity-generalizing cells, 15/84) (*21*).

We next investigated whether the CA1 neuronal population could be used to decode the social context of the flight (social versus alone) and also determine whether a specific bat was present or absent (decoding of identity). We performed Bayesian maximum-likelihood decoding using the whole cell population (separately for the two flight directions) (*21*). We found that, first, we could indeed decode well above chance whether individual flights belonged to social or alone conditions (Fig. 3E, black error bar; mean decoding accuracy = 85%; t test for comparison with the chance level of 50%: P = 0.0068). Second, we were able to decode well above chance whether a specific individual bat was present or absent during a flight (Fig. 3E, yellow error bars; mean decoding accuracy for identity = 82%; t test for comparison with the chance level of 50%, pooling all bat identities together: P = 0.0066; t tests for individual bats: P = 0.024, P = 0.018, P = 0.005, and P = 0.0001). The fact that we could reliably decode bat identity further supports our finding that individual identity is strongly encoded by hippocampal neurons.

We next investigated whether the social modulation to specific individual bats was invariant to the flight direction. We found that, indeed, cells that were up-modulated by the presence (or absence) of a specific individual bat in one flight direction were also up-modulated

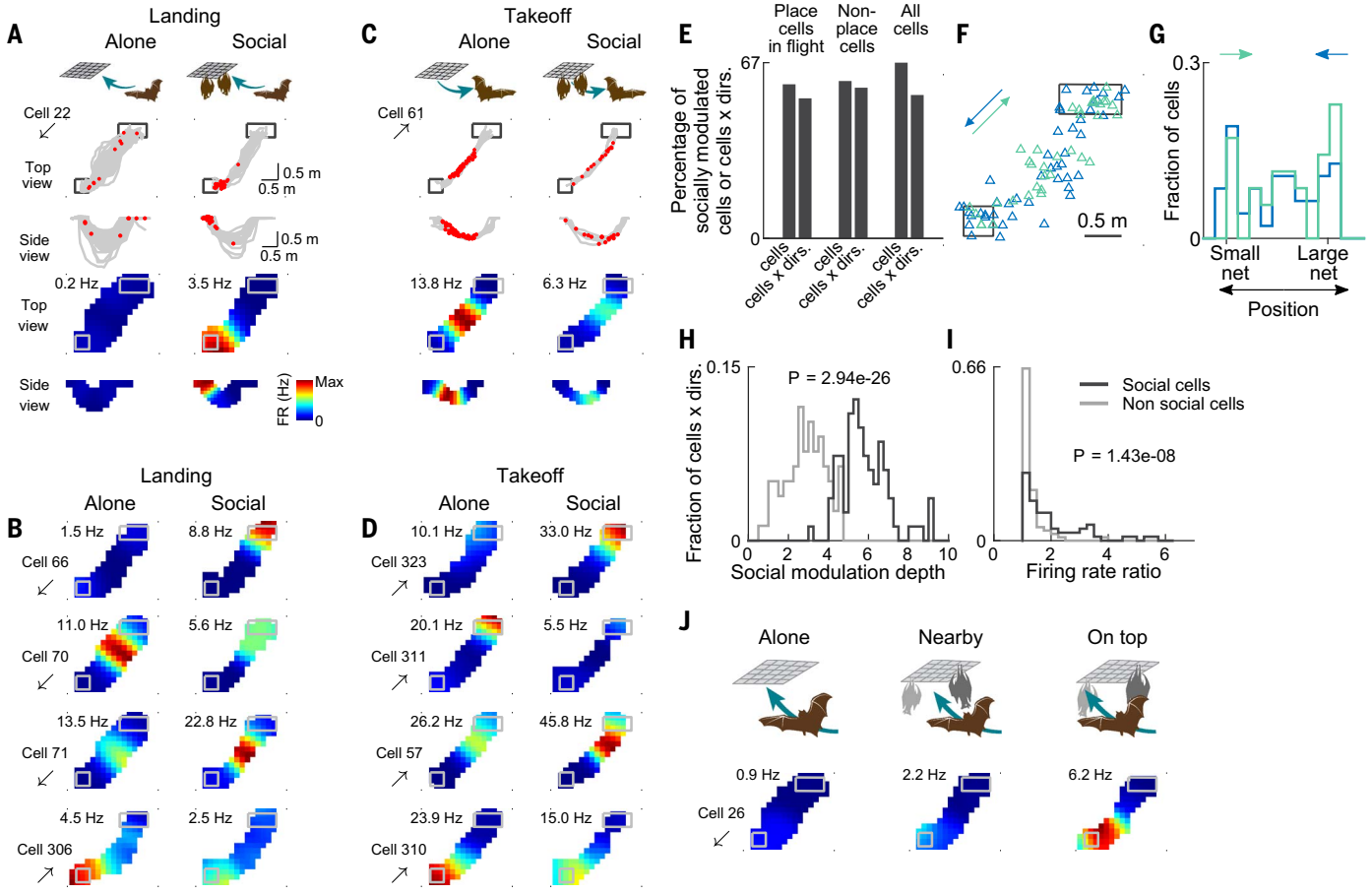

Fig. 2. Hippocampal place coding during flight is strongly modulated by social context. (**A**) Example of a socially modulated neuron during landing. The recorded bat landed on an empty net (left column, "alone") or on a net where other bats were present (right column, "social"). Second and third rows: flight trajectories (gray) with spikes overlaid (red), shown from top view (second row) and side view (third row). Fourth and fifth rows: 2D firing-rate (FR) maps corresponding to the raw data above. The maps are colored from zero (blue) to maximal firing rate [red; value indicated; each pair of maps (social and alone) has the same color scale; see color bar]. Arrow below the cell number indicates flight direction (here, from large net to small net). Note that the neuron barely fired when the bat landed alone (left), but had a clear place field when it landed with other bats present (right; $P < 0.001$) (*21*). (**B**) Examples of four neurons that were significantly socially modulated during landing. Shown are top-view 2D firing-rate maps of different neurons (rows) for the alone condition (left column) and the social condition (right column). Note that the socially modulated place fields occurred throughout the flight trajectory, and that a neuron could be either up-modulated in the social condition (cells 66 and 71) or down-modulated (cells 70 and 306). (**C**) Example of a neuron that was socially modulated by the presence or absence of bats during takeoff, namely whether the bat took off from an empty net (left, "alone") or from a net where other bats were present (right, "social") [plotted as in (A)]. This neuron had a higher firing rate when the bat took off in the alone condition ($P = 0.002$). (**D**) Examples of four neurons that were socially modulated by takeoff [plotted as in (B)]. (**E**) Percentage of significantly socially modulated neurons in-flight for place cells (left pair of bars), nonplace cells (middle pair of bars), and all cells (right pair of bars). Note that most hippocampal neurons were socially modulated [place cells, $n = 47/80$; place cells × directions, $n = 55/103$; nonplace cells, $n = 12/20$; nonplace cells × directions, $n = 27/47$; all cells, $n = 67/100$; all cells × directions, $n = 82/150$; numbers in the denominator indicate cells with sufficient behavioral data (*21*)]. (**F**) Population summary: Top view of the room showing the locations of peak firing of all the significantly socially modulated neurons (triangles) for flights from large net to small net (blue) or in the opposite direction (green) ($n = 82$ cells × directions, which include all of the significantly socially modulated cells × directions regardless of whether they were significant place cells). Note that these fields spanned all locations along the flight trajectories. (**G**) Distribution of the locations of peak firing of socially modulated neurons for flights in each direction. Position was projected onto the diagonal line connecting the two nets for the same cells as in (F). (**H**) Histograms of social modulation depth (effect size, defined as the RMSD between social and alone maps normalized by the SD of the RMSD for the shuffles) for the significant socially modulated cells (black, $n = 82$ cells × directions) and the nonsocial cells (gray, $n = 78$ cells × directions; Wilcoxon rank-sum test of black versus gray, $P = 2.94 \times 10^{-26}$) (*21*). (**I**) Histograms of ratios of peak firing rates in social and alone conditions (FRsocial/FRalone or FRalone/FRsocial, whichever is higher) in socially modulated cells (black) and nonsocial cells (gray; Wilcoxon rank-sum test, $P = 1.43 \times 10^{-8}$; x-axis has been clipped [zoom] for visualization only). (**J**) Example neuron that responded weakly when landing alone (left), moderately when landing near other bats (middle), and strongly when landing on top of other bats (right).

by the presence (or absence) of the same bat in the other flight direction (Fig. 3F: examples; Fig. 3G: population; Pearson $r = 0.55$, $P = 5.77 \times 10^{-6}$; no such correlation was found for the nonsocial cells: fig. S7D, Pearson $r = -0.06$, $P = 0.53$). Thus, unlike spatial coding in CA1, which is known to show remapping between two flight directions (*28*, *30*) (as seen also in Fig. 3F), social identity coding showed invariance between the two flight directions.

Finally, we found that in-flight, identity coding was sex dependent, with a higher percentage of identity-coding cells representing males compared with females (Fig. 3H; χ^2 test: $P = 0.022$; notably, there was no significant difference if the sex of the identity-coded bat was the same or different from the recorded bat: χ^2 test: $P = 0.122$).

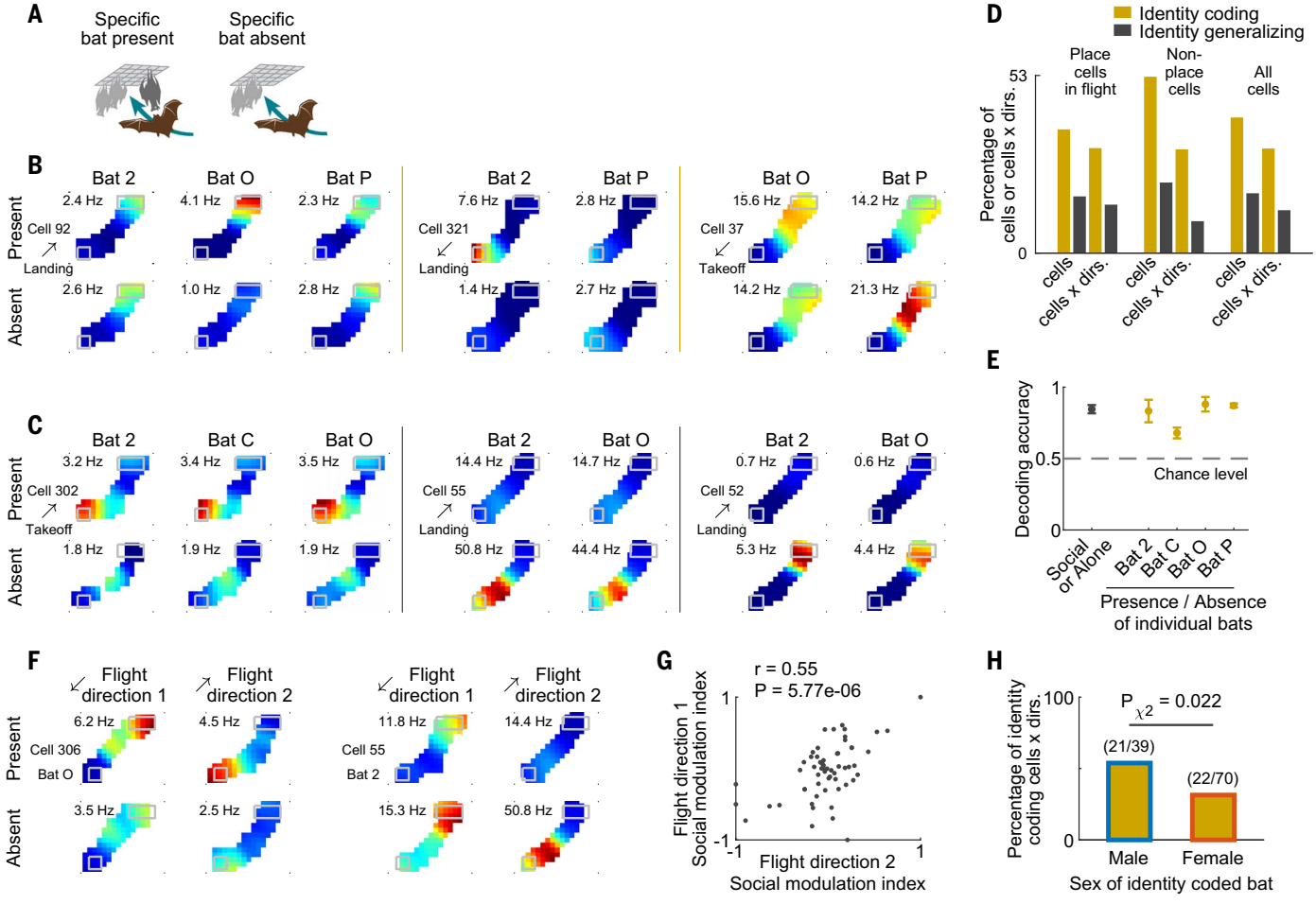

Fig. 3. Hippocampal neurons encode the individual identity of other bats. (**A**) Schematic illustration of flights when a particular conspecific bat is present (left) or absent (right). (**B**) Three example neurons that showed in-flight identity coding for specific bats. Shown are firing-rate maps computed for flights when a particular conspecific was present (top) or absent (bottom) for different conspecifics (columns). Left, neuron showing identity coding for bat O: Significant social modulation was seen when bat O was present compared with absent, but no social modulation is seen for the other two bats (bats 2 and P). Middle, neuron showing identity coding for bat 2: Significant social modulation is seen when bat 2 was present, but not for bat P. Right, neuron showing identity coding for bat P. (**C**) Three example neurons that generalized across bat identities [plotted as in (B)]. All three neurons showed significant social responses, with clear differences between when a bat was present or absent (significant differences between rows), but these responses were similar regardless of the identity of the bat (no differences between columns, i.e., no identity coding). (**D**) Percentage of identity-coding cells [yellow; cells as in (B)] and identity-generalizing cells [gray; cells as in (C)] showing that identity-coding cells were more abundant (identity coding: place cells, n = 24/65, place cells × directions, n = 26/83, nonplace cells, n = 10/19, nonplace cells × directions, n = 13/42, all cells, n = 34/84, all cells × directions, n = 39/125; identity-generalizing: place cells, n = 11/65, place cells × directions, n = 12/83, non-place cells, n = 4/19, nonplace cells × directions, n = 4/42, all cells, n = 15/84, all cells × directions, n = 16/125). Identity-coding and identity-generalizing cells could only be assessed when there were at least two other bats with enough trials for which comparisons could be made. Therefore, the numbers of identity-coding and identity-generalizing cells do not sum up to the total number of socially modulated neurons in-flight (Fig. 2E). (**E**) Decoding accuracy determined using a Bayesian maximum-likelihood decoder. We decoded whether a flight occurred in the social or alone conditions (black error bar; t test, P = 0.0068 compared with chance). We also decoded the presence or absence of specific individual bats during the flight (identity: yellow error bars; t-tests: P = 0.024, P = 0.018, P = 0.005, and P = 0.0001, for bats 2, C, O and P, respectively). Error bars indicate mean ± SEM (n = 4 conditions: the decoding was done separately for the 2 flight directions × 2 social responses to landing/takeoff). (**F**) Two example neurons showing social invariance to flight direction: a similar social modulation in both flight directions for the presence or absence of a specific individual bat. Shown are firing-rate maps computed for flights when bat O (left neuron) or bat 2 (right neuron) was present (top) or absent (bottom) for the two flight directions (columns). Left, a neuron showing social invariance to the presence of bat O on the small net, with higher firing when the recorded bat was flying toward the small net (flight direction 1) and also when it was flying away from the small net (flight direction 2). Right, a neuron showing social invariance to the absence of bat 2 on the large net (higher firing for the absence of bat 2 in both flight directions). (**G**) Population scatter of the social modulation index [contrast index of the peak FR of the maps when a specific individual bat was present versus absent $(FR_{present} - FR_{absent})/(FR_{present} + FR_{absent})$] for one flight direction versus the other flight direction. The social modulation index was significantly correlated between the two flight directions [Pearson r = 0.55, P = 5.77×10^{-6}; n = 59 cells × bats (including both identity-coding and identity-generalizing cells)]. We compared both directions for the same net being occupied by the individual other bat and included all neurons with enough data in both directions and in which at least one of the directions was significantly socially modulated. This positive correlation demonstrates invariant social modulation by individual bats, i.e., social invariance to flight direction, even though the spatial coding exhibited remapping between the two flight directions (F). (**H**) Left, percentage of identity-coding cells × directions representing male bats out of the potential number of male bats that could be assessed in the colony (males with enough data); right, similarly for female bats (χ^2 test for males versus females, P = 0.022; the χ^2 test considers the number of males and females that were encoded by the neurons out of the number that could be assessed).

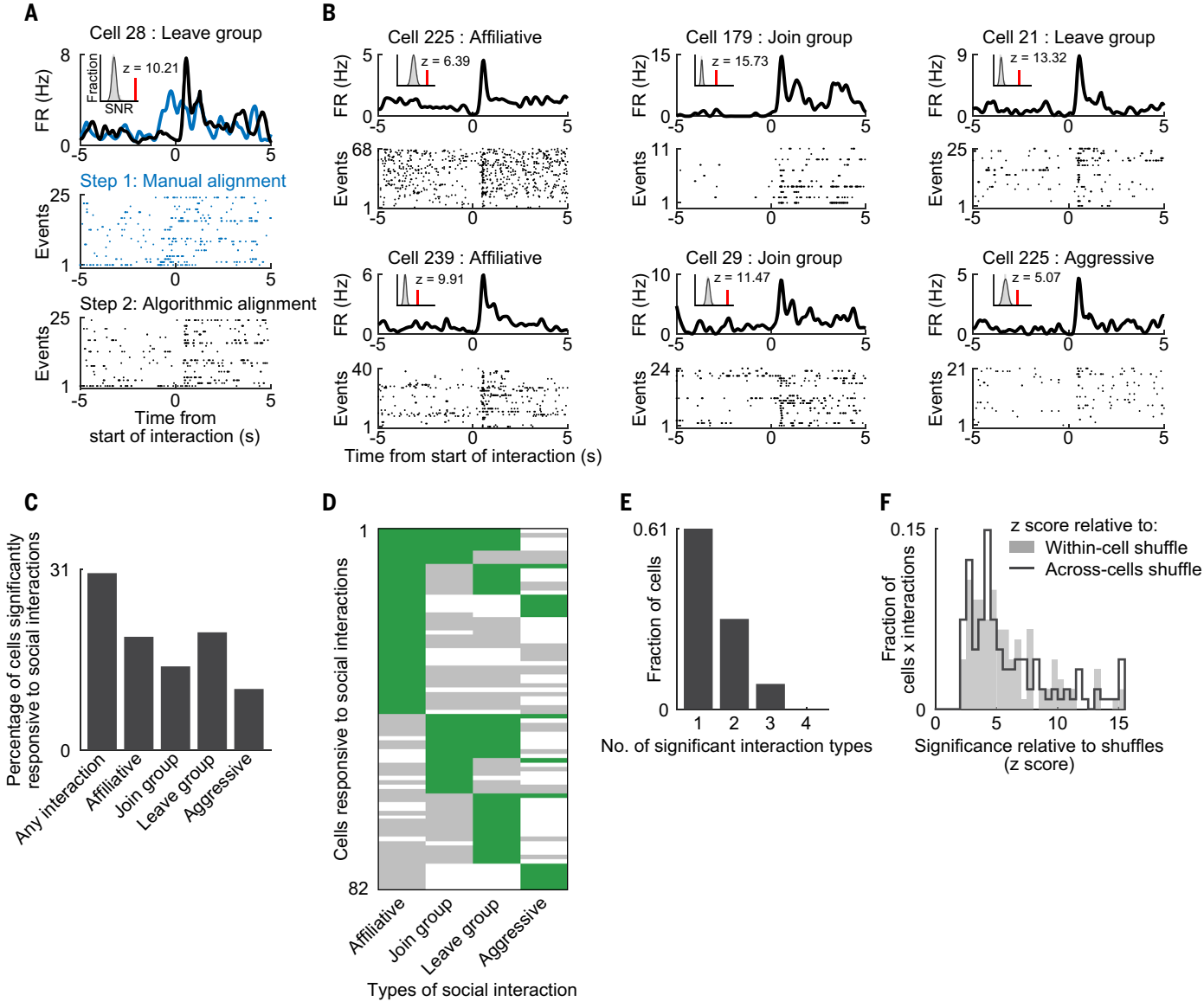

Fig. 4. Hippocampal cells respond to specific social interactions. (**A**) Example cell. Top, peristimulus time histograms (PSTHs) showing the average response (firing rate [FR] versus time) of a neuron to social-interaction events involving the recorded bat, for the social interaction type of leaving a group of bats. Bottom, spike rasters. Events (trials) are aligned to the start of interaction. Blue PSTH and blue raster: first step of interactions alignment based on manually annotated ethograms of the videos. Black PSTH and black raster: second step of interactions alignment, with interactions aligned to the model-estimated interaction time using the neural data itself (*21*, *31*). Inset in top panel shows the SNR for the actual PSTH (red line) and for the PSTHs of the within-cell shuffles (gray, histogram; black line, Gaussian fit; *z*-score of red line compared with Gaussian fit is indicated) (*21*). (**B**) Six additional example cells that were significantly modulated by different types of social interaction events: affiliative (friendly), joining a group, leaving a group, and aggressive interactions. Data are aligned as the black raster in (A); see movie 1 for examples of the different social interactions. (**C**) Percentage of cells significantly responsive to the various social interaction types, normalized separately for each interaction type by the number of cells valid for analysis. "Any interaction" indicates cells responsive to at least one interaction type. (**D**) Population summary of responses of hippocampal neurons (rows) to the various social interactions (columns). Green indicates a significant social response of a neuron to a particular interaction type; gray, no significant social response; white, could not assess the response due to a lack of the minimum number of interactions in that condition. (**E**) Selectivity to social interactions. Bar graph shows how many neurons responded significantly to only one, two, three, or all four social interaction types. Of the 82 neurons that responded significantly to social interactions, most (61%, 50/82 cells, left bar) only responded to a single type of social interaction. (**F**) Histogram of *z*-scores of the neuronal response (SNR) compared with shuffles for significantly responsive cells × interactions (n = 121 cells × interactions; gray bars, *z*-score compared with within-cell shuffles; black line, *z*-score compared with across-cells shuffles) (*21*). Medians of the black and gray histograms: z = 5.0 and z = 4.6, respectively.

Many hippocampal neurons respond to specific types of social interactions

We next examined the responses of dorsal CA1 neurons in the social-interactions behavioral state, i.e., when the recorded bat was involved in explicit social interactions. We categorized four commonly occurring interaction types: affiliative (friendly), joining a group, leaving a group, and aggressive interactions (see examples in movie 1). To align the start of the social-interaction event from an animal's perspective, which may be very different from the sequence of movements observable to us in the videos, we used two steps. In step 1, we determined the approximate start time of the

Movie 1. Social interactions in a colony of wild fruit bats. The movie shows examples of the social interactions that were most commonly observed in the colony of wild Egyptian fruit bats in our experimental setup. The bats most commonly engaged in affiliative interactions (allogrooming), joining a group, leaving a group, and aggressive interactions (boxing). These are the four types of interactions that were analyzed in Fig. 4. Shown are two example instances for each of these four types of social interactions: one example for bats before surgery and one example for implanted bats after surgery.

interaction event based on blinded manual annotation. In step 2, we used a method that estimates more precisely the time of firing-rate change in each social-interaction event from the neural activity itself (*21*, *31*) (Fig. 4A). Hippocampal cells showed significant responses to the four different types of social interactions (Fig. 4, A and B). These social-interaction responses could not be accounted for by velocity differences or by motor movements (fig. S8). In particular, only a minority of the cells responded to self-grooming compared with allogrooming (fig. S8B). Further, the social-interaction responses could not be explained as generalized responses to salient events because the cells did not respond to the nearby landing or takeoff of other bats, a highly salient type of event (fig. S8C).

Many hippocampal cells (30.4%) were significantly responsive to at least one type of social interaction (Fig. 4C, left bar; 82/270 cells; we analyzed here all the 270 cells with enough social-interaction events for analyzing social responses) (*21*). A cell's neural response to an interaction type was considered significant if the signal-to-noise ratio (SNR) of the response was large (≥2.5) and was greater than the 99th percentile of the SNR for two sets of shuffled data: within-cell shuffle and across-cells shuffle (*21*). Most cells were selective to particular social interactions, with 61% of the cells being selective to a single type of social interaction (fig. S9: examples; Fig. 4, D and E: population). The cells showed strong responses: Among the significant social-interaction cells, we found a mean z-scored response of $z = 5.9$ compared with within-cell shuffles and $z = 6.1$ compared with across-cells shuffles (Fig. 4F). These responses could not be explained by location-specific responses (place cells) because almost all of the cells (91.5%) were selective to only one or two types of social interactions (Fig. 4E) even though all four types of social interactions occurred at very similar locations (fig. S10A). For cells that responded to group joining, there was also a tendency to be significantly socially modulated in-flight during landing (χ^2 test: $P = 0.051$). This indicates that the same neurons had a tendency to encode the same social action, joining other bats, invariantly across behavioral states—regardless of whether the joining action was performed through flight or by moving on the net. Together, these results suggest that hippocampal neurons exhibit strong and selective responses to specific types of social interactions.

Encoding the position, direction, and identity of multiple conspecifics

Next, we investigated what hippocampal neurons represented while the bat was active on the net. We reasoned that a neuron could represent several sociospatial behavioral variables during this state: self-location or self-head direction, location of a specific other bat, or the direction and distance to a specific other bat (Fig. 5A). Because there were multiple conspecifics in the colony, this quickly became a highly multidimensional problem. To solve this computational challenge, we took a model-based approach in which we used the aforementioned behavioral variables to predict the responses of single neurons (Fig. 5B and fig. S11A). Specifically, we used a generalized additive model (GAM) (*32*, *33*) and trained two models independently for each cell, one representing allocentric variables [self-place, self-head direction, and the places of other bats (social place cells)] and another representing egocentric variables (directions and distances to other bats). The positions of the different bats were not correlated with each other and likewise the distances and directions to the different bats were not correlated with each other, allowing us to reliably assess each model separately (*21*). However the allocentric and egocentric variables were correlated with each other, precluding a reliable analysis of a mixed allocentric-egocentric model (*21*). We limited this analysis to include only data when at least three other bats were present on the net to allow comparing responses to different individual bats. Results did not change when we removed data around interactions and around sharp-wave ripples (fig. S11, B and C; the rate of ripples was very low, with median rate of 0.13 ripples/min, indicating that the bats were overall very active on the net). The models were fit with 10-fold cross-validation, and we further assessed whether the correlation between the neuronal activity in the data versus the model was significantly higher than the correlations computed for models fit to shuffled data [95th percentile of shuffles (rigid circular shuffling of spike trains)] (*21*). In cases in which both the allocentric and egocentric models provided significant fits, we performed an additional model-selection step using the deviance information criterion (DIC), a standard criterion for model selection (*31*), to determine which model (allocentric or egocentric) better explained the firing of the neuron (fig. S12A; the DIC analysis yielded very conclusive model selection) (*21*). After model selection, we proceeded to evaluate the individual contributions of each of the sociospatial behavioral variables in explaining the responses of the neuron. To this end, we fitted the model using all possible combinations of behavioral variables, and then used a game-theoretic approach of Shapley values (*34*, *35*) to evaluate the contribution of each behavioral variable (*21*). Shapley values could be reliably assessed because within each model, the behavioral variables were not strongly correlated (*21*).

We found that the responses of some cells were better explained by allocentric behavioral variables (Fig. 5, C to E) and some by egocentric behavioral variables (Fig. 5, F to H). Both sets of cells showed good correspondence between the data and the predictions of the model. High correlation of the cell's temporal firing-rate profile was found in the model versus the data [Fig. 5, C and F, top: compare green traces (model) with black traces (data); Spearman ρ = 0.54 and 0.58; these ρ-values are shown also as red lines in the inset (gray histograms are shuffles)]. Also, good correspondence was found between the firing-rate maps of the behavioral variables and the same maps predicted by the model (Fig. 5, C to H). Almost half of the hippocampal neurons were significantly explained by the model (44%, 172/394 cells). We additionally assessed an alternative egocentric model that also included the self-position and self-head direction variables and found that very few neurons were explained by this alternative model (fig. S11D, rightmost bar; 4% of the cells, 17/394). Thus, most egocentric cells tracked only other bats. Because of the small fraction of extra neurons that were captured by this alternative model, we used only the original egocentric and allocentric models (Fig. 5B).

Consistent with previous hippocampal studies reporting strong allocentric representations (*15*, *36*), we found here a larger fraction of allocentric cells than egocentric cells (Fig. 6A: 25% allocentric cells, 99/394; 19% egocentric cells, 73/394). These fractions were similar to previous reports on allocentric place cells and egocentric goal cells in bats navigating toward a goal (*37*). Many allocentric cells jointly encoded behavioral variables representing self and others (Fig. 6B, left matrix). Some of the cells encoded only a few behavioral variables, a sparse representation manifested by relatively

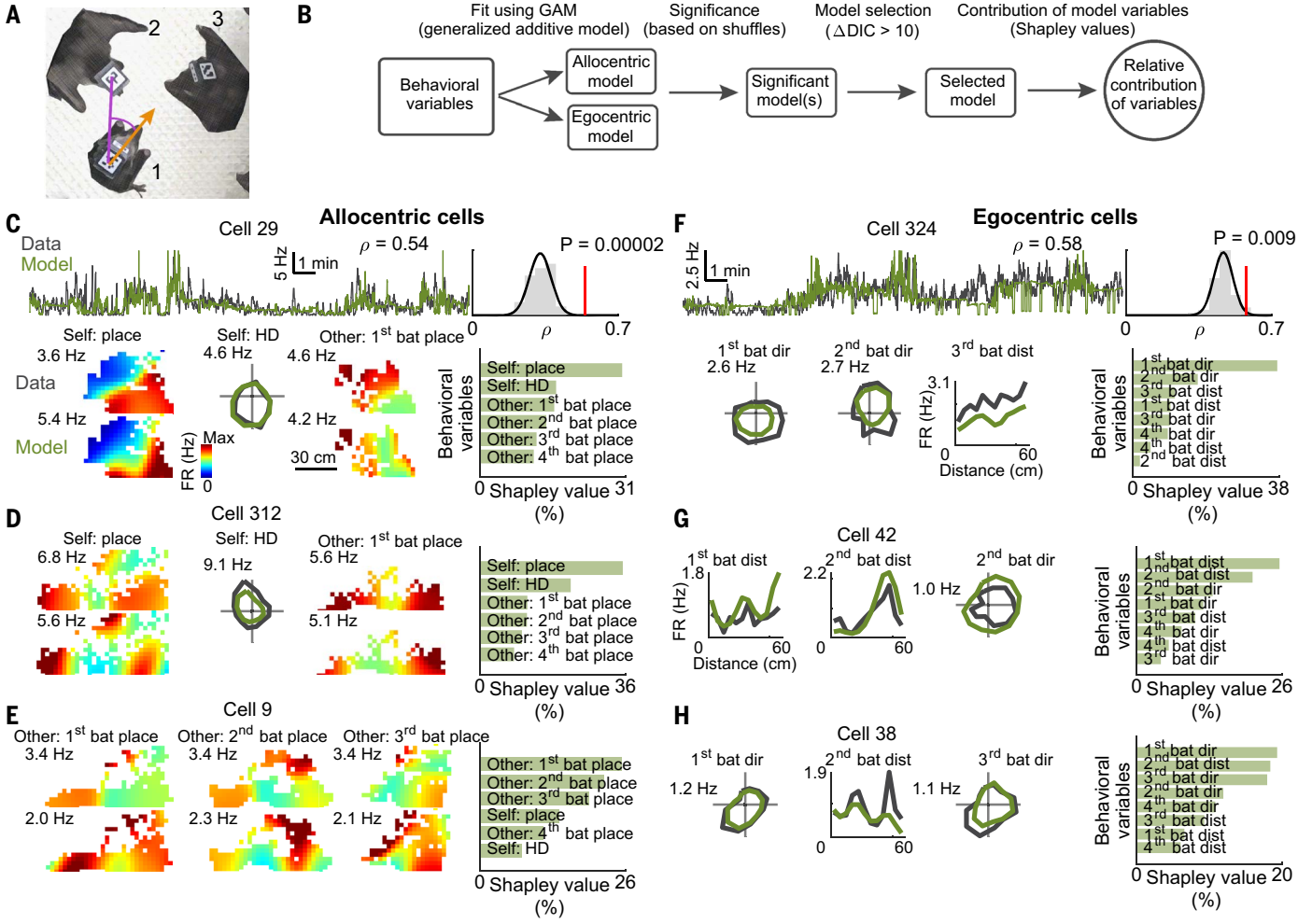

Fig. 5. Hippocampal neurons simultaneously represent position, direction, and distance for self and others. (**A**) Illustration of the behavioral variables for which neuronal coding was tested: self-position and self-head direction for the recorded bat (bat 1, orange), positions of other bats (bats 2 and 3), and directions and distances to other bats (e.g., to bat 2, purple). (**B**) Schematic illustration of the process for assessing whether a neuron represents allocentric or egocentric information and the contribution of the behavioral variables to the firing of the neuron (for an expanded schematic, see fig. S11A) (*21*). (**C**) Example allocentric cell. Top left traces, firing rate of the neuron over 20 min (black) and firing rate predicted by the GAM (green); note the high correlation of model to data (Spearman ρ = 0.54, computed over the entire session). Top right, correlation between data and model (red line) is significantly higher than correlations computed in a similar manner for models fitted to circularly shuffled spikes (gray, histogram for shuffles; black line, Gaussian fit) (*21*). Bottom right, relative contributions of the behavioral variables (Shapley values) to explaining the firing of this neuron. Three bottom left panels show tunings for the three most important variables (i.e., those with the highest Shapley values). Left, self-place firing-rate maps based on data (top) and based on model (bottom); note the similarity of the two maps. Middle, self head-direction tuning curves for data (black) and model (green); note their similarity. Right, tuning to the position of another bat based on data (top) and model (bottom). The tuning curves and maps derived from the model show the partial dependency plots (*21*); maps for both data and model are colored from zero (blue) to maximal firing rate (red; value indicated). (**D** and **E**) Two more examples of allocentric cells showing the maps of the top three most important variables (from left to right) and the Shapley values for all of the allocentric variables (rightmost bar graph). Note that in (E), the top three variables all encoded the positions of other bats in absolute allocentric space (*6*). (**F**) Example of an egocentric cell, plotted as in (C). The top three variables encoded by this neuron were the direction ("dir") to one bat, the direction to a second bat, and the distance ("dist") to a third bat. (**G** and **H**) Two more examples of egocentric cells showing the tunings for the top three most important variables (from left to right) and the Shapley values of all the egocentric variables (rightmost). See Fig. 6 for population analyses.

high Shapley values (high contribution) for only one or two variables and low Shapley values for all other variables [Fig. 6B, sparse-coding cells are plotted in the top rows of the two matrices and have high contribution (high Shapley value, yellow) of only one or two behavioral variables and low contribution of the other variables (blue)]. Other cells had more distributed representation, jointly encoding many behavioral variables [Fig. 6B, bottom rows of the two matrices; these neurons have more uniform contribution of all the variables (medium Shapley value, green or blue for all variables); see also Fig. 6C].

Not all behavioral variables were uniformly represented. Consistent with the known tuning of dorsal CA1 neurons to the animal's self place and self head direction (HD) (*15*, *36*, *38*, *39*), we found that a substantial fraction of the allocentric cells showed high contribution of these two self-variables [Fig. 6B, allocentric cells matrix; note the large Shapley values (yellow) in the "place" and "HD" columns; see also fig. S12B]. This self-tuning was most evident in the

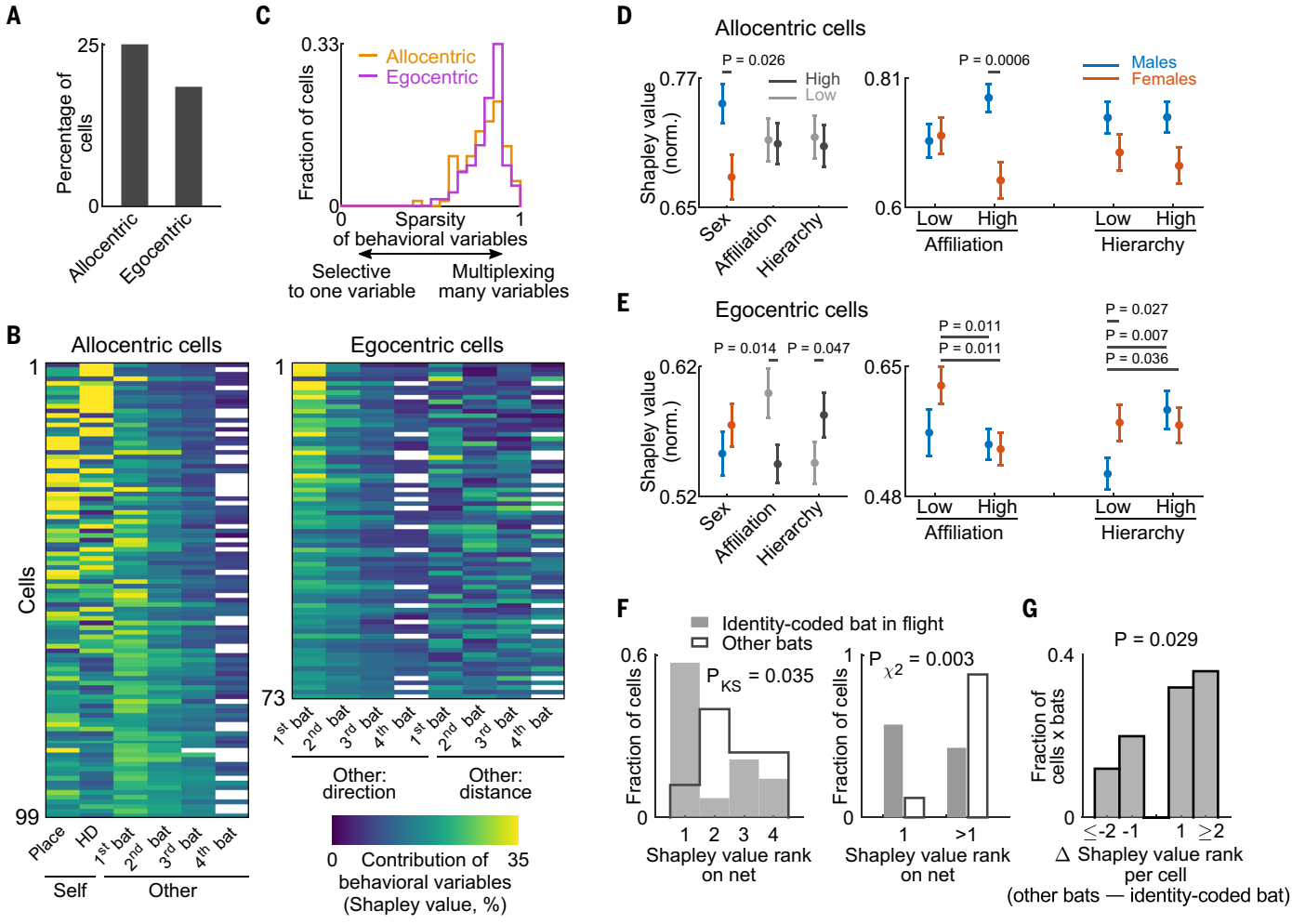

Fig. 6. Hippocampal neurons encode socially important features such as sex, social hierarchy, and social affiliation of other individuals. (**A**) A higher fraction of cells encoded allocentric information (25%, n = 99/394 cells) than egocentric information (19%, n = 73/394 cells); 394 is the number of valid cells that met criteria of sufficient amount of data, with multiple conspecifics being present together on the large net (*21*). (**B**) Population summary for the significant allocentric cells (left) and egocentric cells (right) showing for each of the neurons (rows) the relative contributions (Shapley values) for all of the behavioral variables (columns). Color-coded from blue (zero contribution) to yellow (high contribution; we clipped here the Shapley values at 35% for visualization only). The cells are arranged from top to bottom by the sparsity of the contribution of the behavioral variables, with cells encoding only a few variables plotted at the top and cells with distributed encoding of many variables plotted at the bottom. (**C**) Histograms showing sparsity of behavioral variables of allocentric cells (orange) and egocentric cells (purple). High sparsity indicates multiplexing of many variables, and low sparsity indicates selectivity to one variable (*21*). (**D**) Shapley values for the allocentric cells (normalized by the maximal value in each cell; error bars indicate mean ± SEM). Left, grouping the data by the other bat's sex, social affiliation, or relative social hierarchy (P value indicates main term of a three-way ANOVA). Right, separating the data three-way according to sex (red versus blue), affiliation, and hierarchy of the other bat (P value is after correction for multiple comparisons by Fisher's least-significant difference). "Low" or "high" hierarchy indicates whether the other bat was lower or higher in hierarchy than the recorded bat, respectively, and "low" or "high" affiliation is according to thresholding of the affiliation index (*21*). (**E**) Same as (D) but for egocentric cells. Allocentric cells showed a significant modulation by sex, whereas egocentric cells showed a significant modulation by affiliation and hierarchy (see also table S2). (**F**) Left, histograms of Shapley value rank on the net for the identity-coded bat in-flight (gray bars) and for the other bats that were not identity coded in-flight (white bars). The identity-coded bats in flight had a significantly different distribution of Shapley ranks on the net than the noncoded bats (white bar graph is right shifted compared with the gray; Kolmogorov-Smirnov test, P = 0.035; shown are n = 14 out of the 34 identity-coding cells in Fig. 3 that were also valid for analysis in this figure). Right, most identity-coded bats in-flight (gray bars) had Shapley rank 1 on the net, whereas the noncoded bats in-flight (white bars) had Shapley ranks >1 (χ^2 test: P = 0.003). (**G**) Distribution of the fraction of cells × bats that showed a particular difference in Shapley rank between the noncoded bats in-flight and the identity-coded bat in-flight. Note that many of the cells showed a prominent difference of ≥2 in the Shapley ranks (Wilcoxon signed-rank test, right-tailed, P = 0.029, n = 25 cells × bats).

sparse neurons (the high Shapley values were concentrated mostly in the "place" and "HD" columns at the top part of the matrix): These neurons are classical place cells. However, many cells were not pure place cells but exhibited strong identity coding for one or two other bats (Fig. 6B: Note the yellow color for other bats in the two matrices). Egocentric cells more prominently encoded the directions to other bats compared with the distances to them (Fig. 6B, right matrix: higher Shapley values in the direction columns compared with the distance columns; see also fig. S12C).

To validate that the social encoding specifically represented bats and was not related to

objects, rewards, or prominent locations, we controlled for four alternative locations: (i) the most prominent object (a camera suspended from the center of the ceiling, Fig. 1A); (ii) the nearest food bowl, which served as a primary reward location; (iii) the corner of the net closest to where the bats usually flew from, which is a prominent geometrical feature near the bats; and (iv) the median location of each of the bats in the session. We evaluated the GAM egocentric model by replacing each of the four other bats one at a time by each of these alternative locations (*21*) and found a significant reduction in the performance of the GAM model for all. The prediction of the model was significantly lower for all these four control cases [Wilcoxon signed-rank test for comparing the correlations of the model with the data (Spearman ρ) for the original data versus the correlations for each of the four control cases: $P = 1.71 \times 10^{-4}$, $P = 6.68 \times 10^{-5}$, $P = 6.21 \times 10^{-7}$, $P = 5.39 \times 10^{-5}$, respectively; $P = 3.22 \times 10^{-17}$ when pooling the four controls]. Also, the Shapley values for the four control cases were significantly lower than for the real bats (Wilcoxon rank-sum test: $P = 3.70 \times 10^{-4}$, $P = 8.80 \times 10^{-4}$, $P = 6.19 \times 10^{-6}$, $P = 2.11 \times 10^{-2}$, respectively; $P = 6.63 \times 10^{-12}$ when pooling the four controls; similarly, for the Shapley ranks, we found that the four control cases ranked worse than the data: Wilcoxon rank-sum test: $P = 5.38 \times 10^{-3}$, $P = 4.45 \times 10^{-4}$, $P = 1.38 \times 10^{-2}$, $P = 2.83 \times 10^{-2}$, respectively; $P = 4.31 \times 10^{-8}$ when pooling the four controls). This suggests that the real bats were represented more strongly than prominent objects or reward locations.

Representation of sex, dominance hierarchy, and social affiliation

Allocentric and egocentric cells showed substantial differences in how they represented socially relevant features of the conspecifics, including the sex of the other bat, its relative social hierarchy, and social affiliation, namely how affiliated or "friendly" the other bat was to the recorded bat (Fig. 6, D and E, and fig. S13) (*21*). These three social features, sex, hierarchy, and affiliation, were statistically independent of each other (*21*). We found that allocentric cells were significantly modulated by sex, with males being represented more strongly than females (Fig. 6D, left panel; three-way ANOVA: $P = 0.026$ for the sex term), which is akin to the stronger encoding of males during flights (Fig. 3H). Again, this could not be explained by whether the sex of the other bat was the same or different from the recorded bat (three-way ANOVA: $P = 0.84$). In particular, high-affiliation male conspecifics were represented more strongly than high-affiliation female conspecifics [Fig. 6D, right panel; $P = 0.0006$, corrected for multiple comparisons (Fisher's least-significant difference); see table S2 for full ANOVA results; similar results were obtained when using a mixed-effect linear model (table S2)]. By contrast, egocentric cells were significantly modulated by affiliation and by relative hierarchy, exhibiting stronger coding of low-affiliation bats (less-friendly animals) and of high-hierarchy bats (more-dominant animals) (Fig. 6E, left panel; three-way ANOVA: $P = 0.014$ for the affiliation term, $P = 0.047$ for the hierarchy term). However, the effect was more complex when taking sex into account. The feature that most strongly affected the neural responses to male conspecifics was hierarchy, whereas for female conspecifics it was affiliation. In particular, lower-hierarchy males were represented more weakly than higher-hierarchy males and also more weakly than both lower- and higher-hierarchy females (Fig. 6E, right panel; $P = 0.007$, $P = 0.027$, and $P = 0.036$, respectively, corrected for multiple comparisons; see table S2 for results of ANOVA and mixed-effect linear model). Lower-affiliation females were represented more strongly than both higher-affiliation females and higher-affiliation males (Fig. 6E, right panel; $P = 0.011$ and $P = 0.011$, respectively, corrected for multiple comparisons). Overall, bat hippocampal neurons represented important social features of conspecifics, such as their position, direction, and identity, and were modulated by their sex, social hierarchy, and social affiliation.

Identity coding by hippocampal neurons is context invariant

Next, we investigated whether identity coding by hippocampal neurons is independent of context, with the same bats being represented in different locations and across different behavioral states. To this end, we examined whether the cells that represented the identities of specific bats in-flight (Fig. 3B) also represented the same bats during active observation on-net (Fig. 6B). We found that for most cells, the identity-coded bat in-flight was also the most strongly coded bat on the net, namely the bat with the highest Shapley value among the conspecific bats (Fig. 6F). Conversely, all of the other bats, which were not identity coded in-flight, were also more weakly coded on the net by the cells (Fig. 6F, left panel: Kolmogorov-Smirnov test, $P = 0.035$; right panel: χ^2 test, comparing if the identity-coded bat in-flight had a Shapley rank 1 on-net or not versus the lower-ranked bats: $P = 0.003$). Further, the difference in ranks between the identity-coded and noncoded bats was substantial, often ≥2 (Fig. 6G). Together, these analyses indicate that a given hippocampal neuron encoded the identity of the same bat across different contexts, i.e., across different locations (midroom versus net) and across different behavioral states (flight versus active-on-net)—suggesting an invariant identity coding.

Finally, we investigated which brain regions receive these hippocampal signals encoding social identity, sex, hierarchy, affiliation, and interactions. We examined the anatomical projections from dorsal CA1 in the bat by injecting anterograde tracers into the dorsal CA1 of four additional bats (*21*). We found that the dorsal CA1 sends direct monosynaptic (albeit sparse) projections to multiple brain areas, including the medial prefrontal infralimbic cortex, anterior cingulate cortex, frontal cortex, orbitofrontal cortex, substantia nigra, nucleus accumbens, retrosplenial cortex, and claustrum (fig. S14)—regions that are involved in regulating social behaviors (*40*). We hypothesize that the rich social signals that are represented in the hippocampus during natural behaviors may shape social neural information throughout the brain.

Discussion

We found here that many hippocampal CA1 neurons represented the identity of conspecifics and encoded their social features, such as their sex, dominance hierarchy, and social affiliation, when animals were in a naturalistic social group and allowed to perform unconstrained, untrained, natural social behaviors. These representations were sociospatial in nature (*5*, *6*, *41*), binding together the well-known hippocampal spatial representations (*14*–*16*) with the more social conditions that group-living animals typically encounter in the natural world. We found that during flight, hippocampal spatial coding was strongly modulated by social context through rate remapping, both prospectively and retrospectively, and exhibited strong identity coding (Figs. 2 and 3). Social coding of individual bats exhibited invariance between the two flight directions (Fig. 3, F and G). During social-interaction events, many hippocampal neurons responded selectively to particular types of social interactions (Fig. 4). When the bats were active on the net, hippocampal neurons combined representations of self and other: Cells could encode others' locations in allocentric or egocentric space and could exhibit identity coding, representing one or two individuals or distributed encoding of many individuals (Fig. 6, B and C). The finding of identity coding by hippocampal neurons prompted us to investigate which social features of individuals were being represented, and we found that these neurons represented sex, social hierarchy, and social affiliation (Fig. 6, D and E), all highly important social features. Finally, we found invariance of social representations across behavioral contexts, both in-flight and on-net: Neural encoding of identities was invariant (Fig. 6, F and G) and males were represented more strongly than females (Figs. 3H and 6D) across these contexts. Thus, the hippocampus carries strong and rich social signals when studied in a social group.

Our findings of strong social representations in hippocampal dorsal CA1 are markedly

different from previous studies finding weak social responses in that area (*8*, *42*, *43*). This difference is possibly due to the naturalistic social setting in our study, in which the animals were free to decide what to do, when to do it, and with which other bats to engage socially. The previous experiments typically involved artificial social tasks imposed by the experimenters. This suggests that the hippocampus represents behavioral variables only if they are relevant. Consistent with this view, whereas here we found strong identity coding, this was not the case in a previous study (*44*), where we found that during high-speed collision avoidance between two bats, hippocampal CA1 neurons did not exhibit identity coding, most likely because when avoiding collisions, it is less relevant to encode who you are colliding with. Similarly, we found here that CA1 neurons encoded directions to other bats more strongly than distances to them (Fig. 6B, right, and fig. S12C), possibly because in a very small environment (i.e., the nets), directions are more relevant than distances. Thus, hippocampal neurons seem to represent only relevant social information.

The finding of social encoding during flight cannot be explained as a general gating by internal states such as surprise, arousal, fear, or reward, for the following reasons. Social responses occurred at all possible locations in-flight (Fig. 2F), which is incompatible with a general response to surprise, arousal, fear, or reward, all of which should be focused near the locations of social encounters at the nets. Also, some cells were socially modulated after takeoff from a net (Fig. 2D), i.e., when going away from a social agent, which is also incompatible with surprise, arousal, or reward. Some cells responded more strongly for an empty net (Fig. 2, A to D, "alone"), which is inconsistent with a social reward near other bats or fear response to other bats. Moreover, in simultaneously recorded neurons, one cell could respond more strongly to the social condition and another to the alone condition (e.g., Fig. 2B: cells 71 and 70, respectively), which is inconsistent with a general gating response by an internal state. The fraction of socially modulated cells (Fig. 2E) was >10-fold larger than the previously reported fraction of CA1 cells encoding nonsocial rewards (*45*), indicating that the social responses that we observed could not be explained by cells encoding nonsocial rewards. Many cells showed social identity coding, representing specific bats (Figs. 3, B and D, and 6F), a specificity that is inconsistent with a general gating response by internal states (*46*). Finally, many more cells responded to social interactions than to other salient nonsocial events such as landing and takeoff of other bats near the recorded bat (fig. S8C), indicating that surprise or arousal were unlikely to account for these responses. Together, these findings suggest that the social responses that we observed are not explained by a general response to internal states.

Our findings are distinct from previous reports of social place cells (*5*, *6*), because here we showed hippocampal identity coding in a multianimal group. Our results are also distinct from a previous report on population-level identity coding in mouse hippocampus (*47*), because the task was very artificial and the identity coding was largely driven by training. Further, a recent study (*13*) investigated hippocampal activity in groups of bats flying in a room and showed identity coding only in-flight. Consistent with our results, the latter study showed that reward cannot explain social coding in-flight. However, our naturalistic setup allowed us to also investigate social interactions and to study the representations of sex, dominance hierarchy, and social affiliation, none of which was investigated in previous hippocampal studies (*13*, *47*). In addition, we were able to reveal multiple invariances in social coding, and discover that in a naturalistic group setting, hippocampal neurons represent highly multidimensional social information.

We found that hippocampal neurons responded to social interaction events, and disambiguated between interaction types (Fig. 4). Further investigation would be required to determine whether hippocampal neurons respond to specific motor patterns that occur during social interactions or to the abstract notion of a social interaction. Cells that encode social interactions have been previously observed in the dorsomedial prefrontal cortex (*48*, *49*) and in the anterior cingulate cortex (*50*). However, to our knowledge, our finding is the first in the hippocampus, a brain area that is crucial for encoding memories for events, including events of social interactions (*51*, *52*).

We have shown here that hippocampal CA1 neurons encode several social features that are relevant in natural social settings, specifically, sex, social hierarchy, and social affiliation. These features were previously studied separately (*10*, *26*, *53*, *54*), but here we showed that they are all encoded simultaneously in the same neuronal population (Fig. 6, D and E). Thus, single hippocampal neurons can multiplex information that tracks the multidimensional social information in natural social settings [see also (*55*)]. Allocentric and egocentric cells represented these social features differently, with allocentric neurons encoding sex and egocentric neurons encoding affiliation and hierarchy (Fig. 6, D and E). This may suggest that the allocentric and egocentric cell populations receive different inputs. The social representations that we observed were typically conjoined with spatial representations (Figs. 2 to 6), perhaps indicating that the spatial cognitive map system also evolved to include the coding of social information into a single cognitive map–like framework: a sociospatial cognitive map (*6*, *36*, *54*).

Finally, we found that a large fraction of hippocampal cells were strongly modulated by social identity, both in-flight (Fig. 3) and on-net (Fig. 6). The identity coding was conserved across different locations and contexts: An identity-coding neuron typically represented the same bat both in-flight and on-net (Fig. 6F) and in both flight directions (Fig. 3, F and G). This identity coding was likely based on multisensory information (*56*), including visual, auditory, and olfactory cues, but additional studies would be required to assess the contribution of each sensory modality to the encoding of individual identity and to the coding of social features such as sex, social hierarchy, and social affiliation. The identity coding that we found here is reminiscent of previous reports on identity-coding neurons in the hippocampal formation of humans and monkeys that passively viewed images on a screen (*12*, *56*), but here these were uncovered during active social interactions. The fraction of socially responsive hippocampal neurons in our study was much higher than in the passively viewing humans or monkeys in previous studies. We speculate that our finding of a very high fraction of socially coding cells in the bat hippocampus may be a consequence of three factors: (i) our use of a mixed-sex group, (ii) our highly naturalistic setup and natural social interactions, and (iii) the fact that these were wild bats that have experienced the full natural repertoire of social interactions outdoors. We therefore suggest that future investigations should include brain studies in mixed-sex social groups, in which animals can perform natural social interactions—that are among the most important behaviors that animals have evolved.

Materials and methods summary

We conducted tetrode-based recordings of single neurons in the dorsal hippocampus area CA1 of wild Egyptian fruit bats (*R. aegyptiacus*) of both sexes. The bats lived continuously in a mixed-sex social colony of five to 10 individuals and behaved freely without any tasks. We tracked the positions and identities of all bats using a combination of a radiofrequency-based system and a video-based system, and we video-documented the bats' social interactions. We computed social and spatial responses of individual neurons when the bats were flying, engaged in social interactions, or were active on the landing nets. Further details can be found in the supplementary materials and methods (*21*).

REFERENCES AND NOTES

1. T. D. Seeley, *The Wisdom of the Hive: The Social Physiology of Honey Bee Colonies* (Harvard Univ. Press, 2009). doi: 10.2307/j.ctv1kz4h15
2. A. Strandburg-Peshkin, D. R. Farine, I. D. Couzin, M. C. Crofoot, Shared decision-making drives collective movement in wild

baboons. *Science* **348**, 1358–1361 (2015). doi: 10.1126/science.aaa5099; pmid: 26089514
3. T. Clutton-Brock, *Mammal Societies* (Wiley, 2016).
4. T. Okuyama, T. Kitamura, D. S. Roy, S. Itohara, S. Tonegawa, Ventral CA1 neurons store social memory. *Science* **353**, 1536–1541 (2016). doi: 10.1126/science.aaf7003; pmid: 27708103
5. T. Danjo, T. Toyoizumi, S. Fujisawa, Spatial representations of self and other in the hippocampus. *Science* **359**, 213–218 (2018). doi: 10.1126/science.aao3898; pmid: 29326273
6. D. B. Omer, S. R. Maimon, L. Las, N. Ulanovsky, Social place-cells in the bat hippocampus. *Science* **359**, 218–224 (2018). doi: 10.1126/science.aao3474; pmid: 29326274
7. R. P. Rao, M. von Heimendahl, V. Bahr, M. Brecht, Neuronal responses to conspecifics in the ventral CA1. *Cell Rep.* **27**, 3460–3472.e3 (2019). doi: 10.1016/j.celrep.2019.05.081; pmid: 31216468
8. M. von Heimendahl, R. P. Rao, M. Brecht, Weak and nondiscriminative responses to conspecifics in the rat hippocampus. *J. Neurosci.* **32**, 2129–2141 (2012). doi: 10.1523/JNEUROSCI.3812-11.2012; pmid: 22323725
9. T. Zhou *et al*., History of winning remodels thalamo-PFC circuit to reinforce social dominance. *Science* **357**, 162–168 (2017). doi: 10.1126/science.aak9726; pmid: 28706064
10. Y. Li *et al*., Neuronal representation of social information in the medial amygdala of awake behaving mice. *Cell* **171**, 1176–1190.e17 (2017). doi: 10.1016/j.cell.2017.10.015; pmid: 29107332
11. F. L. Hitti, S. A. Siegelbaum, The hippocampal CA2 region is essential for social memory. *Nature* **508**, 88–92 (2014). doi: 10.1038/nature13028; pmid: 24572357
12. R. Q. Quiroga, L. Reddy, G. Kreiman, C. Koch, I. Fried, Invariant visual representation by single neurons in the human brain. *Nature* **435**, 1102–1107 (2005). doi: 10.1038/nature03687; pmid: 15973409
13. A. Forli, M. M. Yartsev, Hippocampal representation during collective spatial behaviour in bats. *Nature* **621**, 796–803 (2023). doi: 10.1038/s41586-023-06478-7; pmid: 37648869
14. J. O'Keefe, J. Dostrovsky, The hippocampus as a spatial map. Preliminary evidence from unit activity in the freely-moving rat. *Brain Res.* **34**, 171–175 (1971). doi: 10.1016/0006-8993(71)90358-1; pmid: 5124915
15. M. A. Wilson, B. L. McNaughton, Dynamics of the hippocampal ensemble code for space. *Science* **261**, 1055–1058 (1993). doi: 10.1126/science.8351520; pmid: 8351520
16. N. Ulanovsky, C. F. Moss, Hippocampal cellular and network activity in freely moving echolocating bats. *Nat. Neurosci.* **10**, 224–233 (2007). doi: 10.1038/nn1829; pmid: 17220886
17. G. G. Kwiecinski, T. A. Griffiths, Rousettus egyptiacus. *Mamm. Species* **611**, 1–9 (1999). doi: 10.2307/3504411
18. G. Neuweiler, *The Biology of Bats* (Oxford Univ. Press, 2000).
19. M. C. Rose, B. Styr, T. A. Schmid, J. E. Elie, M. M. Yartsev, Cortical representation of group social communication in bats. *Science* **374**, eaba9584 (2021). doi: 10.1126/science.aba9584; pmid: 34672724
20. L. Las, N. Ulanovsky, Bats. *Nat. Methods* **21**, 1135–1137 (2024). doi: 10.1038/s41592-024-02330-6; pmid: 38997589
21. Materials and methods are available as supplementary materials.
22. J. D. Crall, N. Gravish, A. M. Mountcastle, S. A. Combes, BEEtag: A low-cost, image-based tracking system for the study of animal behavior and locomotion. *PLOS ONE* **10**, e0136487 (2015). doi: 10.1371/journal.pone.0136487; pmid: 26332211
23. R. A. Hinde, Interactions, relationships and social structure. *Man (Lond.)* **11**, 1–17 (1976). doi: 10.2307/2800384
24. S. Shultz, C. Opie, Q. D. Atkinson, Stepwise evolution of stable sociality in primates. *Nature* **479**, 219–222 (2011). doi: 10.1038/nature10601; pmid: 22071768
25. S. W. Li *et al*., Frontal neurons driving competitive behaviour and ecology of social groups. *Nature* **603**, 661–666 (2022). doi: 10.1038/s41586-021-04000-5; pmid: 35296863
26. F. Wang *et al*., Bidirectional control of social hierarchy by synaptic efficacy in medial prefrontal cortex. *Science* **334**, 693–697 (2011). doi: 10.1126/science.1209951; pmid: 21960531
27. B. L. McNaughton, C. A. Barnes, J. O'Keefe, The contributions of position, direction, and velocity to single unit activity in the hippocampus of freely-moving rats. *Exp. Brain Res.* **52**, 41–49 (1983). doi: 10.1007/BF00237147; pmid: 6628596
28. M. Geva-Sagiv, S. Romani, L. Las, N. Ulanovsky, Hippocampal global remapping for different sensory modalities in flying bats. *Nat. Neurosci.* **19**, 952–958 (2016). doi: 10.1038/nn.4310; pmid: 27239936
29. W. A. Liberti 3rd, T. A. Schmid, A. Forli, M. Snyder, M. M. Yartsev, A stable hippocampal code in freely flying bats. *Nature* **604**, 98–103 (2022). doi: 10.1038/s41586-022-04560-0; pmid: 35355012
30. T. Eliav *et al*., Multiscale representation of very large environments in the hippocampus of flying bats. *Science* **372**, eabg4020 (2021). doi: 10.1126/science.abg4020; pmid: 34045327
31. K. W. Latimer, J. L. Yates, M. L. Meister, A. C. Huk, J. W. Pillow, Single-trial spike trains in parietal cortex reveal discrete steps during decision-making. *Science* **349**, 184–187 (2015). doi: 10.1126/science.aaa4056; pmid: 26160947
32. K. Hardcastle, N. Maheswaranathan, S. Ganguli, L. M. Giocomo, A multiplexed, heterogeneous, and adaptive code for navigation in medial entorhinal cortex. *Neuron* **94**, 375–387.e7 (2017). doi: 10.1016/j.neuron.2017.03.025; pmid: 28392071
33. J.-P. Noel *et al*., Coding of latent variables in sensory, parietal, and frontal cortices during closed-loop virtual navigation. *eLife* **11**, e80280 (2022). doi: 10.7554/eLife.80280; pmid: 36282071
34. N. L. Goodwin, S. R. O. Nilsson, J. J. Choong, S. A. Golden, Toward the explainability, transparency, and universality of machine learning for behavioral classification in neuroscience. *Curr. Opin. Neurobiol.* **73**, 102544 (2022). doi: 10.1016/j.conb.2022.102544; pmid: 35487088
35. L. S. Shapley, "A value for n-person games" in *Contributions to the Theory of Games*, H. W. Kuhn, A. W. Tucker, Eds. (Princeton Univ. Press, 1953), vol. II, pp. 307–318.
36. J. O'Keefe, L. Nadel, *The Hippocampus as a Cognitive Map* (Oxford Univ. Press, 1978).
37. A. Sarel, A. Finkelstein, L. Las, N. Ulanovsky, Vectorial representation of spatial goals in the hippocampus of bats. *Science* **355**, 176–180 (2017). doi: 10.1126/science.aak9589; pmid: 28082589
38. L. Acharya, Z. M. Aghajan, C. Vuong, J. J. Moore, M. R. Mehta, Causal influence of visual cues on hippocampal directional selectivity. *Cell* **164**, 197–207 (2016). doi: 10.1016/j.cell.2015.12.015; pmid: 26709045
39. A. Rubin, M. M. Yartsev, N. Ulanovsky, Encoding of head direction by hippocampal place cells in bats. *J. Neurosci.* **34**, 1067–1080 (2014). doi: 10.1523/JNEUROSCI.5393-12.2014; pmid: 24431464
40. R. Adolphs, The social brain: Neural basis of social knowledge. *Annu. Rev. Psychol.* **60**, 693–716 (2009). doi: 10.1146/annurev.psych.60.110707.163514; pmid: 18771388
41. M. Murugan *et al*., Combined social and spatial coding in a descending projection from the prefrontal cortex. *Cell* **171**, 1663–1677.e16 (2017). doi: 10.1016/j.cell.2017.11.002; pmid: 29224779
42. X. Mou, D. Ji, Social observation enhances cross-environment activation of hippocampal place cell patterns. *eLife* **5**, e18022 (2016). doi: 10.7554/eLife.18022; pmid: 27692067
43. L. Zynyuk, J. Huxter, R. U. Muller, S. E. Fox, The presence of a second rat has only subtle effects on the location-specific firing of hippocampal place cells. *Hippocampus* **22**, 1405–1416 (2012). doi: 10.1002/hipo.20977; pmid: 21997883
44. A. Sarel *et al*., Natural switches in behaviour rapidly modulate hippocampal coding. *Nature* **609**, 119–127 (2022). doi: 10.1038/s41586-022-05112-2; pmid: 36002570
45. J. L. Gauthier, D. W. Tank, A dedicated population for reward coding in the hippocampus. *Neuron* **99**, 179–193.e7 (2018). doi: 10.1016/j.neuron.2018.06.008; pmid: 30008297
46. M. A. Moita, S. Rosis, Y. Zhou, J. E. LeDoux, H. T. Blair, Hippocampal place cells acquire location-specific responses to the conditioned stimulus during auditory fear conditioning. *Neuron* **37**, 485–497 (2003). doi: 10.1016/S0896-6273(03)00033-3; pmid: 12575955
47. E. Kong, K.-H. Lee, J. Do, P. Kim, D. Lee, Dynamic and stable hippocampal representations of social identity and reward expectation support associative social memory in male mice. *Nat. Commun.* **14**, 2597 (2023). doi: 10.1038/s41467-023-38338-3; pmid: 37147388
48. R. Báez-Mendoza, E. P. Mastrobattista, A. J. Wang, Z. M. Williams, Social agent identity cells in the prefrontal cortex of interacting groups of primates. *Science* **374**, eabb4149 (2021). doi: 10.1126/science.abb4149; pmid: 34672743
49. L. Kingsbury *et al*., Correlated neural activity and encoding of behavior across brains of socially interacting animals. *Cell* **178**, 429–446.e16 (2019). doi: 10.1016/j.cell.2019.05.022; pmid: 31230711
50. K. Haroush, Z. M. Williams, Neuronal prediction of opponent's behavior during cooperative social interchange in primates. *Cell* **160**, 1233–1245 (2015). doi: 10.1016/j.cell.2015.01.045; pmid: 25728667
51. N. Burgess, E. A. Maguire, J. O'Keefe, The human hippocampus and spatial and episodic memory. *Neuron* **35**, 625–641 (2002). doi: 10.1016/S0896-6273(02)00830-9; pmid: 12194864
52. W. B. Scoville, B. Milner, Loss of recent memory after bilateral hippocampal lesions. *J. Neurol. Neurosurg. Psychiatry* **20**, 11–21 (1957). doi: 10.1136/jnnp.20.1.11; pmid: 13406589
53. L. Kingsbury *et al*., Cortical representations of conspecific sex shape social behavior. *Neuron* **107**, 941–953.e7 (2020). doi: 10.1016/j.neuron.2020.06.020; pmid: 32663438
54. R. M. Tavares *et al*., A map for social navigation in the human brain. *Neuron* **87**, 231–243 (2015). doi: 10.1016/j.neuron.2015.06.011; pmid: 26139376
55. E. H. Nieh *et al*., Geometry of abstract learned knowledge in the hippocampus. *Nature* **595**, 80–84 (2021). doi: 10.1038/s41586-021-03652-7; pmid: 34135512
56. T. J. Tyree, M. Metke, C. T. Miller, Cross-modal representation of identity in the primate hippocampus. *Science* **382**, 417–423 (2023). doi: 10.1126/science.adf0460; pmid: 37883535
57. S. Ray *et al*., Data for: Hippocampal coding of identity, sex, hierarchy and affiliation in a social group of wild fruit bats, Zenodo (2025); https://doi.org/10.5281/zenodo.13938638.

ACKNOWLEDGMENTS

We thank T. Kimchi, N. Zilkha, A. Rubin, J. Aljadeff, I. Saraf-Sinik, G. Ginosar, T. Eliav, Y. Waserman, and I. Mashanova-Golikova for comments on the manuscript; S. R. Maimon, A. Sarel, N. Raish, and A. Zarani for assistance with the experiments; I. Beracha, A. Rosenberg, C. Cohen, A. Shalev, N. Simon, E. Gecht, and C. Sole for assistance in analysis; W. Gatome for anatomical tracer injections; A. Tuval for veterinary support; E. Solomon, C. Ra'anan, and R. Eilam for histology; B. Pasmantirer, G. Ankaoua, and L. Goffer for mechanical designs; and G. Brodsky and N. David for graphics. **Funding:** This work was supported by research grants to N.U. from the European Research Council (ERC-SyG oxytocINspace and ERC-CoG NATURAL_BAT_NAV); research grants to N.U. from the Dr. Lou Siminovitch Laboratory for Research in Neurobiology, the Drescher Center for Research on Mental and Emotional Health, Dorraine S. Schwartz, and Debra and Paul Sagues; research grants to N.U. and L.L. from the National Institutes of Health (NIH R01-NS121413), CRCNS NSF-BSF (BSF 2020806), and Israel Science Foundation (ISF 1920/18); the André Deloro Prize for Scientific Research and the Kimmel Award for Innovative Investigation to N.U; and postdoctoral fellowships to S.R. from the European Molecular Biology Organization (ALTF 853-2017) and Human Frontier Science Program (LT000365-2018L). N.U. is the incumbent of the Barbara and Morris Levinson Professorial Chair in Brain Research. **Author contributions:** S.R., L.L., and N.U. conceived and designed the experiments. S.R., L.L., and N.U. set up the experimental systems. S.R. conducted the experiments. S.R., I.Y., N.E., and S.P. analyzed the data with input from K.W.L. L.L. and N.U. guided the data analysis. S.R., L.L., B.J., and M.P.W. performed anatomical injections and analysis. S.R. and N.U. wrote the first draft of the manuscript with major input from L.L. All authors participated in writing and editing the manuscript. N.U. supervised the project. **Competing interests:** The authors declare no competing interests. **Data and materials availability:** All data and code supporting the conclusions of this study are freely accessible online at Zenodo (*57*).

SUPPLEMENTARY MATERIALS

science.org/doi/10.1126/science.adk9385
Materials and Methods
Figs. S1 to S14
Tables S1 and S2
References (*58*–*87*)
MDAR Reproducibility Checklist

Submitted 29 October 2023; accepted 11 November 2024
10.1126/science.adk9385

Science
AAAS

Supplementary Materials for

Hippocampal coding of identity, sex, hierarchy, and affiliation in a social group of wild fruit bats

Saikat Ray *et al*.

Corresponding authors: Liora Las, liora.las@weizmann.ac.il; Nachum Ulanovsky, nachum.ulanovsky@weizmann.ac.il

Science **387**, eadk9385 (2025)
DOI: 10.1126/science.adk9385

The PDF file includes:

Other Supplementary Material for this manuscript includes the following:

Materials and Methods

Subjects and behavioral setup

Subjects. Five adult Egyptian fruit bats (*Rousettus aegyptiacus*), 3 males and 2 females, were included in this study as subjects for electrophysiological recordings (weights 142–165 gr). Nine other adult bats (5 males and 4 females) were part of the social group and were involved in all the behavioral assays. Information on the individual bats is summarized in Table S1. All the male bats were vasectomized to prevent pregnancies (*59*), a procedure which is well-known not to change behavior or hormonal status (*60-62*). Four additional bats were used for anatomical tract-tracing (fig. S14, see below). All bats in this study were caught as adults in the wild (in Israel). All experimental procedures were approved by the Institutional Animal Care and Use Committee of the Weizmann Institute of Science.

Setup. Bats lived together continually (24/7) in mixed-sex groups (between 5–10 bats in each experiment), with approximately equal proportions of males/females in each group, in a medium-sized room (dimensions: 2.7 meters long × 2.3 meters wide × 2.6 meters high; Fig. 1A). The group composition was generally stable over long periods of time (weeks to months), and was changed only when replacing the recorded bats. Group 1 contained the bats – O, 1, 2, 3, C, T, U, X (U was the recorded bat); group 2 contained the bats – O, 2, 3, C, 7, P, T, A1, X (7 and A1 were the recorded bats); group 3 contained the bats – O, 2, 7, P, T (7 was the recorded bat); group 4 contained the bats – O, 2, P, A2, X (A2 was the recorded bat); and group 5 contained the bats – O, 2, S, 6, C, T (6 was the recorded bat, S was present for only the first few days). The bats could stay on two landing nets at two opposite corners of the room, and they were free to perform any behaviors they wanted – there was no particular task to which the bats were trained by the experimenters. The two nets were different in size – a large net (80 × 40 cm) and a small net (40 ×

40 cm) – to create asymmetric conditions for bat behaviors (see below). The bats lived in the room for several months until the conclusion of the experiments, and had food (fruit pieces) available to them *ad libitum* at two central food plates (Fig. 1A, 'food'; the old food was replaced daily by fresh food immediately before the start of the recording session). The room had a dim illumination of 1 lux during the dark phase – when bats are most active, and when the neural recordings were performed (Fig. 1B); this provided ample illumination for these highly-visual bats (*63, 64*). The light level was 220 lux during the light phase (when the bats were inactive, and we did not perform experiments). The experimenter was always outside of the room during the experiments: no humans were present inside the room during the recordings.

Animal localization systems: We used two synchronized tracking systems to localize the animals. We tracked the locations and identities of each of the bats in 3D using a radio-frequency-based system with a set of unique tags that were placed on the bats; this system was used for tracking the bats with 10-cm precision in-flight (see below, system no. 1). Further, we used a set of video-cameras to track barcodes that were placed on each of the bats; this system was used for tracking with mm-level precision the locations, head-directions, and identities of each of the bats when they were on the nets (see below, system no. 2).

Animal localization system no. 1 (radio-frequency based): We tracked the 3D position of all the bats using lightweight ultra-wideband radio-frequency localization tags (*30*) (BeSpoon), which were placed inside a small box on the heads of all the bats, and received and transmitted signals to an array of 9 antennas – eight of which were at the corners of the room and one at its center (Fig. 1A). For each antenna, a spherical estimation of the tag's distance from the antenna was computed based on the time-interval between the signal transmission and arrival. The position of the bat in 3D was then estimated using the intersection of these spheres from all the antennas. Our localization

yielded a good precision of ~10 cm along all the three axes of the room. Each bat had its own radio-frequency tag with a unique ID; the position of each bat was computed with a sample-rate of 25 Hz. All tags were synchronized to the neural recordings using a non-periodic sequence of TTL pulses (precision < 1 ms).

Animal localization system no. 2 (video based): In parallel to the radio-frequency based tracking system, we also used a video-based localization system – which provided tracking at higher spatial resolution (1-millimeter accuracy) but for restricted portions of the room (while the radio-frequency based system provided lower spatial resolution of 10-cm but for the entire room). We used synchronized recordings from 6 cameras (Fig. 1A), recording at 25 Hz each, to perform vision based localization (recordings conducted using Streampix, running on Nvidia Tesla P4 GPU). The cameras (IDS Imaging UI-3060CP) had a highly-sensitive sensor (Sony IMX174), which allowed videography at the relatively low light levels in the room (1 lux). Specifically, 3 cameras had a zoom-in lens, and were directed to the landing-nets (2 on the large net, 1 on the small net), and 3 zoom-out cameras documented flights in the room. We utilized the 3 zoom-in cameras directed to the nets for vision-based localization and tracking of bats on the nets, and for documenting social interactions. Localization was performed by tracking two-dimensional (2D) barcodes on the bats (*22*) (fig. S1A, Fig. 5A), with millimeter resolution. Tracking the 2D barcodes gave both the location and head-direction of the bat, as the barcodes were directional and were always aligned to the nose of the bat. For tracking the recorded bat, 5 simultaneous 2D barcodes were used on the head of the bat (1 on the top and 4 on the 4 sides of the box) to measure the location and head-direction regardless of how the head of the bat was oriented in 3D with respect to the camera. For tracking the conspecific bats, we used one 2D barcode (on the top of the box – to track the location and head-direction) and two 1D barcodes (placed on the front and back of the box): this combination allowed tracking the location of

these bats at all times, regardless of head-orientation in 3D. The 1D barcodes (fig. S1B, Fig. 5A) were based on Hamming codes, to minimize false detection errors. All 6 cameras were synchronous among themselves and were synchronized to the neural recordings using a sequence of TTL pulses (precision < 1 ms).

Social network analysis

For each experimental session, we used the behavioral data recorded while the bats were on the net, in order to assess the stability of the social network of the bats (Fig. 1C-D). This was done in three ways – via three measures of social affiliation: (i) using an affiliation index that was based on the median distances between all pairs of bats during each experimental session, while they were on the nets; (ii) using the rate of all the social interactions involving the recorded bat and its conspecifics in each session, and (iii) using the rate of only the affiliative social interactions (friendly interactions) involving the recorded bat and its conspecifics in each session (see below regarding analysis of interactions). To determine the average social network for each group of bats (i.e. for each recorded-bat), separately for each of the three measures of affiliation, we computed the mean affiliation index over all the days involving the particular recorded bat (e.g., in Fig. 1C this was computed for bat '6', for the distance-based affiliation index). We assessed the stability of the social network, separately for each of the three methods (Fig. 1D), using the closeness network centrality (*65*) – a standard metric for quantifying the structure of graphs (networks). Here, the nodes of the graph are individual bats, and the distances between the nodes in the networks were taken as either the pairwise physical distances between bats (Fig. 1D, left; see also Fig. 1C), or the number of all types of pairwise interactions per hour with the recorded bat (Fig. 1D, middle), or the number of affiliative interactions per hour with the recorded bat (Fig. 1D, right). Closeness network centrality is defined as: $c(i) = (A_i/(N-1))^2(1/W_i)$, where $c(i)$

is the network-centrality of node i, A_i is the number of nodes reachable from node i (a reachable node is a node that can be accessed from node i by travelling along the edges of the graph), N is the number of nodes in the graph, and W_i is the sum of the distances from node i to all reachable nodes in the graph. The network centrality gives a number for each node of the graph, indicating its closeness to the other nodes; this procedure resulted in a vector of network-centralities for each day, with a length equal to the number of nodes (number of bats). We then calculated the Pearson correlation of each day's vector of network-centralities to the median vector of network-centralities, where the median was computed over all the days that involved the particular recorded bat (we note that the group-composition was nearly constant across days for each recorded bat). To determine the chance level, we used the matrix of bat-identities × days (5–10 bats × 99 days: these are the days in which we recorded the bats' behavior; in 92 of these 99 days we also recorded hippocampal CA1 neurons: see below). The entries in the matrix were the centralities of the inter-bat distances or of the rate of interactions. We randomly permuted the bat-identities separately for each day within the matrix. We then determined the correlation again as described above; this was repeated 1,000 times to produce the shuffle distributions (Fig. 1D, gray).

Dominance hierarchy

Bats have a natural instinct to perch at higher locations, because of the need to escape predators (*18, 66*). We exploited this instinct of bats, combined with observations from other flying animals relating their social hierarchy to perching at higher locations (*67*), in order to construct a test to determine the social hierarchy (dominance hierarchy) within our bat colony (fig. S2A). The test apparatus consisted of a narrow vertical box (30 cm wide × 30 cm deep × 100 cm high), in which a pair of bats was placed at the bottom. The narrow box did not allow bats to fly up – and therefore, in

order to reach the top, the bats had to crawl up a ladder. The test started with two bats being placed on the floor of the box, and then a flap was removed, allowing them to access the ladder. The ladder was narrow, and the bats could not climb side-by-side, but instead they had to actively compete and overtake each other – creating a 'race to the top'. Since the task was instinctive, the bats required no training, and performed it from the first trial. In each hierarchy-testing session, we performed this pairwise test between all possible pairs of bats. The hierarchy-testing was performed once a week throughout the period of the neural recordings, over ~1 year. To determine the hierarchy, we used the results of these pairwise tests to calculate the Elo rating for each bat – a standard index of social dominance hierarchy (*68*). The Elo rating of all bats starts at 1,000 by default before the first testing, and then increases over the testing-weeks for the winning bats, and decreases over testing-weeks for the losing bats. To assess the reliability of the Elo ratings – which depend on the order in which the testing sessions are performed – we re-evaluated the Elo ratings on randomly shuffled order of sessions (*2, 69*): we found that the Elo ratings were quite reliable across the shuffles, with low variability (fig. S2B). We further found that our bat colony had a stable social hierarchy over months (Fig. 1E, fig. S2C). To control for movement speed during hierarchy-testing, we quantified the time required for completing the task, and found no significant difference in the mean winning time (40 ± 11 s for the top-ranked bat, and 47 ± 9 s for the bottom-ranked bat, mean ± SEM; *t*-test: $P = 0.51$; Wilcoxon rank-sum test: $P = 0.45$) – confirming that the test indeed assessed social hierarchy and not simply which bat was faster.

We next evaluated the transitivity of the dominance hierarchy (*26*). Transitivity means that if bat A is more dominant than bat B, and bat B is more dominant than bat C, then bat A is also more dominant than bat C. To quantify transitivity, we followed the approach of ref. (*26*), and picked all triads of bats that could be compared to each other (i.e. groups of 3 bats that directly competed

against each other in the dominance hierarchy test). For each triad, we re-evaluated their Elo rating based on pairwise comparisons, and found that most triads were transitive (84%, n = 113/134 triads; the 16% non-transitive triads were cases where two of the bats had close Elo ratings).

We also determined the linearity of the dominance hierarchy, by calculating the linearity index h (*70, 71*), defined as

$$h = \frac{12}{n^3 - n}\sum_{i=1}^{n}\left(v_i - \frac{n-1}{2}\right)^2$$

where n is the total number of individuals, and v_i is the number of individuals dominated by individual i (v_i was determined based on the pairwise dominance hierarchy test described above, namely, based on the Elo ratings; ties between individuals were counted as ½). We obtained h = 0.80. The linearity index h ranges from 0 to 1, with 0 indicating perfect equality between individuals, and 1 indicating a perfect linear relationship. To determine significance of the linearity index (*71*), we randomized the results of the dominance hierarchy between individuals, and re-evaluated the linearity index h. We performed 10^6 such randomizations (10^6 shuffles). All the shuffles had a lower linearity index than in the data ($P < 10^{-6}$).

Behavior segmentation and analysis

Flight analysis (Figs. 2, 3). Individual flights of the bats were extracted from the positional data that we recorded using the radio-frequency-based localization system: the flights were identified based on movement speed. To improve the accuracy in estimating the flight speed, we smoothed the bat's position using a smoothing-spline (*csaps* in Matlab), and used its derivative to extract the instantaneous flight-speed. We then identified individual flights by finding a peak in the speed profile of > 1.25 m/s. The beginning and end of each flight were then defined as the

segment between the two troughs in the speed profile on both sides of this peak (after removing 300 ms from both ends). For behavioral analysis (Fig. 1F-G), all the flights of the recorded bats were used. For the neural analysis (Figs. 2, 3) we used only direct flights of the recorded bat between the two nets – discarding indirect flights or flights to other locations in the room, as follows: (i) Direct flights were defined as flights with a straightness index > 0.5, where the straightness index is the ratio of the direct-line distance between the two nets divided by the actual path-length of the flight (*72*). (ii) Valid flights between the two nets were selected by requiring that both the start and the end of the flight were on one of the nets (this was done by defining 3D 'boxes' around the nets, and discarding flights that did not start or did not end within the area of one of the nets [allowing an extra margin of ±10-cm in each direction; this 10-cm margin was required to accommodate the 10-cm positional accuracy of the bats' 3D tracking]). Flights in which the bat performed a U-turn were bisected: the flight-segment before the U-turn was included only in the take-off analysis, and the flight-segment after the U-turn was included only in the landing analysis.

Social interaction analysis (Fig. 4). The video recordings from the zoom-in cameras, which were directed to the landing-nets, were also used to annotate social interactions on the nets. We annotated only those social interactions that involved the recorded bat. The interactions were manually annotated by human observers, who were blind to the hypotheses and blind to the neural responses. The observers watched the video recordings, and annotated them using a custom-written ethogram program, in which they annotated: (1) which bat interacted with whom, (2) the type of interaction, and (3) the time of the interaction onset. Social interactions were then classified into four categories – affiliative (mostly allo-grooming), joining a group, leaving a group, and aggressive interactions – and were used for further analysis of social interactions (Fig. 4; for the

group-joining and group-leaving interactions we included only those cases where joining or leaving the group happened via crawling and not via flight). Another kind of social interaction (landing on another bat; Fig. 2J) was analyzed separately, as it involved flight behavioral state.

Surgery and neural recording techniques

All surgical procedures were done as described previously (*6, 28, 30, 37, 44*). Briefly, bats were implanted with a 16-tetrode microdrive (weight 3.6 gr; modified from (*73*)), loaded with tetrodes, with each tetrode constructed from four strands of insulated wire (17.8 μm diameter platinum-iridium wire). Tetrodes were gold-plated to reduce wire impedance to 300 kΩ (at 1 kHz). The microdrive was implanted above the dorsal hippocampus (3.0 mm lateral to the midline and 5.8 mm anterior to the transverse sinus that runs between the posterior part of the cortex and the cerebellum), in the right hemisphere (4 bats) or left hemisphere (1 bat); the craniotomy was then covered with an inert silicone elastomer (Kwik-Sil or Kwik-Cast). During the implantation surgery, we used an injectable anesthesia cocktail composed of Medetomidine 0.08 mg/kg, Midazolam 2.5 mg/kg, Fentanyl 0.025 mg/kg, and Ketamine 17 mg/kg – and added supplemental injections as needed, based on the bat's breathing and heart-rate. The microdrive was attached to the skull with bone screws, using a layer of adhesive (Super-Bond C&B) followed by dental acrylic (Lang). We attached the ground wire from the microdrive to a bone-screw that touched the dura in the skull's frontal plate.

Following surgery, the tetrodes were slowly lowered towards the dorsal hippocampal CA1 pyramidal cell layer; positioning of tetrodes in the layer was provisionally done based on the presence of high-frequency field oscillations ("ripples") and associated neuronal firing, and was later verified histologically (e.g., Fig. 1H). For each bat, one tetrode was left in an electrically quiet zone and served as a reference, and the remaining tetrodes served as recording probes.

During recordings, a wireless neural-recording device ('neural-logger'; 64-channels, Deuteron Technologies) was attached to a connector on the microdrive. Signals from all channels were amplified (×200), bandpass filtered (1 – 7,000 Hz), and then sampled continuously at 32 kHz per channel and stored on board the neural-logger. During subsequent processing, the neural recording was further high-pass filtered with a 600-Hz cutoff for spikes – creating a spike bandwidth of 600 – 7,000 Hz – and then a voltage threshold was used for extracting 1-ms spike waveforms.

Histology

Histology was done as described previously (*30, 44*). At the end of recordings, the bats were anesthetized, and electrolytic lesions (DC positive current of 30 μA for 15-s duration) were made in a subset of the tetrodes, to facilitate the reconstruction of tetrode positions. The bat was then given an overdose of sodium pentobarbital and, with tetrodes left *in situ*, was perfused transcardially using 4.5% histofix. The brain was removed and post-fixed. Thin coronal sections were then cut at 40-μm intervals on a freezing microtome. The sections were Nissl-stained with cresyl violet and were photographed to determine the locations of tetrode tracks in dorsal CA1 (e.g., Fig. 1H). All the recording sites were located in dorsal CA1 – thus, all the neurons reported in this study are from dorsal CA1.

Anterograde tracing from CA1. For assessing the projections from dorsal CA1 of the bat to various brain regions involved in social behaviors (fig. S14), we injected anterograde tracers to dorsal CA1 of a separate group of 4 bats, in the same coordinates as the electrophysiological recordings. Five injections were done under anesthesia, using methods as described in detail in (*74*). We injected either Dextran Alexa Fluor 555 10kDa (DA 555) or Dextran Alexa Fluor 647 10kDa (DA 647, Thermo Fisher Scientific). We used a positive, pulsed direct current to inject the tracers (7 s on / 7 s

off, 6 μA for 17–30 min). Ten days post-surgery the bats were euthanized with an overdose of sodium pentobarbital, and were then perfused transcardially with 0.9% phosphate buffer saline followed by fixative (4% paraformaldehyde + 0.1 M phosphate buffer saline). The brains were removed and post-fixed overnight, and subsequently were stored in 30% sucrose at 4°C for at least three days before cutting. Sections of the brains were then cut on a freezing microtome at 40 μm thickness, in the coronal or horizontal plane, and were mounted on microscope slides. The sections were stained with cresyl violet for visualizing cytoarchitecture, and were then scanned using a Zeiss Mirax Midi Scanner or a Zeiss Axio Scan Z.1 scanner (Carl Zeiss GmbH, Germany) using a 20×, 0.8NA objective and either reflected fluorescent light or transmitted white light – to visualize the fluorescent signals.

Spike sorting

Spike-sorting procedures were similar to those described previously (*6, 28, 30, 37, 44*). Briefly, spike waveforms were sorted manually using Plexon Offline Sorter, on the basis of their relative amplitudes on different channels of each tetrode. Well-isolated clusters of spikes were manually selected, and a refractory period (< 2 ms) in the inter-spike-interval histogram was verified. Spike-sorting was done in consecutive time-windows, to allow for drift-correction of the spike clusters.

In total we recorded 489 well-isolated CA1 neurons from 5 bats over 92 sessions (days). Nearly all of these neurons (n = 458) were recorded during sessions involving a single recorded bat, while the remaining cells (n = 31 cells in 3 sessions) were recorded from two bats simultaneously. However, this small number of dual-bat recordings did not permit systematic analysis across the pair of bats. Of the 489 recorded neurons, we further analyzed 444 neurons that passed at least one of the following three inclusion criteria: (i) For flight analysis (Figs. 2, 3): the bat performed ≥5 flights

in a particular direction in the alone condition and ≥5 flights in the same direction in the social condition (see below, section on 'Social modulation and identity-coding in flight', for definitions of 'alone' and 'social' conditions); we also required ≥10 spikes in at least one of these two conditions; or (ii) For social interactions analysis (Fig. 4): the bat had ≥5 interactions in at least one of the four social-interaction types; or (iii) for the analysis during activity on-net (Figs. 5, 6): there were ≥10 minutes and ≥100 spikes when the recorded bat was together on the large net with ≥3 other conspecific bats (see Table S1).

Sharp-wave ripple detection

To detect sharp-wave ripple (SWR) events while the bat was on the net (figs. S3B, S11B-C), we detected SWRs as follows. The LFP signal was filtered in the ripple band, between 100–200 Hz, and the instantaneous power of the signal was computed using the Hilbert transform. SWR events were defined by using the following criteria. First, we extracted events in which the power of the bandpass-filtered LFP (100–200 Hz) exceeded a threshold of 7 standard deviations above the mean. Second, we used a 'ripple/high-gamma ratio' – the ratio between the peak power of the LFP signal between 100–200 Hz (ripple range), and the peak power of the LFP between 60–100 Hz (high gamma range) – and required a ratio of >2 in order to discern clear spectral peaks in the ripple range. And finally, we required the velocity of the bat to be low (< 2 cm/s) during these SWR events. Only SWR events which met all these three criteria were considered. To control for spikes that occur during SWRs, we removed ± 0.5 s around the ripple peak: see fig. S11B-C. We note that the median ripple-rate in our data was 0.13 ripples/min, and the mean ripple-rate was 0.25 ripples/min (fig. S3B) – both of which are much lower than the typical ripple-rates observed during sleep (e.g., 47.4 ripples/min in rats (*75*)).

Allocentric firing-rate maps in flight and place cell classification in flight

Firing-rate maps. All the analyses and statistical tests of neuronal data during flight were performed in this study on the basis of 2D firing-rate maps with fixed bins – using top-view 2D projections. Since the spatial tuning of place-cells in bats and rodents was shown to remap between flight directions (*27, 28, 30*), we performed all flight-related analyses in this study separately for the two flight-directions (flights from large-net to small-net, and vice versa) – in particular, we computed all the firing-rate maps separately for the two flight directions. Firing-rate maps for 2D allocentric position (place tuning; Figs. 2, 3) were computed by counting the number of spikes and the time spent in each spatial bin (0.15 × 0.15 m bins) – with time-spent (occupancy) data and spike counts collapsed onto two dimensions (top view: horizontal plane of the room). Bins of the 2D map which had time-spent < 0.15 s were discarded from the analysis. Then, the spike-count maps and time-spent maps were smoothed (Gaussian kernel with σ = 2 bins = 0.3 m), and we then divided, bin by bin, the smoothed 2D spike-count map by the smoothed 2D time-spent map, to produce the firing-rate map. We computed the spatial information (SI) in bits per spike for each map, as follows (*76*): SI = $\sum p_i(r_i/r)log_2(r_i/r)$, where r_i is the firing rate of the cell in the i^{th} spatial bin, p_i is the probability of the bat being in the i^{th} bin (time spent in the i^{th} bin / total session time), and $r = \sum p_i r_i$ is the overall mean firing rate. For display purpose only (in Fig. 2A,C - bottom row), we similarly computed also the 2D map for a side view: in the vertical plane along the diagonal line connecting the centers of the two nets.

Place cell classification. Place cells were classified using data from direct flights between the nets, separately for each flight-direction, based on the following criteria: (1) There were ≥5 flights in that direction, (2) the cell emitted ≥10 spikes during these flights, and (3) the cell had significant spatial information in its 2D firing-rate map (top-view) as compared to shuffles. To shuffle the spike-

train, we rigidly and circularly shifted in time the spikes of each flight, using a random shift drawn from a uniform distribution; the value of the shift differed randomly between individual flights, so each shuffle consisted of a unique set of temporal shifts that differed randomly across flights. We performed 1,000 such shuffles for each neuron for each direction. To be defined as a significant place-cell, we required the spatial information to be > 95% of the shuffles for that neuron in at least one of the two flight directions (shuffling was done separately for each neuron and each direction); by contrast, a non-place cell is not spatially modulated in any of the flight directions. The spatial tuning of cells × directions was assessed independently for each flight direction.

Social modulation and identity-coding in flight

Social responses and their effect size. Social responses in flight were assessed by analyzing all the direct flights, separately for each direction. Flights of the recorded bat were analyzed based on social context, either at the landing net (Fig. 2A-B) – comparing social versus alone conditions at landing, or at the takeoff net (Fig. 2C-D) – comparing social versus alone conditions at takeoff. We used Bonferroni correction to correct for the two cases of takeoff and landing. In each of these conditions, flights were termed as 'alone' – when no other bats were present, or as 'social' – when any of the other bats was present on the net. Social responses were only assessed on the spatially-overlapping firing-rate maps, namely, using only the spatial regions that were overlapping between the social and alone conditions (fig. S4A-C). Social coding was then assessed only for cells that met the following three inclusion criteria: (1) There were ≥5 flights in the social condition and ≥5 flights in the alone condition, (2) the cell emitted ≥10 spikes in at least one of these two conditions, and (3) there were no significant differences in velocity of flights in the social versus alone conditions (we analyzed 20/22 days × directions with no difference in velocity, see below in the section: 'Controls for flight-velocity, flight-

acceleration, flight-curvature, flight-trajectory, flight overlap in 3D, and number of flights'). For these valid neurons, significant social coding was assessed by comparing their real responses to shuffles, as follows: the root-mean-squared difference (RMSD) between firing-rate maps for social and alone flights was compared to maps for shuffles. The shuffles consisted of random redistribution of the social and alone flights and their corresponding spikes for a cell into two new sets of flights (bootstrapping with repeats). Importantly, we kept the number of flights in each shuffled-social set and shuffled-alone set the same as it was in the original social and alone sets of flights, respectively. The RMSD was determined for the firing-rate maps of the two shuffled sets. We performed 1,000 such shuffles. To be defined as a significant social cell, we required the RMSD between the social and alone condition in the actual data to be >95% of the shuffles. Social effect size, termed *social modulation depth* (Fig. 2H), was defined for each cell as the following ratio: RMSD between the social and alone conditions divided by the standard deviation of the RMSD of the 1,000 shuffles for that cell. An alternative normalized index of effect size, termed the *social modulation effect* (norm.), was also evaluated to confirm the results (fig. S7A): This was defined as the RMSD between the social and alone conditions divided by the median of the RMSD of the 1,000 shuffles for that cell.

In Fig. 2J, where we compared social response when landing near a bat versus on top of a bat, the social condition was separated into two situations: a 'nearby' case, based on flights when the recorded bat landed near other bats but not on top of them; and an 'on top' case, based on flights when the recorded bat landed on top of other bats.

Locations of social responses. For the significant social cells, which met the above criteria, we determined the location of the social response (Fig. 2F-G, fig. S5E-H) based on the peak of the response in the firing-rate map. Since the firing-rate enhancement could be either in the social map or in the alone map, we tested for both options, as follows: (1) The location of the bin with the maximal

firing-rate was determined for the social firing-rate map, and then we computed the absolute difference in firing-rate between the social and alone maps at that location. (2) The same was done for the alone map: the location of the bin with the maximal firing-rate was determined for the alone firing-rate map, and then we computed the absolute difference in firing-rate between the two maps at that second location. Then we took the larger of these two differences (found in steps 1 and 2), and its location was defined as the location of the social response. The social response location was then refined by fitting a Gaussian to the firing-rate map around the selected peak-bin (the peak of the place-field; we used a Gaussian with $\sigma = 2$ bins = 30 cm). This further step of Gaussian fit to the place-field was used because it reduces the noise in estimating the location of the peak of the place-field, since it fits an entire place-field rather than being determined by the location of a single bin. For plotting a one-dimensional histogram of the locations of social responses (Fig. 2G, fig. S5E-H), the two-dimensional location which was determined above was projected onto the diagonal line connecting the centers of the large net and small net.

Pearson correlation (r) was computed between the social map and the alone map (fig. S7B-C); a high correlation indicates that the map structure did not change, namely there was no global remapping – and hence the social modulation in-flight was mainly due to rate remapping (*77*).

Identity-coding cells and identity-generalizing cells. Identity coding in flight was tested for cells that exhibited a social response, as defined above, but now comparing their activity when another *particular* bat was either present or absent at the landing net (or take-off net). We included in this analysis only days where ≥ 2 other bats had enough flights per bat (5 flights for presence and 5 flights for absence) – in order to determine if cells had identity responses to one of those ≥ 2 bats. In determining the identity-response, a Bonferroni correction was applied to account for the number of individual bats compared. A cell was defined as identity-coding (Fig.

3B) if: (1) there was a significant change in firing-rate for one specific bat, but not for other bats; or (2) there was a significant increase in firing-rate for one bat and significance decrease for another bat. A cell was defined as identity-generalizing (Fig. 3C) if there were significant social responses (i.e. significant increase/decrease for social versus alone conditions) that were coherent across all bats.

Overall, neurons were defined as significant social cells (Fig. 2E-I) if: (i) they exhibited significant firing-rate differences between the social and alone condition, as explained above in the subsection on 'Social responses and their effect size'; or (ii) they were significantly identity-coding or significantly identity-generalizing.

In Fig. 3G, we computed a social modulation index for a particular bat, for each flight direction separately – and then compared the social modulation for the same bat between the two flight directions. For each flight direction, the social modulation index was defined as a contrast index between the peak firing-rate of the social map and the alone map for that bat: $(\text{FiringRate}_{\text{social}} - \text{FiringRate}_{\text{alone}}) / (\text{FiringRate}_{\text{social}} + \text{FiringRate}_{\text{alone}})$. A scatter of these indices for one flight-direction versus the other flight-direction was then plotted for the identity-coding cells and identity-generalizing cells (Fig. 3G).

Controls for flight-velocity, flight-acceleration, flight-curvature, flight-trajectory, flight overlap in 3D, and number of flights

Controls for velocity and acceleration. We found that flight velocity could not account for the social modulation observed in flight. First, the mean flight velocities (averaged per-day) for the alone condition and social condition had similar distributions across days, with no significant differences (fig. S5C; Kolmogorov-Smirnov test, $P = 0.275$; Wilcoxon rank-sum test, $P = 0.102$). Second, the

flight-velocity was stable within-day between the social and alone conditions: in 20/22 days × directions there was no significant difference in velocity ($P > 0.05$, Wilcoxon rank-sum test) – and social responses were only computed for those 20 days × directions in which there were no significant differences (fig. S5D, left bar: mean velocity [per flight]). For all the social cells, we also evaluated the instantaneous velocity and instantaneous acceleration of each flight at the location of the social response (namely, at the place-field with largest social modulation; see above subsection 'Locations of social responses' for details) — and we found that in almost all of the social cells there was no significant difference in velocity or acceleration between the social flights and the alone flights (fig. S5D, second and third bars: 90% of the cells did not show significant difference in velocity [at peak of place field], $n = 74/82$ cells × directions; and 95% of the cells did not show significant difference in acceleration [at peak of place field], $n = 78/82$ cells × directions; $P > 0.05$, Wilcoxon rank-sum test for each cell × direction).

Controls for 3D flight overlap, flight curvature, and variability of flight trajectories. The trajectories of flights in the alone condition and social condition each day were binned in spatial voxels of 0.1 × 0.1 × 0.1 m. Voxels with time spent < 0.15 s were discarded from the analysis. The 3D overlap between the alone and social conditions were assessed by determining the Dice coefficient (*78*), as follows:

$$Dice\ Coefficient = 2 \times nVoxels_{overlap} / (nVoxels_{alone} + nVoxels_{social})$$

where $nVoxels_{overlap}$ is the number of overlapping voxels in the alone and social condition and $nVoxels_{alone}$ and $nVoxels_{social}$ are the number of voxels separately in the alone and social conditions. The median Dice coefficient was 0.85, indicating a high degree of 3D spatial overlap between the flights in the alone and social conditions (fig. S5B).

To control for the flight curvature, we computed the straightness index for social and alone flights for all the social cells. We found that for the large majority of social cells, there was no significant difference in the straightness index between the social flights and alone flights (85% of the cells, $n = 70/82$ cells × directions, did not show significant difference; $P > 0.05$, Wilcoxon rank-sum test for each cell × direction; see fig. S5D, rightmost bar).

To control for variability in flight trajectories, for each social neuron we compared the alone flights versus the social flights that had the most similar trajectories to the alone flights in that session; and also compared the alone flights versus the social flights that had the most different trajectories from the alone flights in that session. The similar trajectories were defined as half of the flights among the social flights that had the smallest deviation from the median trajectory of the alone flights at the point where the trajectories diverged the most. Conversely, the different trajectories were the other half of the social flights, which had the largest deviation from the median trajectory of the alone flights at the point the trajectories diverged the most. In other words, 'similar' social flights versus 'different' social flights reflected median bisection of all the social flights, according to their deviation from the median trajectory of the alone flights. We found that the percentage of significant social cells was very comparable in both cases (fig. S6C: compare left panel versus right panel).

We next performed an additional analysis, for each neuron separately, to further test if the variability in flight trajectories could underlie the social modulation. Specifically, we tested if the maximal trajectory variability exhibited by the flights in a particular session (the median of the maximal divergence of all pairs of flights relative to each other) was related to the degree of social modulation exhibited by neurons that were recorded in that session. We found no correlation between the two – neither for the social flights, not for the alone flights, nor for all the flights (fig.

S6E-F). This suggests that that social modulation observed in flight could not be explained by variability in flight trajectories.

Controls for the number of flights. To ensure that the difference in the number of flights between the two conditions did not account for social modulation in-flight, we subsampled the flights from the condition (social or alone) with the higher number of flights, to match the condition with the lower number of flights. The subsampled flights were selected based on minimal deviation from the median trajectory of the other condition – namely, we not only subsampled the number of flights, but also selected the most similar flights. We found that the percentage of significant social cells remained similar, or perhaps slightly increased, when we subsampled (matched) the number of flights between the two conditions (fig. S6B).

Decoding of flight condition (social/alone) and decoding of presence/absence of specific bats (identity)

We used a Bayesian maximum-likelihood decoder (*79, 80*) to decode if a flight happened in the social or alone condition, and also (in a separate analysis) to decode the presence/absence of specific bats (decoding identity) (Fig. 3E). We used for decoding all neurons that had ≥ 5 flights in both social and alone conditions; to increase the number of neurons for the decoder, we performed the decoding using all neurons, even if they were not recorded simultaneously (pseudo-population; the number of neurons is denoted below as N; we could use here a pseudo-population because we decoded here presence/absence). We decoded independently the two flight directions and decoded separately whether social modulation was based on takeoff or landing. Decoding was performed with a leave-one-out cross-validation, where we built a test population-vector by randomly selecting one flight per neuron (i.e. N flights for the N neurons), while the other flights were used to train the decoder. The

training flights were used to determine the neural 'social tuning' for each neuron (the 'social tuning' was defined here as a pair of firing-rates: the mean firing-rate in social flights and the mean firing-rate in alone flights); we thus constructed a training population-vector. We then decoded (predicted) the condition of the test population-vector (namely, we predicted the social versus alone condition) as the one that maximized its log-likelihood:

$$A(condition|\boldsymbol{n}) = \sum_{i=1}^{N} n_i \ln(FR_i) - \sum_{i=1}^{N} FR_i$$

where n_i is the spike count in the test-flight in neuron *i*, with *N* being the total number of neurons, and FR_i is the social tuning of neuron i (there are two firing rates, FR_i (*social*) and FR_i (*alone*), and the one that yields the higher log-likelihood it taken as the predicted condition). When testing for the presence or absence of individual bats (decoding of bat-identity), we applied the same procedure of leave-one-out decoding, and the same criteria for number of minimal flights. Decoding was performed only for bats for which ≥ 10 neurons were available with enough flights for each neuron in both social and alone conditions, when decoding social versus alone conditions; or ≥ 10 neurons in both presence and absence conditions for a particular bat, when decoding bat-identity (these inclusion criteria allowed decoding the identities of 4 other bats in Fig. 3E). We repeated 1,000 times the decoding procedure (by randomly selecting sets of *N* flights to decode), and defined the decoding accuracy as the percentage of correct predictions (predictions of social/alone or presence/absence of a particular bat) out of all these 1,000 repeats.

Responses to social interactions

To examine responses to social interactions (Fig. 4), we computed for each cell the peri-stimulus time histogram (PSTH), separately for each of the four different types of social interactions that

involved the recorded bat – affiliative (friendly) interactions, joining a group, leaving a group, and aggressive interactions (see movie 1). Affiliative interactions consisted only of allogrooming events, while aggressive interactions mainly comprised boxing events, with some events of aggressive displays (wing-opening). All types of social interactions were mutually exclusive, and thus each interaction-event contributed to only one category of social interactions. There were not enough interaction-events to analyze selectivity to interaction-type × bat-identity – so here we focused on analyzing response selectivity to interaction-type. The individual events for the PSTH were initially aligned to the onset of the social interactions as marked in the ethograms for the recorded bat, as described above; each interaction was used only once in the PSTH, regardless of the length of the interaction; we extracted event-trials of duration ±5 s around the onset of the interaction-event. The PSTHs to social interactions were then computed separately for each of the 4 interaction-types, based on the following inclusion criteria: (1) We included in the PSTH only events which were temporally well-separated from other events with a gap of ≥ 5 s – in order to avoid influences of one social interaction-event on another; (2) there were ≥ 5 events for determining the PSTH for a particular interaction type; (3) there were ≥ 20 spikes for the PSTH of that interaction type; (4) over 25% of the events had spikes; (5) we excluded from analysis time epochs of flights that occurred too close to an interaction-event (±5 seconds from interaction-onset).

Alignment of social-interaction responses. Since the start of a social-interaction event from an animal's perspective may be temporally different than what is observable for humans in the videos – we used a two-step procedure. The first step was to manually align the interaction-onset by human observers, as explained above. The second step refined the temporal alignment, by using a method that allows finding the time of change in the firing-rate in each event, based on the neural activity itself (as detailed in ref. (*31*)). This method models each event as a Poisson process, and

finds if there was a step up, step down, or no change in the firing-rate during the event. The model has several parameters that are estimated from the data: the mean and standard deviation of the step time (relative to the human-labeled event), the probability of a step occurring during each event, the pre-step firing rate (the baseline rate), and the post-step firing rate. The step probability, pre-step firing rate and post-step firing rate are estimated assuming they are the same for all the events of the cell (i.e. for all trials of a given interaction-type); the step times are latent variables and are estimated separately for each event (each trial), and the model inference takes into account the uncertainty in estimating steps on individual trials. We used the mean of the step times estimated for each interaction-event as the model-alignment point for that event. Specifically, the model uses a Markov chain Monte Carlo (MCMC) method to sample from the posterior distribution of the model parameters and latent variables given the observed spike trains. For each event, the model discarded the first 2,000 MCMC iterations (the 'burn in' period), and then used the next 10,000 iterations to determine the posterior distributions of the model parameters: this was done to ensure that the Markov chain converged to its asymptotic distribution – the true posterior. The mean of this distribution was used as a point estimate of the model parameters – including the probability of the step – which then allowed us to infer the step time (*31*). We used the instantaneous firing-rate in each event (from 5 seconds before the onset of the interaction to 5 seconds after it, as described above), smoothed by a 1 second rectangular window, to estimate the step change in each event (this 1-second window was used only for finding the step, not for computing PSTHs). We only used events (trials) that had ≥3 spikes in them for this procedure – and left the remaining ones as-is. We then aligned the events based on the step time determined by the model, and then computed the PSTH on the aligned spike trains. To this end, the aligned spike trains of individual events were

smoothed (Gaussian kernel with $\sigma = 100$ ms) and averaged, to obtain the PSTH. Figure 4A shows an example of a raster and PSTH before (blue) and after this algorithmic alignment (black).

Significance of social-interaction responses. To assess if the social response of the neuron for a particular interaction-type was significant, we required the response to pass *all* the three following criteria: (1) The signal-to-noise ratio of the response was ≥ 2.5, where the signal-to-noise ratio was defined as the peak firing-rate of the PSTH between –1 sec to +3 sec, after alignment, normalized by the mean firing-rate of the PSTH. (2) Within-cell shuffle: The signal-to-noise ratio of the social-interaction response was >99th percentile of the signal-to-noise ratios of the shuffles. We randomly shuffled each of the spikes in each event – thus preserving the spike counts – and then performed the above MCMC-based event-alignment procedure to generate a shuffled PSTH, which underwent the same alignment pipeline as the real data. We repeated this shuffling process 1,000 times. To evaluate the significance at the 99th percentile level, we did the following: we fitted a Gaussian to the distribution of signal-to-noise ratios for the 1,000 shuffles (see examples in Fig. 4A-B, insets), and determined the *z*-score of the data signal-to-noise ratio compared to this Gaussian. We considered a cell to have a significant response if its *z*-score was larger than the *z*-score corresponding to the 99th percentile of the Gaussian distribution. We did not use circular rigid shifting of spikes for these shuffles, because the MCMC step-alignment algorithm finds the step time in the given event interval – which would un-shift the rigid shifts of the shuffles; therefore, such rigid shifting is not possible as a shuffling method in this step-alignment algorithm. Instead, we randomly shifted each spike individually (Poisson shuffling). (3) Across-cells shuffle: Here again, we required the signal-to-noise ratio of the social response to be > 99th percentile of the signal-to-noise ratios of the shuffles. For this across-cells shuffle, we pooled together the algorithm-aligned spike trains for all cells and all trials (i.e. the algorithm-based alignment was identical for the data

and shuffles) – pooling all the individual interaction-events (trials) for all the interaction-types across all the cells – generating one large "population pool" of events (events × interaction-types × cells). Importantly, this shuffle thus preserves the firing pattern of hippocampal cells. Then, for each social-response raster of each cell, we randomly picked from the "population pool" the same number of trials as in the original raster, to generate a shuffle PSTH. We repeated this shuffling process 1,000 times. The significance was determined by fitting a Gaussian to the distribution of signal-to-noise ratios from the shuffles, and determining how much larger the data signal-to-noise ratio was compared to the Gaussian fit, by evaluating its *z*-score. Results did not change qualitatively when using other thresholds for signal-to-noise ratio and for significance percentiles for the two shuffles (for example, see fig. S10B-C for 95% and 99.5% percentile thresholds).

In summary: to be defined as a significant social response for a particular social interaction type, we required the PSTH and raster of that neuron to pass *all* the above 3 criteria – namely: (1) to have a large signal-to-noise ratio (≥ 2.5), (2) to pass the within-cell shuffle at the 99^{th} percentile level, and (3) to pass the across-cells shuffle at the 99^{th} percentile level.

Social and spatial responses while active on the net

We analyzed the social-spatial responses on the net using a modeling-based approach, which involved a series of steps (Fig. 5B, fig. S11A) that are detailed below.

Generalized additive model. To determine neural responses when the bat was active on the net (Figs. 5, 6), we employed a generalized additive model (GAM), using the python library pyGAM. GAM is related to generalized linear models (GLM), but it is generally more powerful than GLM – because it allows modeling neural tuning functions with *any* smooth shape (*33, 81, 82*). This was achieved by modelling the tuning functions with B-splines. This approach has been applied in multiple

studies for investigating neuronal multiplexing of several kinematic variables (*32, 33, 83*) – but here we used this approach for the first time in a social context, with socio-spatial variables. Importantly, GAM combines the power of non-parametric models with the interpretability of linear models – and it enables assessing the contribution of each behavioral variable to the model (see below). We used the GAM with a Poisson distribution and a log link function to predict the firing of a neuron at a 40 ms temporal resolution (25 Hz – the video rate), based on the behavioral variables – including identities, positions, directions, and distances of all the bats. The B-splines for the GAM had 10 knots for each of the 1D variables (directions and distances). For the 2D variables (positions), the B-spline had 10 knots along the longer axis and 5 knots along the shorter axis of space (we used here a 2:1 ratio because the net was 80 × 40 cm in size, namely had a 2:1 aspect ratio). The angular variables (directions) also had a circular continuity constraint between 0° and 360°. We conducted the GAM analysis on cells which met the following two inclusion criteria: (i) The recording-session had ≥10 minutes of behavioral data of the recorded bat being present on the large net while 3 or 4 other bats were also present on the same net (one cell was analyzed with only 2 other bats). This requirement was needed in order to allow comparing responses to different individual bats. If more than four other bats were present in the session, we analyzed the data of the four other bats which spent the most time together with the recorded bat. (ii) The cell emitted ≥100 spikes during this epoch. Cells that passed these two criteria were then fit using two independent models: (1) allocentric model – based on the position and head-direction of the recorded bat and the positions of all the other bats, and (2) egocentric model – based on the directions and distances to the other bats with respect to the recorded bat (Fig. 5A-B). The direction to other bats was defined as the angle between the self head-direction, and the line connecting the position of the recorded bat to the other bat (Fig. 5A, angle between the orange line and purple line). Both types of models were evaluated with 10-fold cross-validation, where the data were divided into 5-

sec segments – to prevent leakage between the train data and test data. The final model was taken as the average over the 10 models determined from each of the 10-fold cross-validations.

Model significance and model selection. As an index of model-quality, we computed for each model (allocentric and egocentric) the Spearman correlation ρ between the firing-rate of the actual data across the entire session, versus the fitted firing-rate of the model across the entire session (e.g. in Fig. 5C [top], the correlation of the black trace [data] versus the green trace [model]: $\rho = 0.54$). To determine if the model predicted the data significantly better than chance, we shuffled the data by rigidly and circularly shifting the spike train with respect to the behavioral data, by a random time-shift (uniform distribution), and then fitted the allocentric and egocentric models to these shuffles. To ensure independence of each shuffle, we used a temporal shift of at least 5 seconds compared to all other shuffles (100 shuffles for each cell). Each shuffle was then fitted with the exact same pipeline as the data (with 10-fold cross-validation, as described above). We then assessed if the Spearman correlation ρ for the actual data was > 95% of the Spearman correlations for the shuffled data (e.g., see top-right panel in Fig. 5C: ρ of data [red line] is larger than all the shuffles [gray histogram]). More specifically, to determine the *P*-value, we fitted a Gaussian to the distribution of Spearman correlations of the shuffles (e.g., see the black curve in the top-right panel of Fig. 5C – which is fitted to the gray histogram of shuffles) – and then we used the *z*-score of the actual data relative to this Gaussian to determine at what percentile was the ρ of the data compared to the shuffles. If both the allocentric and egocentric models could predict the data better than chance – better than 95% of the shuffles – then we used the deviance information criterion (DIC), a standard method for model-selection (*31*), in order to determine which model explained the data better. DIC is defined as:

$$DIC = 2 \times \log \mathrm{p}(y \mid \bar{\theta}) - 4 \times \mathbb{E} \log \mathrm{p}(y \mid \theta)$$

where $\mathrm{p}(y \mid \bar{\theta})$ is the likelihood function over the parameter posterior means, given the data; and $\mathbb{E} \log \mathrm{p}(y \mid \theta)$ is the expected value of the log-likelihood of the samples. The model with lower DIC was selected as the better model for that cell. We only selected a model if the |ΔDIC| between the two models was >10 – a standard threshold that is typically used for model-selection (*31*); in case of |ΔDIC| ≤ 10, the neuron was neither classified as allocentric, nor as egocentric. Notably, the DIC typically yielded a very conclusive model selection, with 63% of the neurons having |ΔDIC| ≥ 100 (fig. S12A). We also note that the number of variables in the two models was quite similar (six variables in the allocentric model and eight variables in the egocentric model: see Fig. 6B) – allowing a direct comparison.

Data maps. To visualize the neural tuning to different variables, we computed 2D firing-rate maps for self position and for positions of other bats, and computed 1D tuning-curves for self head-direction, and for the distances to other bats and directions to other bats. The firing-rate maps for the 2D allocentric position (for both self and other bats) were computed by counting the number of spikes and the time spent in each spatial bin (bins of 3 × 3 cm) – with time spent (occupancy) data corresponding to either self positions (for place tuning) or to the position of another bat (for social place tuning). Bins with time spent < 0.2 s were discarded from analysis. Spike-count maps and time-spent maps were then smoothed (Gaussian kernel σ = 2.5 bins), and we then divided, bin by bin, the smoothed 2D spike-count map by the smoothed 2D time-spent map, to yield a firing-rate map – for self or other (e.g., Fig. 5C-E [top]). The tuning curves for 1D variables – self head-direction, directions to other bat, and distances to other bat – were computed as follows: (i) for directional variables (self head-direction and direction to other bat): by counting the spikes and time-spent in 30° angular bins, and (ii) for distance variables (distance from the recorded bat to the other bat): by counting the spikes and time-spent in 5-cm distance bins. Bins with time spent < 0.5 s were discarded

from analysis. The 1D spike-count maps and time-spent maps were then divided, bin by bin (without smoothing), to obtain tuning curves for self head-direction (e.g. Fig. 5C-D), directions to other bats and distances to other bats (Fig. 5F-H).

Model maps. The model maps of behavioral variables, as predicted by the GAM, were determined as the partial dependency plots (*58*) of the GAM: these partial dependency plots indicate the marginal response of the neuron to a particular behavioral variable, as predicted by the model, taking into account the other behavioral variables (*58*) – generating the predicted 2D maps for position (e.g., the model maps [bottom] in Fig. 5C-E), and 1D tuning curves for direction and distance (e.g., green tuning-curves in Fig. 5C-D, F-H). A minimum occupancy criterion, identical to the data map, was also applied to the model map.

Shapley values. To assess the contribution of each behavioral variable to the firing of the neuron, we computed the Shapley values (*35*) for each of the behavioral variables. Shapley values are a standard metric that provides the optimal estimation of how much a variable contributes to a model (*34, 35*). Here we used Shapley values to assess the contribution of each of the behavioral variables to the neuronal response (*34, 35*). The Shapley value is the average marginal contribution of each of the variables, considering all possible combinations of models, and is defined as:

$$\varphi_m(v) = (1/n)\sum_{S}[v\,(S\,\cup\{m\})\,-\,v(S)]/\binom{n-1}{l(S)}\,, \qquad m = 1, 2, 3 \ldots n$$

where $\varphi_m(v)$ is the Shapley value for the behavioral variable m, $v(S)$ is the explained variance (pseudo R^2) of all the model subsets S involving the variables 1 to n, excluding m, $v\,(S\,\cup\{m\})$ is the explained variance of the models including the variable m, and $l(S)$ indicates the size of the subset S. Specifically, we trained all possible 2^n models for the n behavioral variables, and used the explained variance of each model to compute the Shapley value.

Control for salient locations and reward locations in the GAM analysis. To test if the hippocampal CA1 neurons in the recorded bats represented the direction and distance to the other bats, or whether they represented the direction and distance to *any* type of salient or rewarding places, we computed the egocentric GAM for all the significant egocentric cells, for four additional control-locations: (i) the closest food bowl – which is the key reward location; (ii) the corner of the net closest to where the bats usually flies from (fig. S5A) – which is a very salient geometrical feature for the bat; (iii) a salient hanging object on the ceiling – specifically, the most prominent camera in the middle of the room; and (iv) the median location of each of the bats over the entire session. To keep the number of variables identical, we re-evaluated the GAM for each neuron, by replacing the location of one of the other bats in the GAM with one of these four control-locations. This procedure was repeated by replacing each of the conspecific bats one-by-one. We then assessed the prediction of the model as before, by determining the correlation between the predicted firing-rate and the real firing-rate (Spearman ρ) across the entire session, and compared it to the correlation between the model and the data for the real bats. We found that the predictions were significantly poorer (lower ρ) for the control locations than for the real bats (Wilcoxon signed-rank test, $P = 3.22 \times 10^{-17}$). We also computed the Shapley values for these control locations, and found that they were also significantly poorer (lower Shapley values) than for the real bats (Wilcoxon rank-sum test, $P = 6.63 \times 10^{-12}$). We performed this control for the egocentric model, and not for the allocentric model, because the allocentric locations of these control-objects were stationary, and thus there was no dynamic range to evaluate the neurons' allocentric encoding; by contrast, their egocentric encoding could be evaluated, because the egocentric variables (direction and distance from the recorded bat) did vary all the time, due to the movements of the recorded bat. (We also note that our previous study on social allocentric encoding of other bats (*6*) showed that when we moved objects [both

rewarding and non-rewarding objects], these moving objects were represented more weakly [less significant neurons] than social agents – i.e., more weakly than other bats).

Variance inflation factor. Computing reliable Shapley values requires independence or near-independence of the behavioral variables (*84*). To determine if the behavioral variables that we used in the models were correlated to each other (multicollinear) – or were independent of each other – we computed the variance inflation factor (VIF). The VIF indicates the degree of multicollinearity among the variables, and is defined as:

$$VIF_m = 1/(1 - R^2_{m|-m})$$

where VIF_m is the variance inflation factor for variable m, and $R^2_{m|-m}$ is the variance in predicting the variable m, using all other variables apart from m – employing the prediction model (GAM). A VIF of 1 indicates complete independence of the variable from all the other variables, and VIF < 10 is a standard threshold that indicates low multicollinearity among the variables (*85*) – namely, that the variables are nearly independent, and are *not* strongly correlated to each other. We assessed the VIF for all the variables within the allocentric model and within the egocentric model, and found near-independence of the behavioral variables within each model (median VIF [allocentric cells] = 3.3; median VIF [egocentric cells] = 4.4). In other words, the positions of the different bats were not correlated with each other – and likewise the distances and directions to the different bats were not correlated with each other (no correlations across bats, and no correlations between directions and distances). This independence allowed us to reliably assess the contribution of each of the behavioral variables to the neuronal firing, using the Shapley values – separately for the allocentric model and egocentric model (however, we note that the allocentric and egocentric variables were correlated to each other [VIF > 10], which is the main reason why we could not reliably estimate a

mixed allocentric-egocentric model for the neurons, and instead we estimated separately a model for allocentric variables and another model for egocentric variables).

Sparsity of behavioral variables. The degree of multiplexing exhibited by neurons to the different behavioral variables was evaluated for significant neurons, by measuring the sparsity (range from 0 to 1) of the Shapley values across all the allocentric or egocentric behavioral variables for each neuron. Sparsity is defined as (*86*):

$$Sparsity = < \varphi_m >^2 / < \varphi_m^2 >$$

where φ_m is the Shapley value for behavioral variable m. Sparsity values close to 0 indicate high selectivity to a single behavioral variable – and values close to 1 indicate multiplexed encoding of all the behavioral variables, whereby all the behavioral variables are being equally encoded.

Encoding of sex, social hierarchy, and social affiliation. To determine if hippocampal neurons represent one of the following 3 social features of other individuals – sex, social hierarchy, and social affiliation – we parsed in a 3-way manner the Shapley values that represent the conspecific bats (Fig. 6D-E; the Shapley values of each cell were normalized here by their maximum). Specifically, to investigate the effect of sex, the Shapley values were grouped by the sex of the conspecific: male or female. To investigate the effect of hierarchy, the Shapley values were grouped by bats who were higher in hierarchy than the recorded bat, or were lower in hierarchy. To investigate the effect of affiliation, we computed an affiliation index. The affiliation index was evaluated as the median distance that a conspecific bat spent from the recorded bat on a given day – capturing the intuition that you tend to be closer to your friends (*87*) – and was then normalized by the maximum of the median across all the bats and all the days of that social network. Notably, the affiliation index was strongly correlated to an alternative measure of affiliation, namely the rate of affiliative interactions with the conspecific (fig. S13). The affiliation index was then thresholded to

classify bats with high affiliation to the recorded bat, versus bats with low affiliation – and the Shapley values corresponding to these two groups were parsed accordingly. These 3 sets of groups (Fig. 6D-E) were then evaluated using a 3-way ANOVA (Sex × Affiliation × Hierarchy, using *anovan* in Matlab), and subsequently the differences between the specific groups were evaluated using a standard multiple-comparison correction (Fisher's least-significant difference, computed using *multcompare* in Matlab).

We note that affiliation, sex, and hierarchy were independent from each other: (1) The affiliation index was uncorrelated with hierarchy (Pearson $r = –0.10$, $P = 0.22$). (2) The affiliation index was independent of the sex of the other bat (Wilcoxon rank-sum test between affiliation of male and female bats: $P = 0.45$). (3) The hierarchy was independent of the sex of the other bat (Wilcoxon rank-sum test between hierarchy of male and female bats: $P = 0.09$; see also fig. S2B).

To complement the ANOVA, we also fitted a mixed-effects linear model (using Matlab's function *fitlme*). See Table S2 for the results of this model (Matlab's function *anova* on the fitted mixed-effects linear model). This type of model can deal better with unbalanced designs, and can also include random factors in the model. The model included as fixed effects our three factors of interest: sex, affiliation, and hierarchy (and their interactions). In addition, the model included as random effects two additional factors: self bat identity – the identity of the recorded bat for each neuron, and target bat identity – the identity of the represented bat for each Shapley value. The model was fit using Maximum Likelihood. The results of the ANOVA and the mixed-effects linear model agreed with each other very well (Table S2).

Comparison of identity-coded bats across contexts. To determine if the bats that were identity-coded in-flight were also the same bats that were identity-coded on the net (Fig. 6F-G), we did the following. We determined for each cell the Shapley rank for the specific bat that was

identity-coded in-flight (Fig. 6F-left, gray bars; the Shapley rank was determined by the Shapley value: rank 1 corresponds to the bat with the highest Shapley value and rank 4 to the one with the lowest Shapley value). This was then compared to the Shapley ranks of the bats that were not identity-coded in-flight (Fig. 6F, left; white bars). We also compared the results using a χ^2 test, comparing which bats had a Shapley-rank 1 versus rank > 1 (Fig. 6F, right: gray bars, identity-coded bats in-flight; white bars, non-coded bats in-flight). In other words, we performed a χ^2 test for the following 2×2 comparison:

(identity-coded bat in-flight , non-coded bats in-flight) × (rank = 1 on-net , rank > 1 on-net).

Statistics

Distributions were compared using Wilcoxon rank-sum test and Kolmogorov-Smirnov test, unless noted otherwise. Correlations were based on Pearson correlation or Spearman correlation (see above). Contingency tests were performed using χ^2 test. To assess the significance of responses, we compared the real data to shuffled distributions (95^{th} percentile or 99^{th} percentile): the details of the shuffles are indicated in the sections above, together with the details of the respective analysis.

Data and code availability

All the behavioral and neural data in this study were analyzed using custom code written in Matlab, and the GAM analysis was performed in Python. The data and code that support the conclusions of this study are available from the authors upon a reasonable request, and are also accessible online at Zenodo (*57*). The code for the GAM analysis is archived on Github, and is freely available at: https://github.com/1tux/neural-analysis.

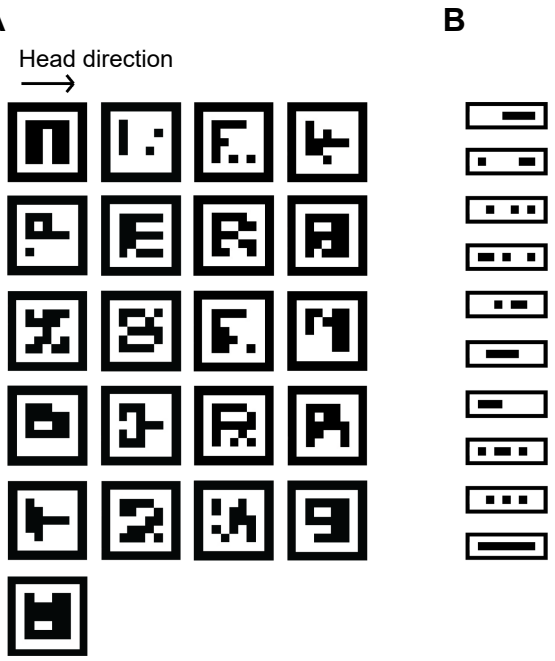

fig. S1. Barcodes used for camera-based tracking. (**A**) Two-dimensional barcodes (*22*) used for tracking the position and head-direction of bats. These two-dimensional barcodes were placed on the top of the box on the bat's head (for the recorded bat they were placed on the top and on the 4 sides of the box). The two-dimensional barcodes have a directional orientation, indicated here by the arrow, that shows the direction towards the bat's nose – which we used to track the bat's head-direction. (**B**) One-dimensional barcodes used for tracking the positions of the other bats. These one-dimensional barcodes were placed on the sides of the box on the other bat's head (in addition to the two-dimensional barcode that was placed on top of the box) (*21*).

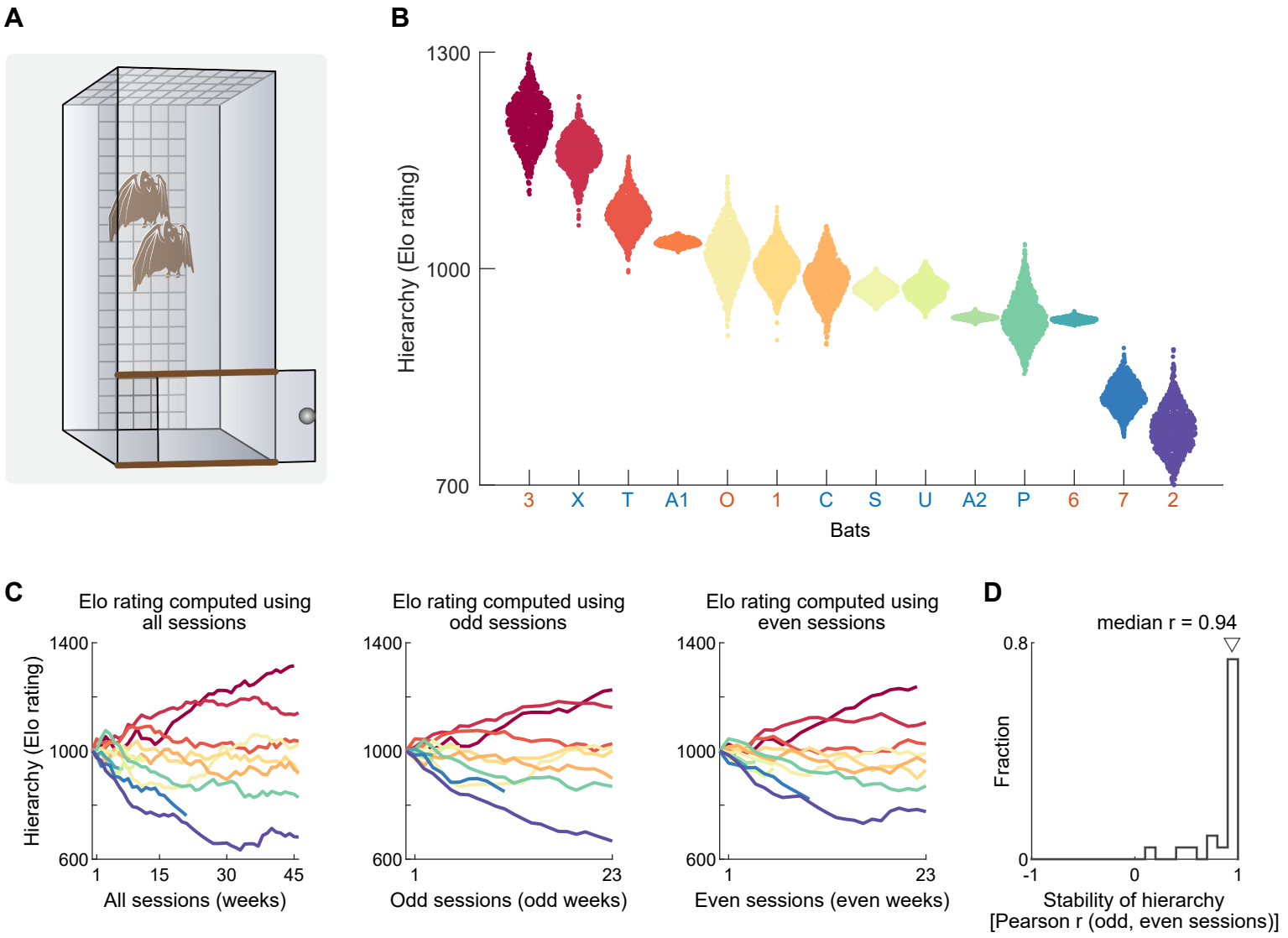

fig. S2. Setup for testing dominance hierarchy, and stability of Elo ratings for hierarchy. (**A**) A schematic illustrating the setup used for determining dominance hierarchy within pairs of bats. This setup relies on the inherent tendency of bats to hang at high locations. Here, two bats were placed at the bottom of a vertically-oriented box (30 cm wide × 30 cm deep × 100 cm high), and were allowed to climb simultaneously up to the top of the box by using a ladder placed on the box's wall. The first bat to reach the top was deemed the higher in hierarchy. (**B**) Distribution of hierarchy (Elo rating) for each of the bats in the experiment (n = 14), obtained by shuffling across sessions the temporal order of pairwise tests between the bats, which were used for determining the Elo ratings (*2, 69*). Colors match the colors of the curves in Fig. 1E and fig. S2C. The letters/digits below the x-axis indicate the bat's name, and the color of the letter/digit indicates the sex (blue, male; red, female). Bats A1, U, A2, 6, 7 were the five bats in which we conducted neural recordings; the other bats were conspecific members of the bat colony. (**C**) Left: Hierarchy (Elo ratings) of the bats computed using all the sessions – this is the same data as in Fig. 1E, replotted here to facilitate comparison to the other two panels. Middle: Elo ratings recomputed using only the odd sessions (odd weeks). Right: Elo ratings recomputed using only the even sessions (even weeks). (**D**) Stability of hierarchy: Distribution of the Pearson correlations (Pearson r) of the vector of Elo ratings for the bat-group calculated using the odd sessions versus the vector of Elo ratings calculated using the even sessions. In other words, these are the correlations between the Elo ratings of the bats in fig. S2C-middle versus fig. S2C-right. Note the stable hierarchy, as evidenced by the high correlations (median r = 0.94).

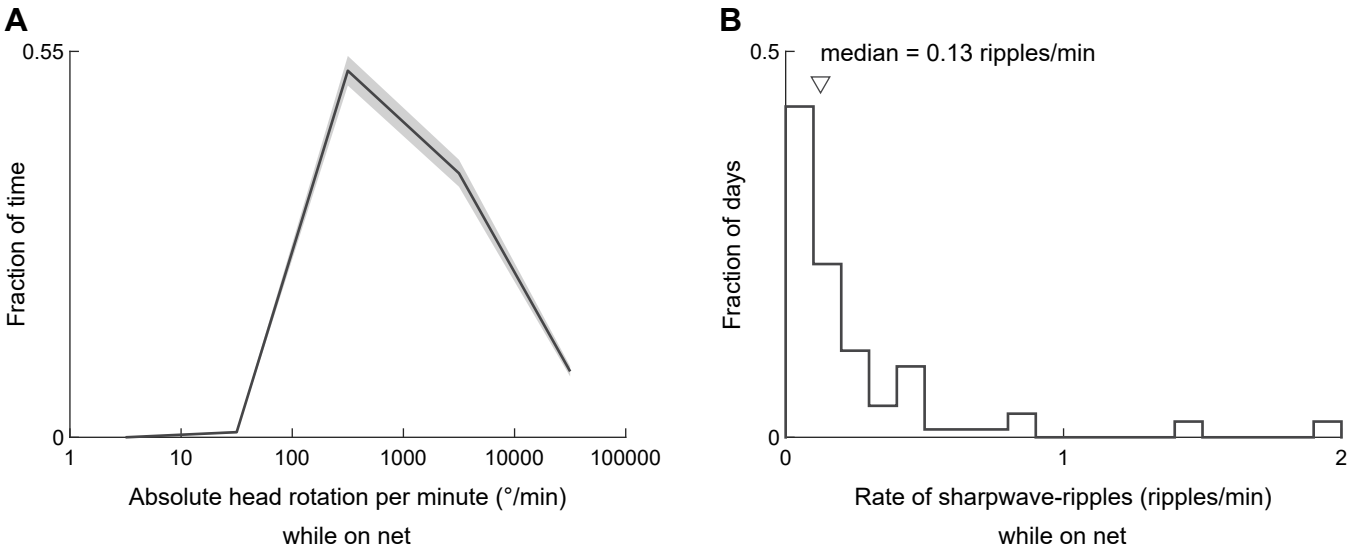

fig. S3. The recorded bats were active on the nets. (**A**) Distribution of the cumulative absolute head-rotation per minute (°/min) by the recorded bats, during the active-on-net behavioral state (i.e., excluding epochs of explicit social interactions, and excluding flights). Displayed is the mean (black line) ± SEM (gray area) over all the recording sessions (n = 92 sessions, i.e. n = 92 recording-days). The large values of cumulative absolute rotation per minute indicate that the recorded bats were quite active on the nets. (**B**) Histogram of the rates of sharpwave-ripples in the recorded bats (number of ripples per minute in each recording session). Note that the median ripple-rate in our data was 0.13 ripples/min, and the mean ripple-rate was 0.25 ripples/min – both of which are much lower than the typical ripple-rates observed during sleep (e.g. 47.4 ripples/min in rats (*75*)). This ultra-low rate of ripples further illustrates that the bats were active on the net during the recording sessions.

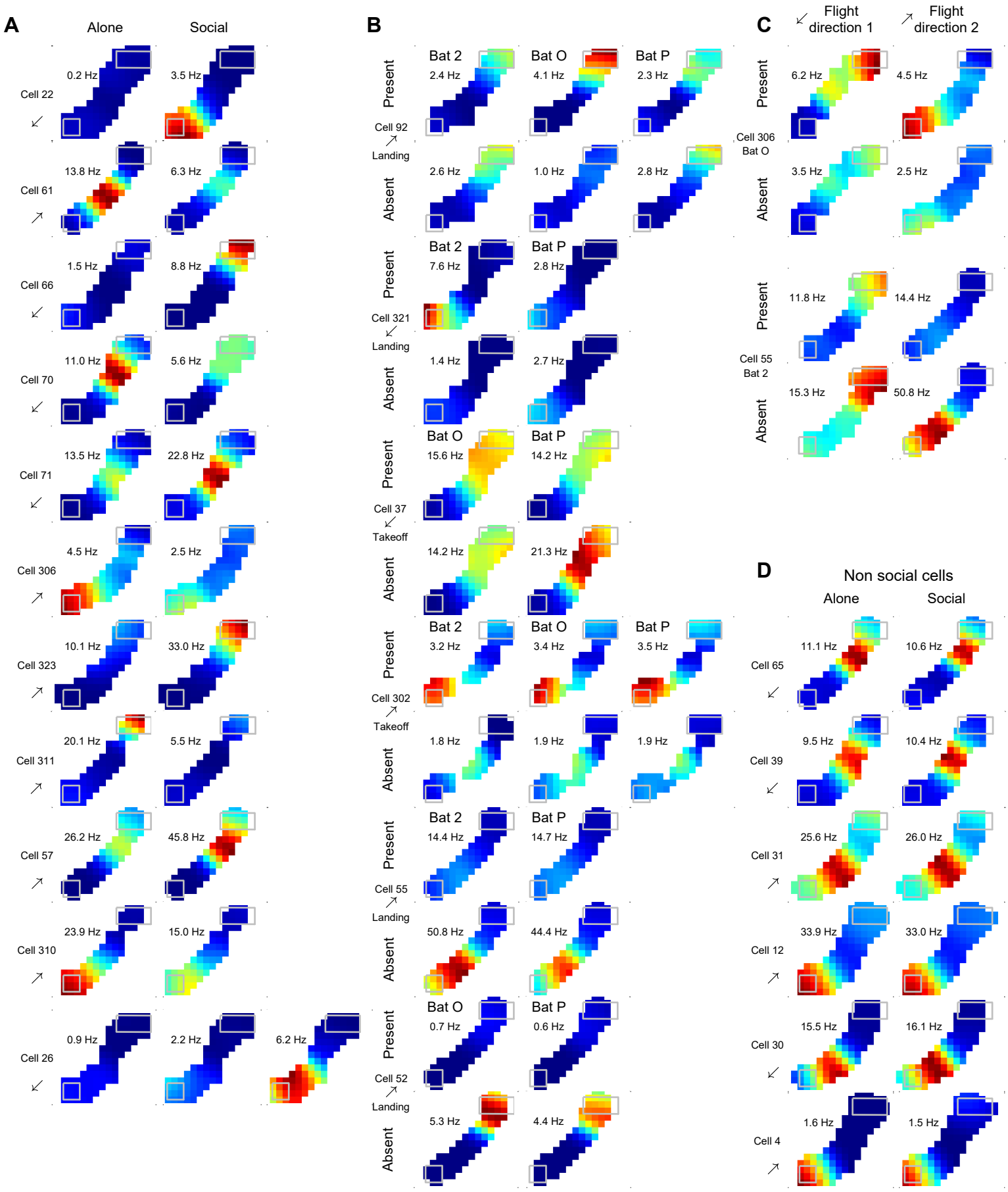

fig. S4. Overlap regions of the firing-rate maps of social cells in-flight, during social and alone flights, and examples of non-social cells in-flight. Figure legend on next page.

fig. S4. Overlap regions of the firing-rate maps of social cells in-flight, during social and alone flights, and examples of non-social cells in-flight. (**A**) Two-dimensional firing-rate maps during flight (top-view), plotted separately for social flights (right) and alone flights (left). These are the same neurons as in Fig. 2A-D and 2J, but showing here only the overlapping pixels between the maps for the social flights and for the alone flights for each cell. We note that all the statistical comparisons in Figs. 2, 3 were made only using these overlapping portions. (**B**) Two-dimensional firing-rate maps during flight (top-view) for six cells. For each neuron, firing-rate maps were computed separately for flights when a particular conspecific was present (top) or absent (bottom), for different conspecifics (columns). These are the same neurons as in Fig. 3B-C, but showing here only the overlapping pixels between the maps (overlap between the top map and bottom map for each cell). (**C**) Two-dimensional firing-rate maps during flight (top-view) for two cells. For each neuron, firing-rate maps were computed separately for flights when a particular conspecific bat was present (top) or absent (bottom), for different flight directions (columns). These are the same neurons as in Fig. 3F, but showing here only the overlapping pixels between the maps (overlap between the top map and bottom map for each cell $\times$ direction). (**D**) Six examples of place cells that were not socially-modulated in-flight; plotted as in **A**.

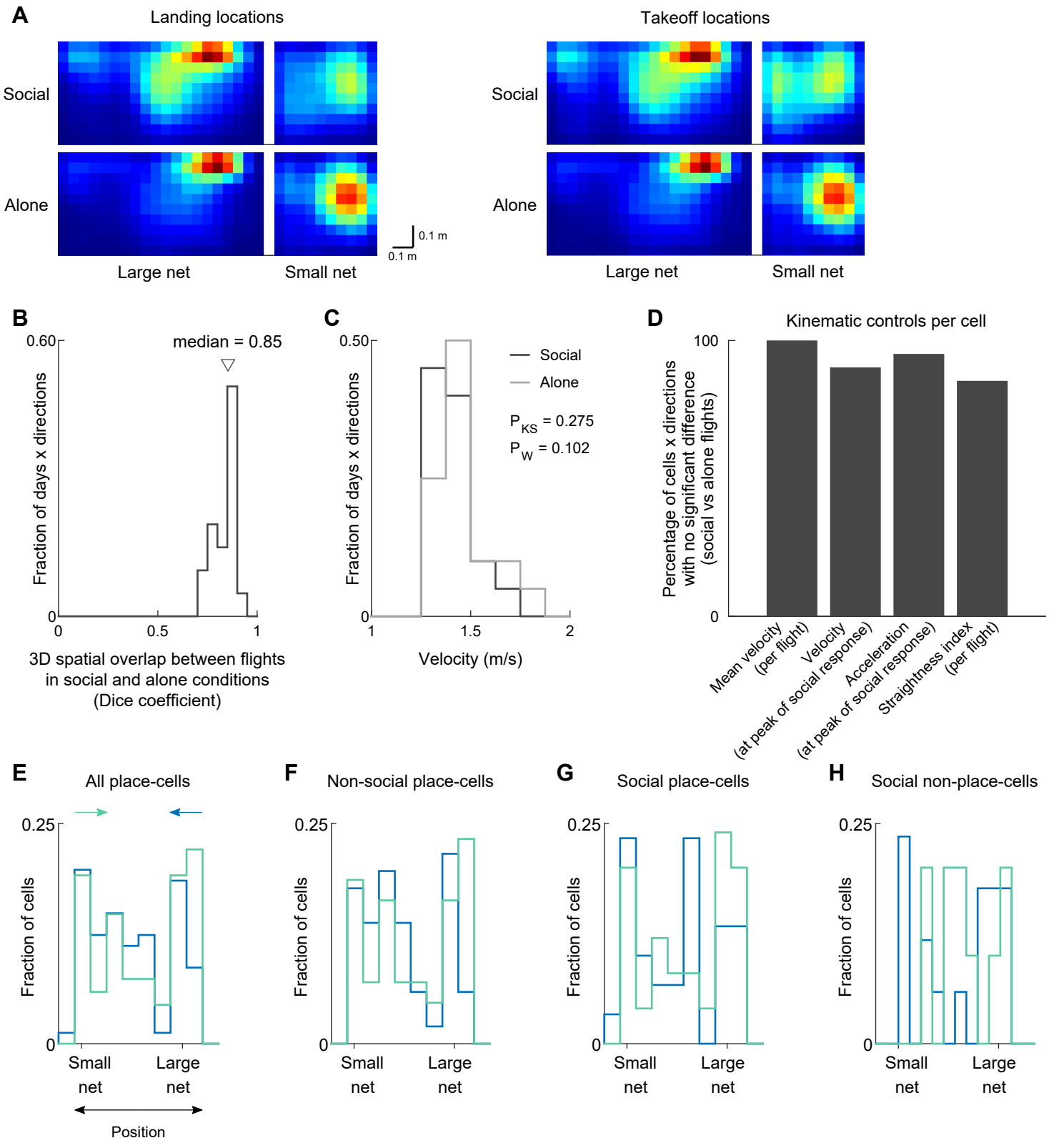

fig. S5. Controls for social and alone flights: spatial overlap, flight-velocity, acceleration, and straightness of trajectories; and distribution of place-fields in-flight. Figure legend on next page.

fig. S5. Controls for social and alone flights: spatial overlap, flight-velocity, acceleration, and straightness of trajectories; and distribution of place-fields in-flight. (**A-B**) Controls for flight trajectories. (**A**) Control for locations of landing and takeoff. Occupancy (time-spent) maps showing the locations of the recorded bats on the nets, for all the recording days: these locations were computed using 1-s of positional data after landing (left maps), and 1-s before takeoff (right maps) – separately for the social flights (top maps) and alone flights (bottom maps). There was a high map-correlation between the social and alone occupancy maps for landings (Pearson r = 0.86) and also for takeoffs (Pearson r = 0.79). This indicates that landing locations of the bats were similar for both the social and alone flights, and likewise for the takeoff flights – and thus, differences in landing-locations (or takeoff-locations) cannot explain the differences in neural responses observed between social and alone flights. (**B**) Control for 3D spatial overlap. Shown is the distribution of Dice coefficients – a standard index of spatial overlap (*21*) – showing the 3D spatial overlap between the flights in the social condition and the alone condition, for all the days in which we recorded significant social-coding cells in-flight (n = 20 days × directions). The triangle shows the median Dice coefficient, 0.85 – indicating very high volumetric overlap of the flights in 3D. (**C**) Control for flight velocity. Histograms of flight velocities in the social condition (black) and alone condition (gray), for all the days in which we recorded significant social-coding cells in-flight, and which showed no significant difference in velocity between the conditions (n = 20 days × directions, out of a total of 22 days × directions). There was no significant difference between the two distributions (Kolmogorov-Smirnov test: P = 0.275; Wilcoxon rank-sum test: P = 0.102). (**D**) Kinematic controls per cell. Shown are the percentages of cells × directions, which showed significant social neural responses, but which exhibited no significant difference in kinematic variables (velocity, acceleration, or straightness) between the social flights versus alone flights. In particular: 100% of the cells × directions had no significant differences in mean flight velocity between social and alone flights (left bar, n = 82/82); 90% and 95% cells × directions had no significant differences in neither velocity nor acceleration at the peak of the social response, when comparing between the social and alone flights (velocity near peak: second bar from left [n = 74/82], acceleration near peak: third bar from left [n = 78/82]); and 85% of the cells × directions had no significant differences in the straightness index (related to flight curvature) between the social and alone flights (rightmost bar, n = 70/82). (**E-H**) Distribution of locations of place-fields for different sub-populations of neurons, plotted as in Fig. 2G. (**E**) Distribution of locations of place-fields for all the place-cells. This distribution was similar to the distribution for the socially-modulated neurons (Fig. 2G; Kolmogorov-Smirnov tests comparing Fig. 2G to fig. S5E: P = 0.79 and P = 0.64 for the two flight-directions). (**F**) Distribution of locations of place-fields for all the non-social place-cells (Kolmogorov-Smirnov tests comparing Fig. 2G to fig. S5F: P = 0.54 and P = 0.59). (**G**) Distribution of locations of place-fields for all the social place-cells (Kolmogorov-Smirnov tests comparing Fig. 2G to fig. S5G: P = 0.92 and P = 0.89). (**H**) Distribution of locations of peak-firing for all the social non-place cells (Kolmogorov-Smirnov tests comparing Fig. 2G to fig. S5H: P = 0.46 and P = 0.96).

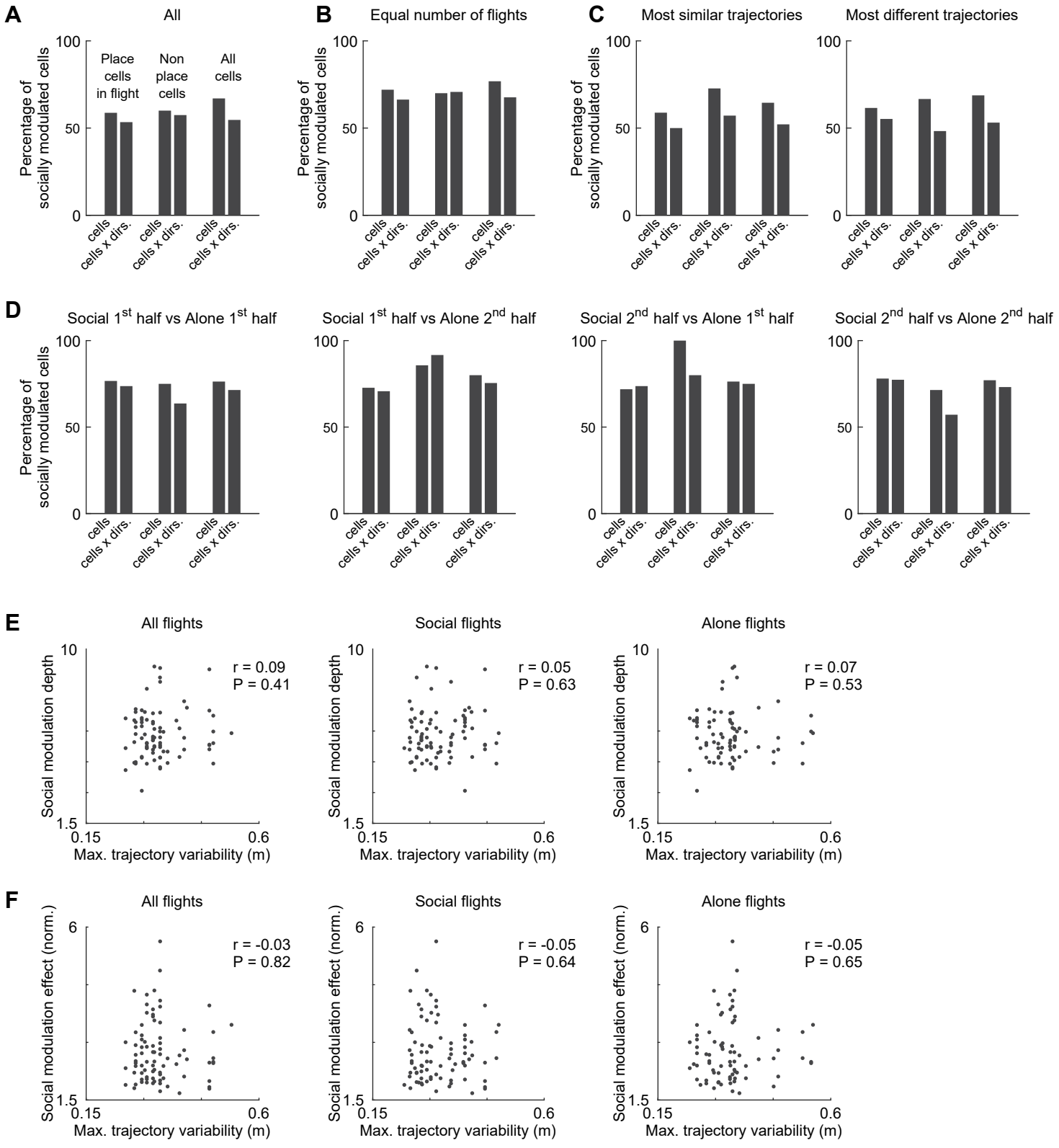

fig. S6. Controls for social modulation in flights: social coding cannot be explained by variations in flight numbers or in flight trajectories. Figure legend on next page.

fig. S6. Controls for social modulation in flights: social coding cannot be explained by variations in flight numbers or in flight trajectories. (**A-D**) Percentage of significantly socially-modulated neurons in-flight, among place-cells (left pair of bars), non-place cells (middle pair of bars), and all cells (right pair of bars), for different controls. Note that most hippocampal neurons were socially-modulated across all conditions. (**A**) All flights: this is identical to main Fig. 2E, and is shown here for reference. (**B**) Equal number of flights: Subsampling the number of flights in the social or alone condition (whichever had more flights), to match the number of flights in both conditions. The subsampling was done as follows: Suppose there are N social flights and M alone flights, and N < M: we first computed the median flight trajectory for the N social flights (the condition with fewer flights). We then selected N out of the M alone flights based on the criterion that these N alone flights were the closest (in terms of maximal absolute deviation) to the median trajectory of the N social flights (and vice versa if N > M). As shown here, we found that this subsampling (matching) did not affect qualitatively the results (if anything, the number of neurons showing significant difference between social and alone flights was slightly increased here as compared to panel **A**). (**C**) 'Most similar trajectories' (left) and 'most different trajectories' (right) refers to taking half of the trajectories in the social flights that were the most similar to the median trajectory of the alone flights, or half of the trajectories in the social flights that were the most different from the median trajectory of the alone flights – doing this for each neuron separately – and then using those subsets of trajectories in order to determine social modulation in that neuron. The results show that the percentage of socially modulated cells did not depend on which set of trajectories were used – the most similar trajectories or the most different trajectories: both sets yielded very comparable percentages of significantly socially-modulated cells. (**D**) Percentage of significant socially-modulated cells when comparing the 1st and 2nd halves of the social flights versus the alone flights for each cell, for all the four possible comparisons. (**E**) Population scatters showing the social modulation depth for each cell versus the maximal trajectory variability (median of the maximal trajectory divergence) for that cell – plotted for all flights (left), only social flights (middle) or only alone flights (right). There was no correlation between the social modulation depth of a cell and the maximal trajectory variability of its flights, in any of the conditions (see the Pearson *r* correlations and their *P*-values written on the three scatter-plots): this indicates that differences in trajectory do not account for the social modulation of the cells. (**F**) Same scatters as in **E** using an alternative index of social effect size – the social modulation effect (norm.) (*21*). Similar to **E**, there was no correlation between the social modulation effect (norm.) of a cell and the maximal trajectory variability of its flights, in any of the conditions.

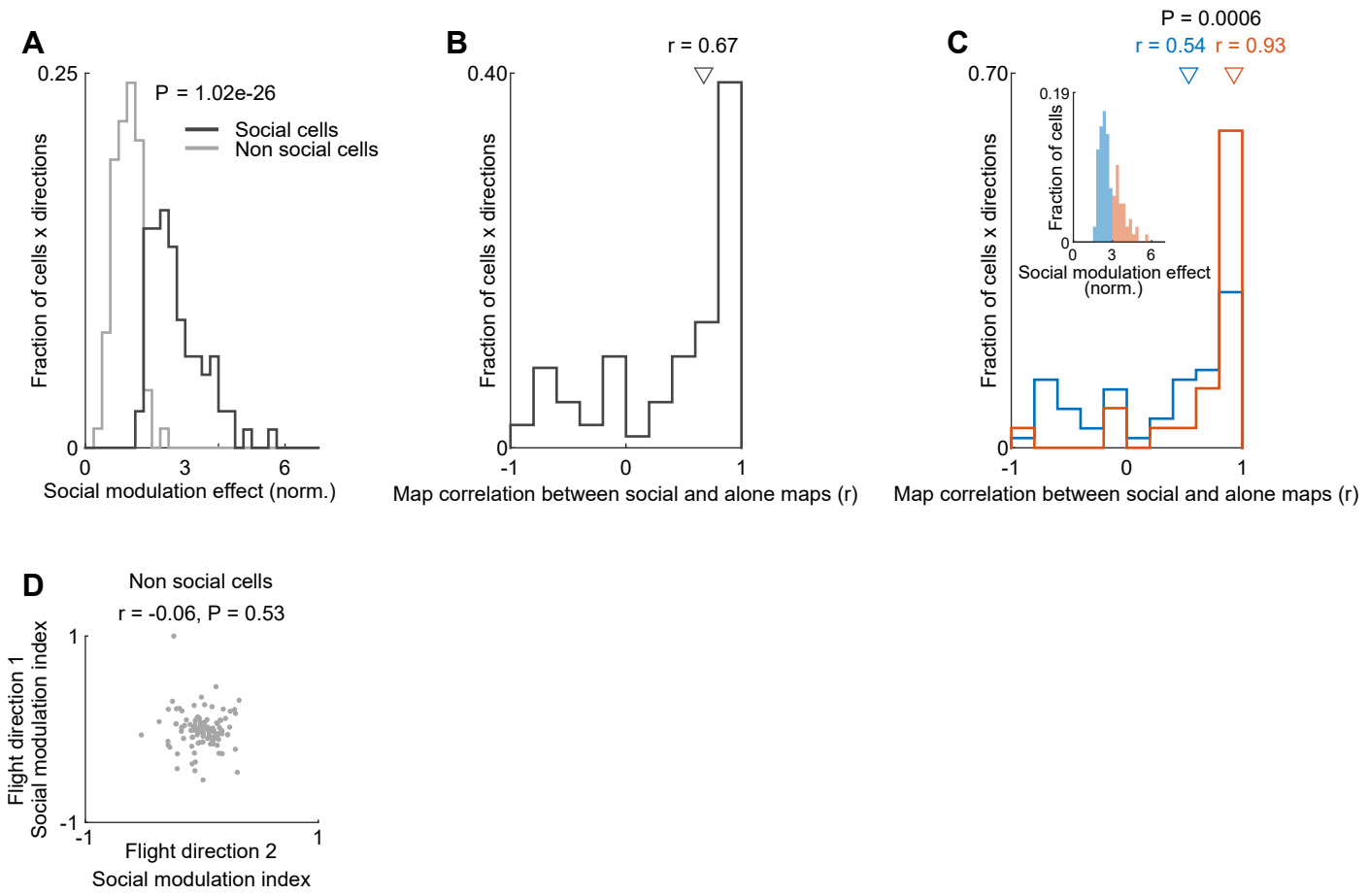

fig. S7. Social modulation in flight occurs mainly through rate remapping. (**A**) Histograms of social modulation effect (norm.) – plotted for the significant socially-modulated cells (black, n = 82 cells × directions) and for the non-social cells (gray, n = 78 cells × directions; Wilcoxon rank-sum test of black versus gray, $P = 1.02 \times 10^{-26}$) (*21*). The social modulation effect (norm.) is an alternative index of effect size than the social modulation depth used in main Fig. 2H (*21*). (**B**) Histogram of Pearson correlation (r) between firing-rate maps for flights in the social condition versus the alone condition, for all the significantly socially-modulated cells in flight (n = 82 cells × directions; these are the correlations between the 'Social' maps and 'Alone' maps for all cells, e.g. between the 'Social' and 'Alone' top-view maps in main Fig. 2A-D). The triangle shows the median map correlation, r = 0.67 – a high value, indicating that map structure did not change, namely there was no global remapping. Instead, the social modulation in-flight was mainly due to rate remapping (*77*). (**C**) Same data as in **B**, separated into two groups of neurons: cells that showed a particularly strong social-modulation effect (red, social modulation effect (norm.) ≥ 3, see inset; n = 27 cells × directions), and cells that showed a significant but somewhat weaker social-modulation effect (blue, social modulation effect (norm.) < 3, see inset; n = 55 cells × directions). Red and blue triangles show the median correlation values for the red and blue histograms (median r = 0.93 and r = 0.54, respectively); the red and blue histograms differed significantly (Wilcoxon rank-sum test: P = 0.0006; Kolmogorov-Smirnov test: P = 0.005). The high map-correlation values for the red histogram (median r = 0.93) – which are the neurons that showed a particularly large difference in firing-rate between the social condition versus alone condition (social modulation effect (norm.) ≥ 3) – indicates that these strongly socially-modulated neurons showed rate-remapping, and did not exhibit a global change in their map structure (no global remapping). Inset is the same data as the black line in **A** (with different bins), and shows the distribution of social modulation effect for the socially-modulated cells, colored by cells which showed a large effect (≥ 3, red) and those which showed a smaller effect (< 3, blue). (**D**) Population scatter of the social modulation index in one flight-direction versus the other flight-direction (*21*), plotted for the subpopulation of non-social cells × bats (in contrast to main Fig. 3G, which shows the same scatter for identity-coding and identity-generalizing cells × bats). There was no correlation in the social modulation index between the two flight directions for these non-social cells × bats (Pearson r = –0.06, P = 0.53; n = 115 cells × bats).

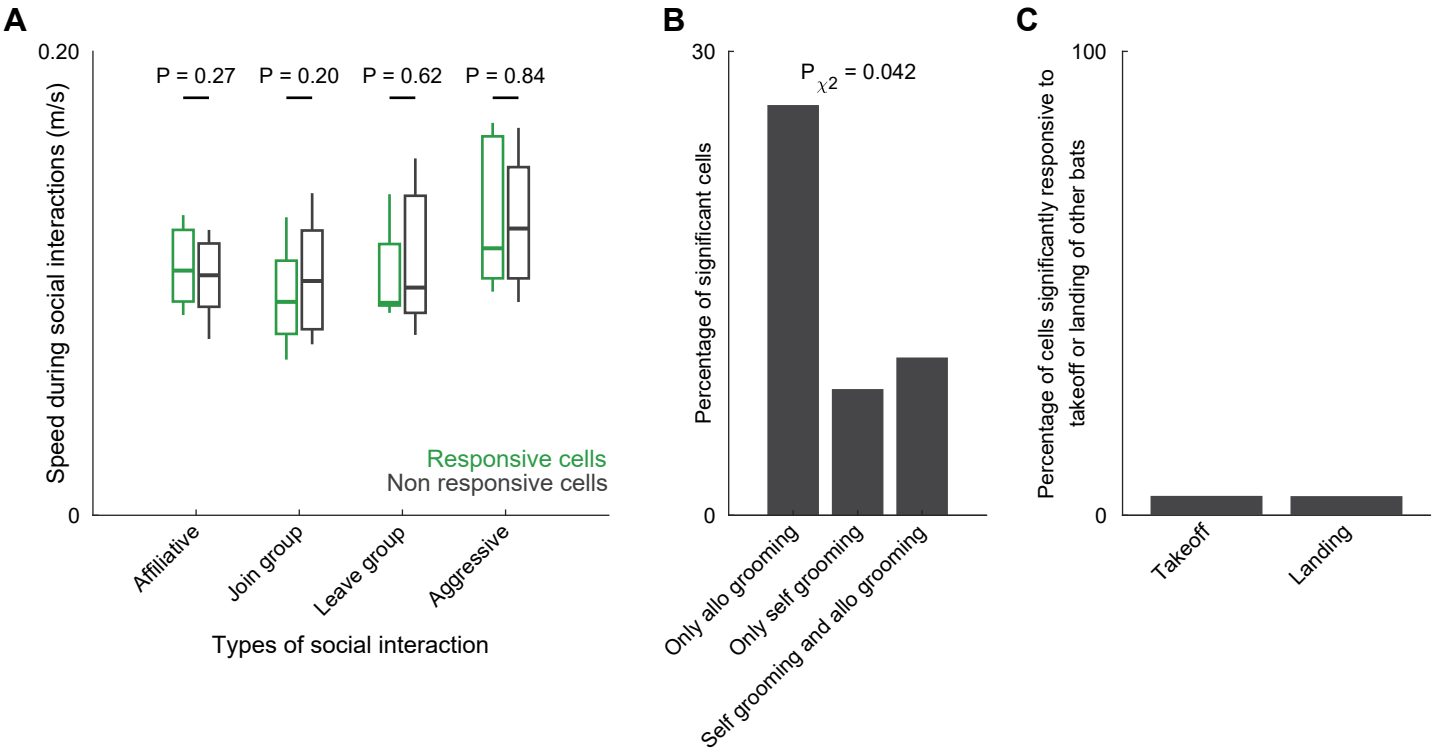

fig. S8. Social interactions: controls for movement and arousal. (**A**) Speed of the recorded bat during the four types of social interactions, plotted separately for socially-responsive cells (green) and non-responsive cells (gray). There was no significant difference in the median speed between the socially-responsive cells and non-responsive cells, in any of the interaction types (Wilcoxon rank-sum test, *P*-values indicated on the plot; 2-way ANOVA, $P = 0.54$). Box-plots denote the median (horizontal line), 25^{th} to 75^{th} percentiles (box), and 10^{th} to 90^{th} percentiles (whiskers). (**B**) Percentage of cells that responded only to allo-grooming (27%), only to self-grooming (8%), or to both (10%). These percentages indicate that allo-grooming responses cannot be explained as a general grooming response (χ^2 test for cells responsive to allo-grooming versus self-grooming: $P = 0.042$). This control was performed to control for motor movements, which are broadly similar between allo-grooming and self-grooming (here we analyzed a subset of 5 days with the largest number of allo-grooming responsive neurons; for these days we also delineated self-grooming events; $n = 65$ total cells from 3 different recorded bats). (**C**) Percentage of cells that showed responses to salient non-social events: the landing and takeoff of other bats from the same net on which the recorded bat was located. The events of landing and takeoff were automatically detected as the end-points and start-points of flights, respectively, and we computed their rasters and PSTHs using the exact same analysis-pipeline as for the social interaction events (i.e., as in Fig. 4B-C). The low percentage of cells that responded to these events (4% to landing, 4% to takeoff) indicates that the much-stronger responses observed during social interactions (see Fig. 4C) cannot be accounted for by arousal or attention to salient events.

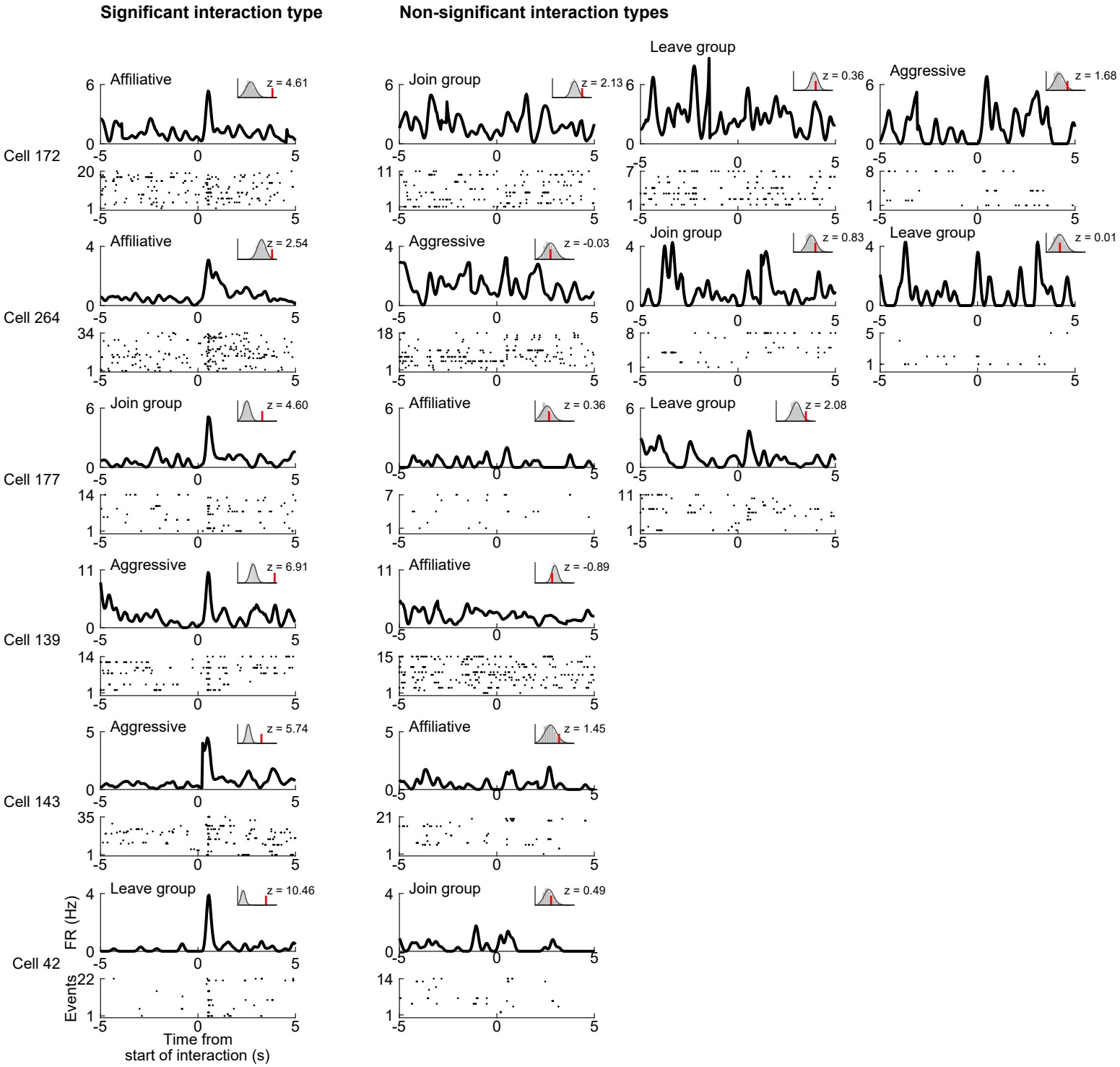

fig. S9. Examples of hippocampal cells that were selective to specific social interactions. For each cell, shown are the rasters and PSTHs for all the types of social interactions for which ≥ 5 events (trials) occurred; rasters are aligned as in main Fig. 4B (aligned to the model-estimated interaction time, i.e. using the algorithmic alignment). FR, firing-rate. Note that these neurons showed high selectivity: each cell responded to a particular type of social interaction, but not to others.

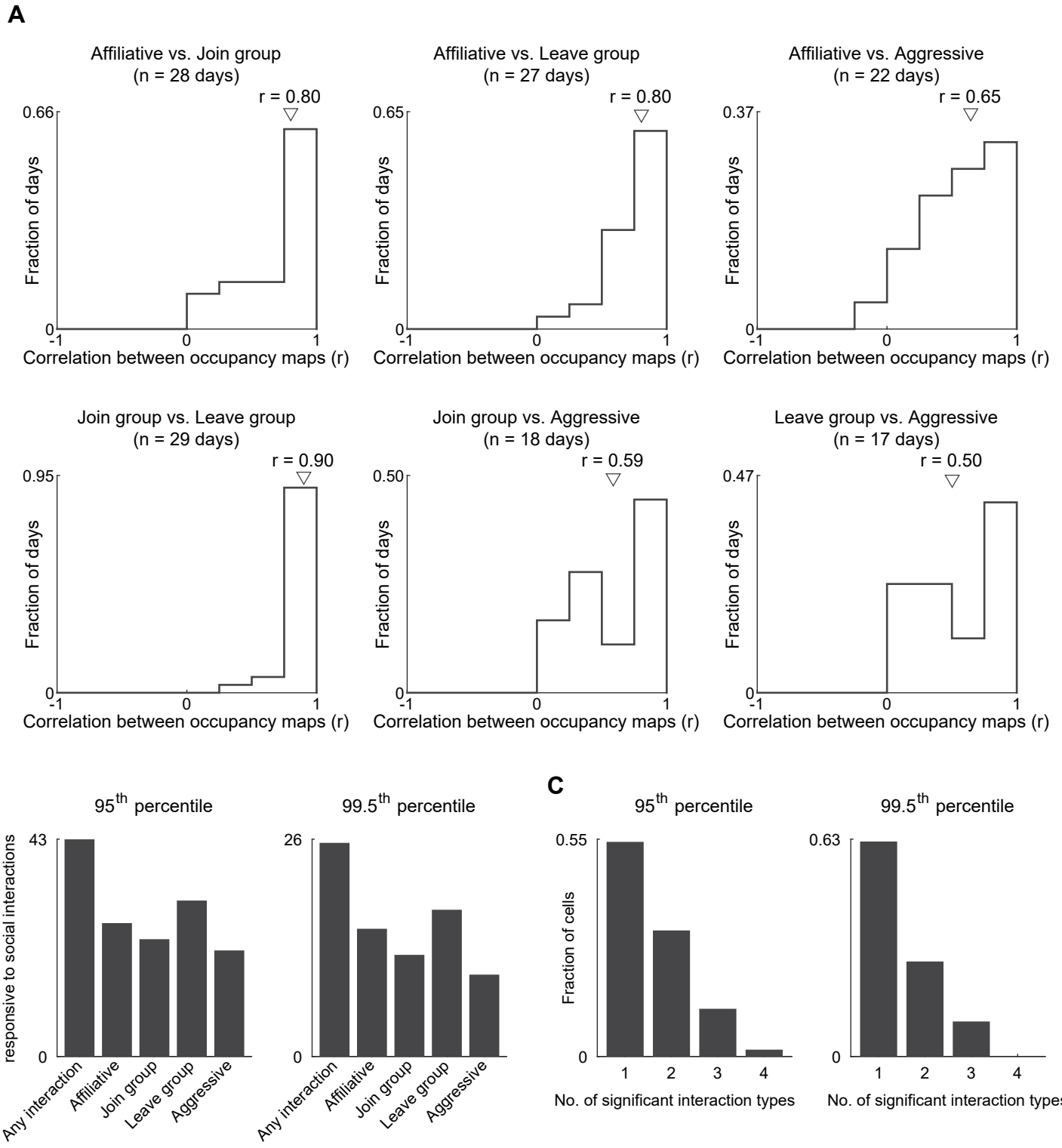

fig. S10. Different social interactions occurred at similar locations on the nets; and population summary of social-interaction results for different significance thresholds. Figure legend on next page.

fig. S10. Different social interactions occurred at similar locations on the nets; and population summary of social-interaction results for different significance thresholds. (**A**) Histograms of the Pearson correlations (*r*) of the per-day occupancy maps (time-spent maps) of the recorded bat when it engaged in different types of social interactions. The six histograms show comparisons of all the possible pairs of the four types of social interactions, for each day (Affiliative, Join group, Leave group, and Aggressive interactions; included are only days in which there were enough interactions of a particular type to assess social responses (*21*); number of days is indicated above each histogram). Triangles denote the median correlations of the distributions; note the high correlations for all pairs of interactions, which indicate that all the four interaction types occurred at similar locations. (**B-C**) Similar plots to Fig. 4C,E, but with different significance-thresholds compared to shuffles. (**B**) Percentage of cells significantly responsive to the various social interaction types: plotted similarly to Fig. 4C. Left: using a 95th percentile significance threshold. Right: using a 99.5th percentile significance threshold. Note that in Fig. 4C we used a 99th percentile significance threshold. (**C**) Bar graphs showing how many neurons responded significantly to only one, two, three, or all four social interaction types: plotted similarly to Fig. 4E. Left: using a 95th percentile significance threshold. Right: using a 99.5th percentile significance threshold. Note that in Fig. 4E we used a 99th percentile significance threshold.

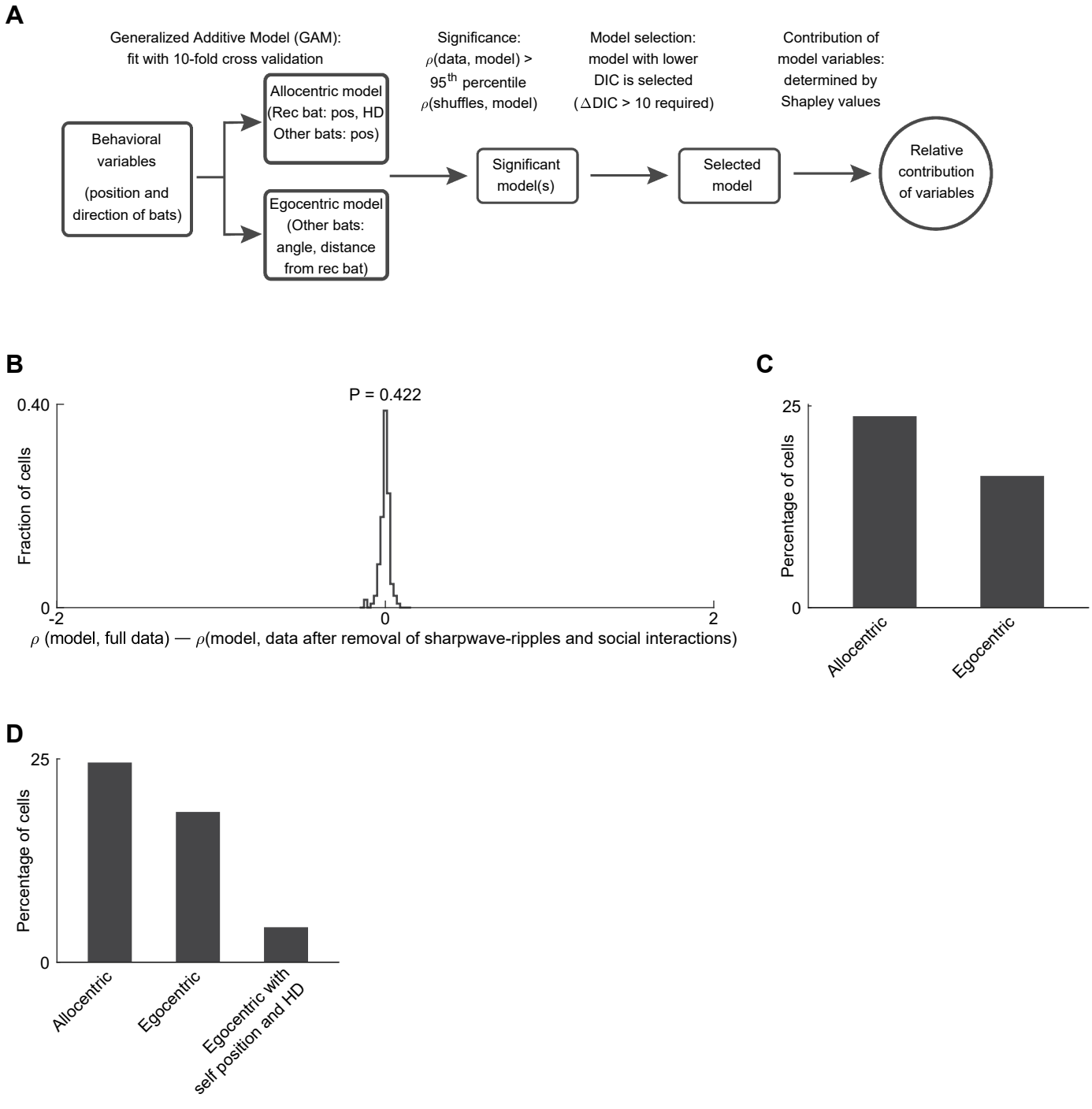

fig. S11. Assessment procedure of GAM model, results of GAM model after removal of social-interactions and sharp-wave ripples, and analysis of egocentric model with self variables. Figure legend on next page.

fig. S11. Assessment procedure of GAM model, results of GAM model after removal of social-interactions and sharp-wave ripples, and analysis of egocentric model with self variables. (**A**) Schematic illustration of the process for determining whether a neuron encodes allocentric or egocentric information, and assessing the contribution of the various behavioral variables to the firing of the neuron. (**B-C**) While in main Figs. 5,6 we ran the GAM model for all the data collected during the active-on-net behavioral state, here we re-ran the GAM model after removing ±2 sec around the start of each social interaction and ±0.5 sec around each sharpwave ripple (for ripple detection see ref. *21*). (**B**) Distribution of the differences in the model-data Spearman correlations ρ, before versus after removal of interactions and sharpwave-ripples. Note the histogram is very narrow and is centered around zero (t-test: $P = 0.422$). The x-range of –2 to +2 covers the full range of potential possible differences in ρ. (**C**) Fraction of significant allocentric and egocentric neurons, after removal of interactions and sharpwave-ripples. The results are very similar to Fig. 6A. (**D**) Fraction of significant neurons captured by each model, when assessing the GAM with three model options (instead of two as in Figs. 5, 6): (1) allocentric model, (2) egocentric model, and (3) a model comprising the egocentric variables (distances and angles to the other bats) combined with self position and self head-direction (HD). The fraction of allocentric and egocentric neurons remained the same as in Fig. 6A (25% allocentric cells, 19% egocentric cells), with a small fraction of additional neurons that were best described by the 3rd model, which encoded egocentric variables with self position and self head-direction (4%, n = 17/394 neurons). Furthermore, we note that there was a 97% overlap of the allocentric neurons and egocentric neurons between the two approaches – namely, the same cells were identified as allocentric and egocentric cells, respectively, when we ran the 3-model comparison (this panel) as compared to the original 2-model comparison (Fig. 6A-B).

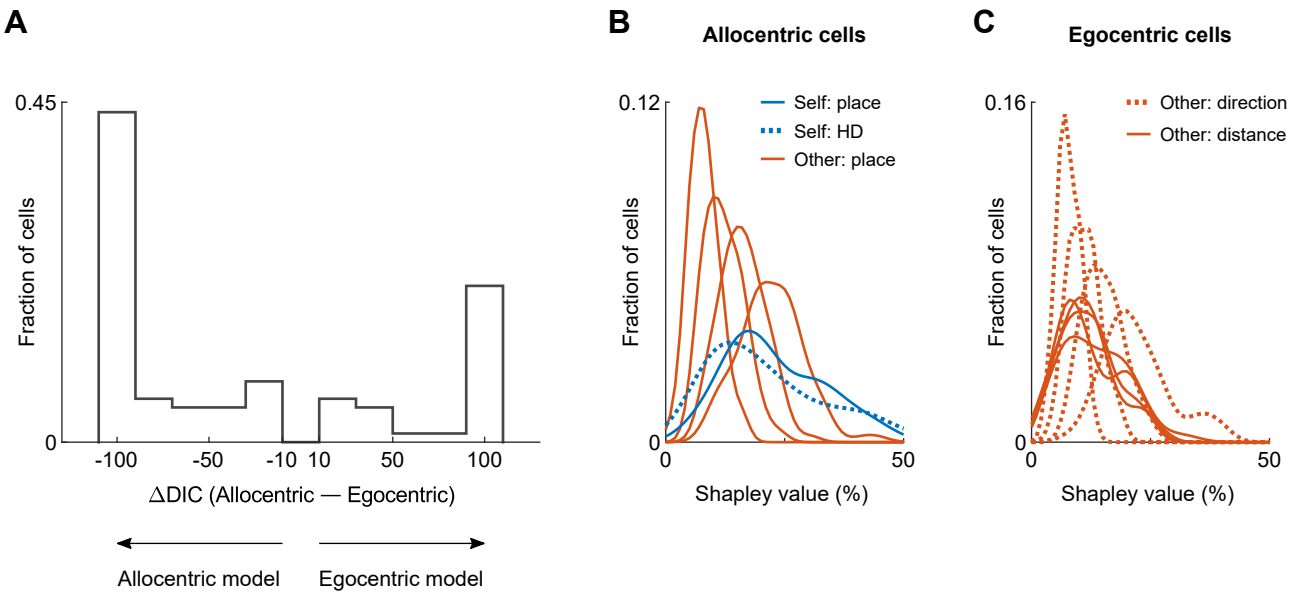

fig. S12. Model selection, and Shapley values of allocentric and egocentric cells. (**A**) Distribution of differences in deviance information criterion (DIC, see ref. *21*) between the allocentric model and egocentric model, for all the cells where both models were significant compared to shuffles (n = 87 cells). A lower value of DIC indicates a better model, hence negative values of ΔDIC support an allocentric model and positive values of ΔDIC support an egocentric model. The two extreme bins show cases of |ΔDIC| ≥ 100. Since for model selection we used a standard threshold of |ΔDIC| > 10 (see (*31*)), there is a notch between –10 and +10. Note that for most neurons, the |ΔDIC| was much larger than this standard threshold of 10 (in 63% of the neurons, the |ΔDIC| was ≥ 100: see the two extreme bins in the histogram). (**B**) Distributions (kernel density plots) of Shapley values for the different behavioral variables, for allocentric cells (n = 99 cells). Blue solid line and blue dotted line indicate the self position and self head-direction (HD) of the recorded bat; red lines indicate the positions of the other bats (rightmost histogram is pooled over the strongest-represented bat in each day [highest Shapley value], and leftmost histogram is pooled over the weakest-represented bat in each day [lowest Shapley value]). Note the rightward skew (higher Shapley values) of the two blue lines (self place and self head-direction) as compared to the four red lines (other bats) – indicating that there is stronger coding for self than for others in dorsal hippocampus CA1, as expected from the known self place-coding and self head-direction coding in the dorsal hippocampus CA1. (**C**) Distributions (kernel density plots) of Shapley values for the different behavioral variables, for egocentric cells (n = 73 cells). Red solid lines indicate the distance-coding variables to the other bats, and red dotted lines indicate the direction-coding variables to the other bats (data pooled as in **B**). Note the higher Shapley values for the dotted lines, indicating that the egocentric directions to other bats had a stronger representation than egocentric distances to other bats.

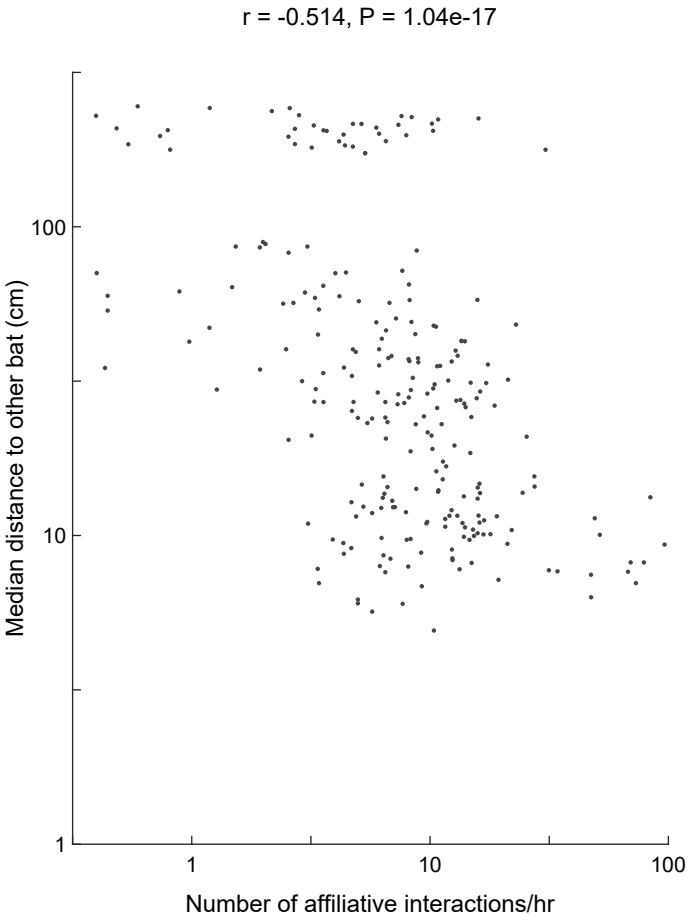

fig. S13. Correlation between two different indices for social affiliation: index based on inter-bat distances is correlated with index based on affiliative interactions. Scatter plot (log-log scale) showing the relation between the median distance to other bat (median per session, y-axis), and the rate of affiliative interactions between the bats during the same session (x-axis). Each dot represents one other bat (conspecific) in a session (n = 242 bats × sessions). In Fig. 6D-E we used the distance-based index for social affiliation, in which lower distance to other bats indicates higher affiliation to them. The strong negative correlation seen here between the two indices (Pearson $r = -0.514$, $P = 1.04 \times 10^{-17}$) indicates that the distance-based affiliation index, used in Fig. 6D-E, reflects also the affiliation computed from an independent index that is based on the rate of affiliative interactions between the bats.

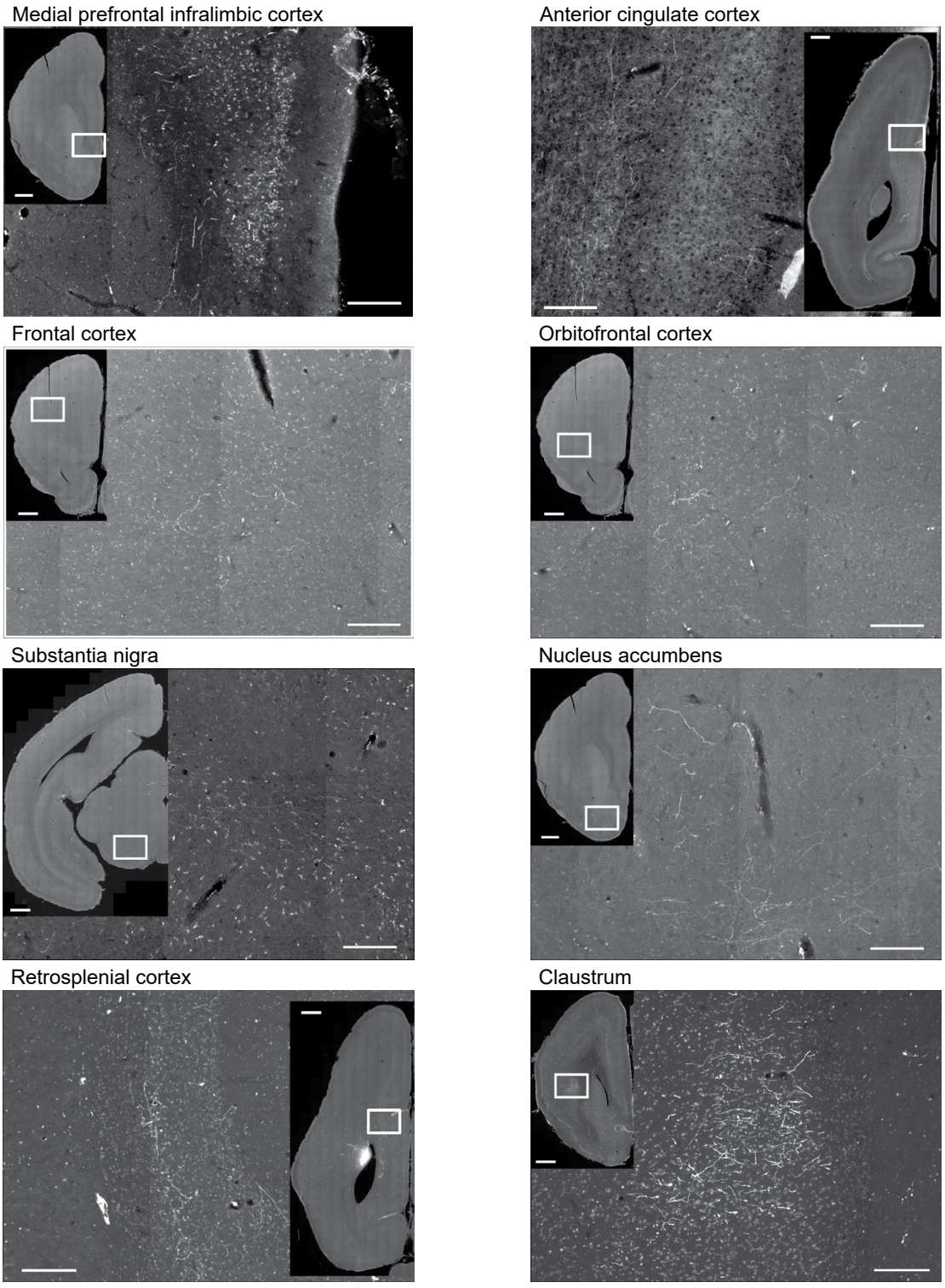

fig. S14. Direct anatomical projections from bat dorsal hippocampal CA1 reach many brain areas that are important for social interactions. Here we injected 4 additional bats with anterograde tracers (DA647, DA555) in dorsal CA1 (*21*). Shown are examples illustrating some of the brain regions involved in regulating social behavior, in which we found direct monosynaptic (albeit sparse) projections from dorsal CA1. These regions include the medial prefrontal infralimbic cortex, anterior cingulate cortex, frontal cortex, orbitofrontal cortex, substantia nigra, nucleus accumbens, retrosplenial cortex, and claustrum. Scale bars: main panels, 200 μm; insets, 1 mm. Anterior cingulate cortex and retrosplenial cortex are horizontal sections, all other six regions are coronal sections.

				Flights		Social interactions	Active on net
	Bat name	*Sex*	*Hemi-sphere*	*Cells*	*Cells × directions*	*Cells*	*Cells*
Recorded bats	U	M	Right	-	-	30	20
	A1	M	Right	11	17	22	14
	7	F	Right	-	-	16	17
	A2	M	Right	61	101	83	168
	6	F	Left	28	32	119	175
All recorded bats: summary				100	150	270	394
Other bats (non-recorded bats)	O	F					
	1	F					
	2	F					
	3	F					
	C	M					
	P	M					
	S	M					
	T	M					
	X	M					

Table S1: Summary of all bats and neuronal recordings. The numbers of cells and cells × directions shown here refer to the cells which were valid for analysis: namely, cells which met criteria of minimal amount of behavioral data and minimal number of spikes allowing analysis (see Materials and Methods). A total of 444 cells were valid for analysis in at least one of the three behavioral states (flights, social interactions, active on net). Bats U and 7 did not exhibit enough flights during the recording period, and were not included in the flight analysis. In addition to the 14 bats listed in this table, 4 additional bats were used for anatomical tract tracing (fig. S14).

Cell type	Term	3-way ANOVA (*P*-value)	Mixed-effects model (*P*-value)
Allocentric cells	sex	0.026	0.025
	hierarchy	0.625	0.621
	affiliation	0.987	0.987
	sex × hierarchy	0.806	0.803
	sex × affiliation	0.011	0.010
	hierarchy × affiliation	0.243	0.238
	sex × hierarchy × affiliation	0.938	0.937
Egocentric cells	Sex	0.378	0.374
	hierarchy	0.047	0.046
	affiliation	0.014	0.013
	sex × hierarchy	0.034	0.032
	sex × affiliation	0.387	0.384
	hierarchy × affiliation	0.779	0.777
	sex × hierarchy × affiliation	0.348	0.344

Table S2: Summary of 3-way ANOVA and mixed-effects linear model for the encoding of sex, social hierarchy, and social affiliation of other bats by hippocampal neurons during active observation on-net. Top half, allocentric cells (Fig. 6D). Bottom half, egocentric cells (Fig. 6E). As described in the Materials and Methods, the mixed-effects model also uses an ANOVA, but unlike the standard 3-way ANOVA, this model includes also random effects. The fact that similar *P*-values were obtained using the 3-way ANOVA and the mixed-effects linear model indicates that the random effects included in the mixed-effects model had a very small impact – and in particular, this means that including the identity of the recorded bat as a random effect did not influence the results.

References and notes

1. T. D. Seeley, *The Wisdom of the Hive: The Social Physiology of Honey Bee Colonies* (Harvard Univ. Press, 2009).

2. A. Strandburg-Peshkin, D. R. Farine, I. D. Couzin, M. C. Crofoot, Shared decision-making drives collective movement in wild baboons. *Science* **348**, 1358–1361 (2015). doi:10.1126/science.aaa5099 Medline

3. T. Clutton-Brock, *Mammal Societies* (Wiley, 2016).

4. T. Okuyama, T. Kitamura, D. S. Roy, S. Itohara, S. Tonegawa, Ventral CA1 neurons store social memory. *Science* **353**, 1536–1541 (2016). doi:10.1126/science.aaf7003 Medline

5. T. Danjo, T. Toyoizumi, S. Fujisawa, Spatial representations of self and other in the hippocampus. *Science* **359**, 213–218 (2018). doi:10.1126/science.aao3898 Medline

6. D. B. Omer, S. R. Maimon, L. Las, N. Ulanovsky, Social place-cells in the bat hippocampus. *Science* **359**, 218–224 (2018). doi:10.1126/science.aao3474 Medline

7. R. P. Rao, M. von Heimendahl, V. Bahr, M. Brecht, Neuronal responses to conspecifics in the ventral CA1. *Cell Rep.* **27**, 3460–3472.e3 (2019). doi:10.1016/j.celrep.2019.05.081 Medline

8. M. von Heimendahl, R. P. Rao, M. Brecht, Weak and nondiscriminative responses to conspecifics in the rat hippocampus. *J. Neurosci.* **32**, 2129–2141 (2012). doi:10.1523/JNEUROSCI.3812-11.2012 Medline

9. T. Zhou, H. Zhu, Z. Fan, F. Wang, Y. Chen, H. Liang, Z. Yang, L. Zhang, L. Lin, Y. Zhan, Z. Wang, H. Hu, History of winning remodels thalamo-PFC circuit to reinforce social dominance. *Science* **357**, 162–168 (2017). doi:10.1126/science.aak9726 Medline

10. Y. Li, A. Mathis, B. F. Grewe, J. A. Osterhout, B. Ahanonu, M. J. Schnitzer, V. N. Murthy, C. Dulac, Neuronal representation of social information in the medial amygdala of awake behaving mice. *Cell* **171**, 1176–1190.e17 (2017). doi:10.1016/j.cell.2017.10.015 Medline

11. F. L. Hitti, S. A. Siegelbaum, The hippocampal CA2 region is essential for social memory. *Nature* **508**, 88–92 (2014). doi:10.1038/nature13028 Medline

12. R. Q. Quiroga, L. Reddy, G. Kreiman, C. Koch, I. Fried, Invariant visual representation by single neurons in the human brain. *Nature* **435**, 1102–1107 (2005). doi:10.1038/nature03687 Medline

13. A. Forli, M. M. Yartsev, Hippocampal representation during collective spatial behaviour in bats. *Nature* **621**, 796–803 (2023). doi:10.1038/s41586-023-06478-7 Medline

14. J. O'Keefe, J. Dostrovsky, The hippocampus as a spatial map. Preliminary evidence from unit activity in the freely-moving rat. *Brain Res.* **34**, 171–175 (1971). doi:10.1016/0006-8993(71)90358-1 Medline

15. M. A. Wilson, B. L. McNaughton, Dynamics of the hippocampal ensemble code for space. *Science* **261**, 1055–1058 (1993). doi:10.1126/science.8351520 Medline

16. N. Ulanovsky, C. F. Moss, Hippocampal cellular and network activity in freely moving echolocating bats. *Nat. Neurosci.* **10**, 224–233 (2007). doi:10.1038/nn1829 Medline

17. G. G. Kwiecinski, T. A. Griffiths, Rousettus egyptiacus. *Mamm. Species* **611**, 1–9 (1999). doi:10.2307/3504411

18. G. Neuweiler, *The Biology of Bats* (Oxford Univ. Press, 2000).

19. M. C. Rose, B. Styr, T. A. Schmid, J. E. Elie, M. M. Yartsev, Cortical representation of group social communication in bats. *Science* **374**, eaba9584 (2021). doi:10.1126/science.aba9584 Medline

20. L. Las, N. Ulanovsky, Bats. *Nat. Methods* **21**, 1135–1137 (2024). doi:10.1038/s41592-024-02330-6 Medline

21. Materials and methods are available as supplementary materials.

22. J. D. Crall, N. Gravish, A. M. Mountcastle, S. A. Combes, BEEtag: A low-cost, image-based tracking system for the study of animal behavior and locomotion. *PLOS ONE* **10**, e0136487 (2015). doi:10.1371/journal.pone.0136487 Medline

23. R. A. Hinde, Interactions, relationships and social structure. *Man (Lond.)* **11**, 1–17 (1976). doi:10.2307/2800384

24. S. Shultz, C. Opie, Q. D. Atkinson, Stepwise evolution of stable sociality in primates. *Nature* **479**, 219–222 (2011). doi:10.1038/nature10601 Medline

25. S. W. Li, O. Zeliger, L. Strahs, R. Báez-Mendoza, L. M. Johnson, A. McDonald Wojciechowski, Z. M. Williams, Frontal neurons driving competitive behaviour and ecology of social groups. *Nature* **603**, 661–666 (2022). doi:10.1038/s41586-021-04000-5 Medline

26. F. Wang, J. Zhu, H. Zhu, Q. Zhang, Z. Lin, H. Hu, Bidirectional control of social hierarchy by synaptic efficacy in medial prefrontal cortex. *Science* **334**, 693–697 (2011). doi:10.1126/science.1209951 Medline

27. B. L. McNaughton, C. A. Barnes, J. O'Keefe, The contributions of position, direction, and velocity to single unit activity in the hippocampus of freely-moving rats. *Exp. Brain Res.* **52**, 41–49 (1983). doi:10.1007/BF00237147 Medline

28. M. Geva-Sagiv, S. Romani, L. Las, N. Ulanovsky, Hippocampal global remapping for different sensory modalities in flying bats. *Nat. Neurosci.* **19**, 952–958 (2016). doi:10.1038/nn.4310 Medline

29. W. A. Liberti 3rd, T. A. Schmid, A. Forli, M. Snyder, M. M. Yartsev, A stable hippocampal code in freely flying bats. *Nature* **604**, 98–103 (2022). doi:10.1038/s41586-022-04560-0 Medline

30. T. Eliav, S. R. Maimon, J. Aljadeff, M. Tsodyks, G. Ginosar, L. Las, N. Ulanovsky, Multiscale representation of very large environments in the hippocampus of flying bats. *Science* **372**, eabg4020 (2021). doi:10.1126/science.abg4020 Medline

31. K. W. Latimer, J. L. Yates, M. L. Meister, A. C. Huk, J. W. Pillow, Single-trial spike trains in parietal cortex reveal discrete steps during decision-making. *Science* **349**, 184–187 (2015). doi:10.1126/science.aaa4056 Medline

32. K. Hardcastle, N. Maheswaranathan, S. Ganguli, L. M. Giocomo, A multiplexed, heterogeneous, and adaptive code for navigation in medial entorhinal cortex. *Neuron* **94**, 375–387.e7 (2017). doi:10.1016/j.neuron.2017.03.025 Medline

33. J.-P. Noel, E. Balzani, E. Avila, K. J. Lakshminarasimhan, S. Bruni, P. Alefantis, C. Savin, D. E. Angelaki, Coding of latent variables in sensory, parietal, and frontal cortices during closed-loop virtual navigation. *eLife* **11**, e80280 (2022). doi:10.7554/eLife.80280 Medline

34. N. L. Goodwin, S. R. O. Nilsson, J. J. Choong, S. A. Golden, Toward the explainability, transparency, and universality of machine learning for behavioral classification in neuroscience. *Curr. Opin. Neurobiol.* **73**, 102544 (2022). doi:10.1016/j.conb.2022.102544 Medline

35. L. S. Shapley, "A value for n-person games" in *Contributions to the Theory of Games*, H. W. Kuhn, A. W. Tucker, Eds. (Princeton Univ. Press, 1953), vol. II, pp. 307–318.

36. J. O'Keefe, L. Nadel, *The Hippocampus as a Cognitive Map* (Oxford Univ. Press, 1978).

37. A. Sarel, A. Finkelstein, L. Las, N. Ulanovsky, Vectorial representation of spatial goals in the hippocampus of bats. *Science* **355**, 176–180 (2017). doi:10.1126/science.aak9589 Medline

38. L. Acharya, Z. M. Aghajan, C. Vuong, J. J. Moore, M. R. Mehta, Causal influence of visual cues on hippocampal directional selectivity. *Cell* **164**, 197–207 (2016). doi:10.1016/j.cell.2015.12.015 Medline

39. A. Rubin, M. M. Yartsev, N. Ulanovsky, Encoding of head direction by hippocampal place cells in bats. *J. Neurosci.* **34**, 1067–1080 (2014). doi:10.1523/JNEUROSCI.5393-12.2014 Medline

40. R. Adolphs, The social brain: Neural basis of social knowledge. *Annu. Rev. Psychol.* **60**, 693–716 (2009). doi:10.1146/annurev.psych.60.110707.163514 Medline

41. M. Murugan, H. J. Jang, M. Park, E. M. Miller, J. Cox, J. P. Taliaferro, N. F. Parker, V. Bhave, H. Hur, Y. Liang, A. R. Nectow, J. W. Pillow, I. B. Witten, Combined social and spatial coding in a descending projection from the prefrontal cortex. *Cell* **171**, 1663–1677.e16 (2017). doi:10.1016/j.cell.2017.11.002 Medline

42. X. Mou, D. Ji, Social observation enhances cross-environment activation of hippocampal place cell patterns. *eLife* **5**, e18022 (2016). doi:10.7554/eLife.18022 Medline

43. L. Zynyuk, J. Huxter, R. U. Muller, S. E. Fox, The presence of a second rat has only subtle effects on the location-specific firing of hippocampal place cells. *Hippocampus* **22**, 1405–1416 (2012). doi:10.1002/hipo.20977 Medline

44. A. Sarel, S. Palgi, D. Blum, J. Aljadeff, L. Las, N. Ulanovsky, Natural switches in behaviour rapidly modulate hippocampal coding. *Nature* **609**, 119–127 (2022). doi:10.1038/s41586-022-05112-2 Medline

45. J. L. Gauthier, D. W. Tank, A dedicated population for reward coding in the hippocampus. *Neuron* **99**, 179–193.e7 (2018). doi:10.1016/j.neuron.2018.06.008 Medline

46. M. A. Moita, S. Rosis, Y. Zhou, J. E. LeDoux, H. T. Blair, Hippocampal place cells acquire location-specific responses to the conditioned stimulus during auditory fear conditioning. *Neuron* **37**, 485–497 (2003). doi:10.1016/S0896-6273(03)00033-3 Medline

47. E. Kong, K.-H. Lee, J. Do, P. Kim, D. Lee, Dynamic and stable hippocampal representations of social identity and reward expectation support associative social memory in male mice. *Nat. Commun.* **14**, 2597 (2023). doi:10.1038/s41467-023-38338-3 Medline

48. R. Báez-Mendoza, E. P. Mastrobattista, A. J. Wang, Z. M. Williams, Social agent identity cells in the prefrontal cortex of interacting groups of primates. *Science* **374**, eabb4149 (2021). doi:10.1126/science.abb4149 Medline

49. L. Kingsbury, S. Huang, J. Wang, K. Gu, P. Golshani, Y. E. Wu, W. Hong, Correlated neural activity and encoding of behavior across brains of socially interacting animals. *Cell* **178**, 429–446.e16 (2019). doi:10.1016/j.cell.2019.05.022 Medline

50. K. Haroush, Z. M. Williams, Neuronal prediction of opponent's behavior during cooperative social interchange in primates. *Cell* **160**, 1233–1245 (2015). doi:10.1016/j.cell.2015.01.045 Medline

51. N. Burgess, E. A. Maguire, J. O'Keefe, The human hippocampus and spatial and episodic memory. *Neuron* **35**, 625–641 (2002). doi:10.1016/S0896-6273(02)00830-9 Medline

52. W. B. Scoville, B. Milner, Loss of recent memory after bilateral hippocampal lesions. *J. Neurol. Neurosurg. Psychiatry* **20**, 11–21 (1957). doi:10.1136/jnnp.20.1.11 Medline

53. L. Kingsbury, S. Huang, T. Raam, L. S. Ye, D. Wei, R. K. Hu, L. Ye, W. Hong, Cortical representations of conspecific sex shape social behavior. *Neuron* **107**, 941–953.e7 (2020). doi:10.1016/j.neuron.2020.06.020 Medline

54. R. M. Tavares, A. Mendelsohn, Y. Grossman, C. H. Williams, M. Shapiro, Y. Trope, D. Schiller, A map for social navigation in the human brain. *Neuron* **87**, 231–243 (2015). doi:10.1016/j.neuron.2015.06.011 Medline

55. E. H. Nieh, M. Schottdorf, N. W. Freeman, R. J. Low, S. Lewallen, S. A. Koay, L. Pinto, J. L. Gauthier, C. D. Brody, D. W. Tank, Geometry of abstract learned knowledge in the hippocampus. *Nature* **595**, 80–84 (2021). doi:10.1038/s41586-021-03652-7 Medline

56. T. J. Tyree, M. Metke, C. T. Miller, Cross-modal representation of identity in the primate hippocampus. *Science* **382**, 417–423 (2023). doi:10.1126/science.adf0460 Medline

57. S. Ray, I. Yona, N. Elami, S. Palgi, K. W. Latimer, B. Jacobsen, M. P. Witter, L. Las, N. Ulanovsky, Data for: Hippocampal coding of identity, sex, hierarchy and affiliation in a social group of wild fruit bats, Zenodo (2025); https://doi.org/10.5281/zenodo.13938638.

58. J. H. Friedman, Greedy function approximation: A gradient boosting machine. *Ann. Stat.* **29**, 1189–1232 (2001). doi:10.1214/aos/1013203451

59. M. Lafortune, S. O. Canapp Jr., D. Heard, L. L. Farina, A vasectomy technique for Egyptian fruit bats (Rousettus aegyptiacus). *J. Zoo Wildl. Med.* **35**, 104–106 (2004). doi:10.1638/03-020 Medline

60. P. L. Garrison, C. J. Gamble, Sexual effects of vasectomy. *J. Am. Med. Assoc.* **144**, 293–295 (1950). doi:10.1001/jama.1950.02920040007002 Medline

61. C. H. Phoenix, Sexual behavior in rhesus monkeys after vasectomy. *Science* **179**, 493–494 (1973). doi:10.1126/science.179.4072.493 Medline

62. J. M. McGlynn, M. J. Erpino, Effects of vasectomy on the reproductive system and sexual behaviour of rats. *J. Reprod. Fertil.* **40**, 241–247 (1974). doi:10.1530/jrf.0.0400241 Medline

63. S. Danilovich, A. Krishnan, W.-J. Lee, I. Borrisov, O. Eitan, G. Kosa, C. F. Moss, Y. Yovel, Bats regulate biosonar based on the availability of visual information. *Curr. Biol.* **25**, R1124–R1125 (2015). doi:10.1016/j.cub.2015.11.003 Medline

64. M. Geva-Sagiv, L. Las, Y. Yovel, N. Ulanovsky, Spatial cognition in bats and rats: From sensory acquisition to multiscale maps and navigation. *Nat. Rev. Neurosci.* **16**, 94–108 (2015). doi:10.1038/nrn3888 Medline

65. A. Bavelas, Communication patterns in task-oriented groups. *J. Acoust. Soc. Am.* **22**, 725–730 (1950). doi:10.1121/1.1906679

66. M. J. Vonhof, R. M. R. Barclay, Roost-site selection and roosting ecology of forest-dwelling bats in southern British Columbia. *Can. J. Zool.* **74**, 1797–1805 (1996). doi:10.1139/z96-200

67. S. J. Portugal, L. Sivess, G. R. Martin, P. J. Butler, C. R. White, Perch height predicts dominance rank in birds. *Ibis* **159**, 456–462 (2017). doi:10.1111/ibi.12447

68. P. C. H. Albers, H. de Vries, Elo-rating as a tool in the sequential estimation of dominance strengths. *Anim. Behav.* **61**, 489–495 (2001). doi:10.1006/anbe.2000.1571

69. A. Sánchez-Tójar, J. Schroeder, D. R. Farine, A practical guide for inferring reliable dominance hierarchies and estimating their uncertainty. *J. Anim. Ecol.* **87**, 594–608 (2018). doi:10.1111/1365-2656.12776 Medline

70. H. Landau, On dominance relations and the structure of animal societies: I. Effect of inherent characteristics. *Bull. Math. Biophys.* **13**, 1–19 (1951). doi:10.1007/BF02478336

71. H. de Vries, An improved test of linearity in dominance hierarchies containing unknown or tied relationships. *Anim. Behav.* **50**, 1375–1389 (1995). doi:10.1016/0003-3472(95)80053-0

72. S. Benhamou, How to reliably estimate the tortuosity of an animal's path: Straightness, sinuosity, or fractal dimension? *J. Theor. Biol.* **229**, 209–220 (2004). doi:10.1016/j.jtbi.2004.03.016 Medline

73. J. Voigts, J. P. Newman, M. A. Wilson, M. T. Harnett, An easy-to-assemble, robust, and lightweight drive implant for chronic tetrode recordings in freely moving animals. *J. Neural Eng.* **17**, 026044 (2020). doi:10.1088/1741-2552/ab77f9 Medline

74. B. Jacobsen, H. Kleven, W. Gatome, L. Las, N. Ulanovsky, M. P. Witter, Organization of projections from the entorhinal cortex to the hippocampal formation of the Egyptian fruit bat Rousettus aegyptiacus. *Hippocampus* **33**, 889–905 (2023). doi:10.1002/hipo.23517 Medline

75. V. Ego-Stengel, M. A. Wilson, Disruption of ripple-associated hippocampal activity during rest impairs spatial learning in the rat. *Hippocampus* **20**, 1–10 (2010). doi:10.1002/hipo.20707 Medline

76. W. E. Skaggs, B. L. McNaughton, K. M. Gothard, E. J. Markus, An information-theoretic approach to deciphering the hippocampal code" in *Advances in Neural Information Processing Systems*, M. Kaufman, S. J. Hanson, J. D. Cowan, C. L. Giles, Eds. (Curran Associates, 1992), vol. 5, pp. 1030–1037.

77. S. Leutgeb, J. K. Leutgeb, C. A. Barnes, E. I. Moser, B. L. McNaughton, M.-B. Moser, Independent codes for spatial and episodic memory in hippocampal neuronal ensembles. *Science* **309**, 619–623 (2005). doi:10.1126/science.1114037 Medline

78. L. R. Dice, Measures of the amount of ecologic association between species. *Ecology* **26**, 297–302 (1945). doi:10.2307/1932409

79. K. Zhang, I. Ginzburg, B. L. McNaughton, T. J. Sejnowski, Interpreting neuronal population activity by reconstruction: Unified framework with application to hippocampal place cells. *J. Neurophysiol.* **79**, 1017–1044 (1998). doi:10.1152/jn.1998.79.2.1017 Medline

80. D. B. Omer, L. Las, N. Ulanovsky, Contextual and pure time coding for self and other in the hippocampus. *Nat. Neurosci.* **26**, 285–294 (2023). doi:10.1038/s41593-022-01226-y Medline

81. A. Schneider, C. Zimmermann, M. Alyahyay, F. Steenbergen, T. Brox, I. Diester, 3D pose estimation enables virtual head fixation in freely moving rats. *Neuron* **110**, 2080–2093.e10 (2022). doi:10.1016/j.neuron.2022.04.019 Medline

82. D. Servén, C. Brummitt, "pyGAM: Generalized additive models in Python" (Zenodo, 2018); https://zenodo.org/records/1208724.

83. J. J. Moore, J. D. Cushman, L. Acharya, B. Popeney, M. R. Mehta, Linking hippocampal multiplexed tuning, Hebbian plasticity and navigation. *Nature* **599**, 442–448 (2021). doi:10.1038/s41586-021-03989-z Medline

84. K. Aas, M. Jullum, A. Løland, Explaining individual predictions when features are dependent: More accurate approximations to Shapley values. *Artif. Intell.* **298**, 103502 (2021). doi:10.1016/j.artint.2021.103502

85. G. James, D. Witten, T. Hastie, R. Tibshirani, *An Introduction to Statistical Learning* (Springer, 2013).

86. W. E. Skaggs, B. L. McNaughton, M. A. Wilson, C. A. Barnes, Theta phase precession in hippocampal neuronal populations and the compression of temporal sequences. *Hippocampus* **6**, 149–172 (1996). doi:10.1002/(SICI)1098-1063(1996)6:2<149:AID-HIPO6>3.0.CO;2-K Medline

87. J. B. Silk, S. C. Alberts, J. Altmann, Social bonds of female baboons enhance infant survival. *Science* **302**, 1231–1234 (2003). doi:10.1126/science.1088580 Medline